INFORMATION TO USERS

The most advanced technology has been used to photograph and reproduce this manuscript from the microfilm master. UMI films the text directly from the original or copy submitted. Thus, some thesis and dissertation copies are in typewriter face, while others may be from any type of computer printer.

The quality of this reproduction is dependent upon the quality of the copy submitted. Broken or indistinct print, colored or poor quality illustrations and photographs, print bleedthrough, substandard margins, and improper alignment can adversely affect reproduction.

In the unlikely event that the author did not send UMI a complete manuscript and there are missing pages, these will be noted. Also, if unauthorized copyright material had to be removed, a note will indicate the deletion.

Oversize materials (e.g., maps, drawings, charts) are reproduced by sectioning the original, beginning at the upper left-hand corner and continuing from left to right in equal sections with small overlaps. Each original is also photographed in one exposure and is included in reduced form at the back of the book.

Photographs included in the original manuscript have been reproduced xerographically in this copy. Higher quality 6" x 9" black and white photographic prints are available for any photographs or illustrations appearing in this copy for an additional charge. Contact UMI directly to order.

UMI

University Microfilms International
A Bell & Howell Information Company
300 North Zeeb Road, Ann Arbor, MI 48106-1346 USA
313/761-4700 800/521-0600

Order Number 9119688

Transport properties of photoexcitations in stretched trans-polyacetylene

Walser, Ardie Darnel, Ph.D.

City University of New York, 1991

U·M·I
300 N. Zeeb Rd.
Ann Arbor, MI 48106

TRANSPORT PROPERTIES OF PHOTOEXCITATIONS IN STRETCHED TRANS-POLYACETYLENE

by

ARDIE DARNEL WALSER

A dissertation submitted to the Graduate Faculty in Engineering in partial fulfillment of the requirement for the degree of Doctor of Philosophy, The City University of New York.

1991

This manuscript has been read and accepted by the Graduate Faculty in Engineering in satisfaction of the dissertation requirement for the degree of Doctor of Philosophy.

1/28/91
Date

Chair of Examining Committee
Prof. R. R. Alfano

Co-Chair of Examining Committee
Prof. R. Dorsinville

1/29/91
Date

Executive Officer
Prof. Gerard Lowen

Supervisory Committee
Prof. S. Ahmed
Prof. P. P. Ho
Dr. A. M. Johnson

The City University of New York

Abstract

TRANSPORT PROPERTIES OF PHOTOEXCITATIONS IN STRETCHED TRANS-POLYACETYLENE

by

Ardie Darnel Walser

Advisers: **Prof. Robert R. Alfano**
Prof. Roger Dorsinville

The temperature, sample orientation (1D and 3D), intensity, and optical field polarization dependence of the picosecond photoconductive response of highly oriented stretched trans-polyacetylene has been measured . The results of these experiments strongly suggest that solitons and polarons are the main mobile charged carriers in this quasi one-dimensional organic semiconductor.

The main results are summarized as follows:

i) The fast component of the photoconductivity parallel to the polymer chains (1D configuration) is temperature independent for both above- and below-gap photoexcitation.

ii) The fast component of the photoconductivity perpendicular to the chains (3D configuration) decreases exponentially with 1/T for both above- and below- gap excitation each with an activation energy E_A of 48 meV and 63 meV respectively.

iii) The 1D and 3D cw photoconductivity decreases with 1/T exhibiting approximately the same activation energy of $E_A = 0.15$ eV.

iv) The fast component of the photoresponse is roughly three orders of magnitude higher than the cw response with a decay time of about 400 ps. The transient mobility μ is approximately 0.04 $cm^2/V\text{-}s$ along the chain. The mean drift distance of the photogenerated charge carriers <x> along the chain is estimated at 13 angstroms.

v) The I-V characteristic curve of the 1D picosecond photoconductive response is superlinear for both above- and below gap excitation, while the I-V characteristic curve for the 3D picosecond photoconductive response is linear.

vi) The intensity dependence of the picosecond 1D and 3D photocurrent varied linearly with the laser intensity, independent of the polarization and wavelength (0.53 μm and 1.06 μm) of the incident beam.

vii) The anisotropy with below gap excitation is constant at 2.4, while with above gap excitation it decreases from 7.4 to 4.5 as the laser intensity increases. It has also been found, that the photoconductive response is greatest for below gap excitation independent of the optical field polarization.

These results were accounted for by a combination of a direct interchain generation model, which was derived from an extended tight binding model, laser heating and bimolecular recombination. Solitons dominant the 1D picosecond photocurrent and polarons dominant the 3D picosecond photocurrent.

ACKNOWLEDGEMENT

I wish to thank Prof. Robert Alfano for giving me the opportunity to fulfill my potential as a scientist- for this I shall always be grateful. I appreciate his sincere interest to make me and this thesis first rate. I also thank Prof. Roger Dorsinville, with whom I worked closely with these past years, for his guidance and insight. I thank Dr. Nate Ockman for his stimulating comments and challenging conversation. I wish to thank Prof. Ricardo Tubino for the acquisition of samples (for without them, this thesis would not have been possible) and for the many fruitful discussions. Thanks to Dr. Anthony M. Johnson for his technical expertise and moral support. I wish to thank the IUSL where all my experiments were performed and thank all my friends there for their assistance. My deepest gratitude to NASA (grant number 449521), GPOP and CASI for financial support throughout my graduate studies. And finally, I thank all my family and friends for their support and inspiration.

This work is dedicated with respect and love to my mother, Mary Ruth Walser as a testament of her contribution to humanity and to my wife Patricia Veronica Phillips-Walser and my son Jarrett Dakar Walser.

TRANSPORT PROPERTIES OF PHOTOEXCITATIONS IN STRETCHED TRANS-POLYACETYLENE

by

ARDIE DARNEL WALSER

List of Tables

List of Figures

I. Introduction

Over the past three decades, the scientific community has expressed considerable interest in conducting organic materials for their unique applications in a variety of fields (ie. photoconductor, battery, nonlinear optics, etc.). The past 16 years have seen the level of activity grow rapidly as new and unanticipated phenomena were observed which were not found in nonconducting organic materials and were rarely found in inorganic materials. The prediction that superconductivity might occur in organic solids at technologically feasible temperatures stimulated this field further. Unfortunately, this prediction has not been fulfilled, although some organic materials have shown superconducting properties at very low temperatures ($T < 5$ K). The field is highly interdisciplinary involving the skills and expertise of chemist, material scientist, and theoretical and experimental physicist and engineers, whose interaction has produced new chemistry, physics and technology. When using the term "conducting organic materials" we are referring to a large class of polymers each having different structural features (varying from simple to complex) and conducting properties.

The interest in polyacetylene stems from its expected applications as well as the simplicity of its structure. In fact it appears to behave as a quasi-one-dimensional conductor showing a Peierls transition to a degenerated ground state which may give rise

to the formation of localized intrinsic defects such as solitons and polarons. Due to its chain structure, polyacetylene may be doped with a variety of chemical substances. These dopants interact with the molecular chains of the polymer, as electron donors or acceptors increasing the conductivity of the sample more than twelve orders of magnitude, up to $10^3\ \Omega^{-1}\ cm^{-1}$ at room temperature for concentrations of about 10%. Hence, this materials conductivity ranges from insulating to metallic levels[1,2,3]. Since the doped molecules are weakly coupled to the chain they may be introduced and removed electrochemically allowing for storage of electrical energy[4] . The possibility of doping with donors (reducing agents) or acceptors (oxidizing agents) allows the construction of p-n junctions and Schottky barriers which exhibit a photoresponse to light. Undoped polyacetylene has a photoconductive response as well.

This very versatile material has numerous technological applications, several of them being:

1) Polyacetylene may serve as an organic conductor replacing conventional metals.

2) Reversible electrochemical doping of polyacetylene allows for the construction of light-weight, high-energy-density batteries.

3) The photovoltaic effect in heterojuctions with polyacetylene as one component, may be used to produce low-cost solar photovoltaic cells. It is conceivable that the heterostructure could be fabricated entirely of polyacetylene. Where each component of the heterostructure is a polyacetylene sample doped appropriately for the purpose it is to serve. This would apply similarly to integrated circuit technology.

4) Polyacetylene high third order susceptibility makes it an excellent candidate for use in nonlinear optics.

5) Polyacetylene may be used as an picosecond optical switch due to the short life time of its photocarriers.

Before we can effectively exploit polyacetylene and other conjugated polymers (as well as the entire family of conducting organic materials) for technological applications, we must first have a better understanding of their fundamental properties. A theoretical picture of the elementary excitations in conjugated polymers was developed by Su, Schrieffer and Heeger[5], the SSH model. In this picture, the excitations are quite different from the electron-hole pairs of conventional semiconductors. Instead of electrons and holes, the proper description of the quasi-particles in conjugated polymers is one-dimensional (1D) domain walls, or kinks, or solitons, which separate degenerate ground-state structures. In view of this theory, solitons are responsible for the transport of energy along the polymer chains. There has been considerable interest in testing just how applicable this model is to real materials. Much of the attention has focused on polyacetylene, whose two isomers, trans- and cis-, are expected to represent all the conjugated polymers. Dopant molecules may act as electron donors (ie. Na, K) or acceptors (ie. I_3, AsF_5, $FeCl_3$) distorting the trans-polyacetylene chain and thus introducing polarons or solitons to the chain. Solitons and polarons may also be created by optical excitation. Su and Schrieffer employed the SSH model and showed that an electron-hole pair excited at the band gap relaxes to a soliton-antisoliton pair within 100 fs. An electron

electron-hole pair excited higher up in the band had to pass a more complicated process. There is also a channel of direct soliton-antisoliton pair generation as concluded from the onset of photoconductivity for excitation below the band gap. Once created, these excitations could be probed through measurements of their effect on optical absorption, electron spin resonance and conductivity. Photoexcitation of solitons and polarons is a convenient way to investigate these entities without the influence of impurities in pristine trans-polyacetylene and even cis-polyacetylene, where doping inevitably would initiate isomerization.

In spite of the considerable attention received by the conjugated polymer trans-polyacetylene in terms of theoretical models and experimentation, it is still not clear that solitons and polarons are the main charge carriers. The question to be addressed here is: are they the main charge carriers (soliton and polaron) and what role do these excitations play in the picosecond photoconductive response of polyacetylene?

1.1) Thesis Statement

The objective of this research is to determine the nature and character of the photogenerated charged carriers in the highly oriented organic semiconductor stretched trans-polyacetylene, trans(PA); to determine whether or not solitons and polarons are these charge carriers and if so, their behavior under given conditions. A picosecond optical switch will be used to detect these charge

carriers and scrutinize the effects of, temperature, electric field orientation, and optical excitation energy and polarization on the picosecond photoconductive response of trans-(PA).

1.2) Thesis Outline

In chapter II, I will review the basic background of trans(PA). Here, the physical structure of trans(PA) and the SSH model inspired by it will be discussed. In the second and third sections a brief discussion of the techniques used to fabricate, isomerize and orient the samples used in this study will be given. And finally, a brief summary of some of the experimental results used to prove the validity of the SSH model will be dicussed.

In chapter III, I discuss the experimental technique and apparatus used to investigate the picosecond photoconductive response of trans(PA). A description of the laser system, and sampling scope are given, as well as, some of the fundamental principles of picosecond photoconductivity.

In chapter IV, I report on the investigation of the temperature dependence of the 1D and 3D picosecond photoconductivity of trans(PA) with above gap excitation. These experiments demonstrate for the first time the two distinct behaviors of the mobile charge carriers (solitons and polarons) in highly oriented trans(PA). I find that the picosecond photoconductive response in the 1D configuration (a long the polymer chain) is

independent of temperature, while the response in the 3D configuration (perpendicular to the polymer chain) is temperature dependent.

In chapter V, I report on the investigation of the temperature dependence of the 1D and 3D picosecond photoconductive response of trans(PA) for below gap excitation. I find that the picosecond photoconductivity of trans-(PA) has the same relationship with temperature for below gap excitation as it does for above gap excitation, strongly suggesting that the charge carriers are one in the same.

In chapter VI, I investigated the 1D picosecond photoconductive response of trans-(PA) as a function of polarization (the angle between the optical electric field and the polymer chain) for both above and below gap excitation. The anisotropy ratio for the picosecond photoresponse for both above and below gap excitations was investigated. I report that the above gap anisotropy decreased from 7.4 to 4.5 as the laser intensity increased and the below gap anisotropy remained fixed at an approximate value of 2.4. These results demonstrate the photoproduction of nonlinear charged carriers (solitons and polarons) at energies below the principle interband absorption edge. The possible application of several models such as interchain excitation and bimolecular recombination in explaining the results of this study is discussed.

Chapter VII summarizes the major results and conclusions drawn from this thesis.

Chapter VIII discusses possibilities for future research and applications.

II. Polyacetylene

2.1) Introduction

This chapter is a synopsis of the prevailing school of thought on the structure, properties and models of polyacetylene.

2.2) Structure and theory

Polyacetylene is a linear polymer; it consist of weakly coupled chains of CH units forming a quasi-one dimensional lattice. It is one of the simplest polymer chains. Three of the four carbon valence electrons are in sp^2 hybridized orbitals (mainly a mixing of the 2s and two of the 2p atomic orbitals of the carbon atom, Appendix A), where two of the σ type bonds connect neighboring carbon atoms along the one-dimensional (1D) backbone, while the third (2p) forms a bond with the hydrogen atom side group. The optimal bond angle of 120^0 between these three bonds can be achieved by two possible arrangements of the carbon atoms, trans-(PA) and cis-(PA), with four CH monomers per unit cell respectively (Figs. 2.2-1(a) and 2.2-1(b)). While a cis-bond changes the direction of the chain by 60^0, a trans-bond does not alter the chain direction. The remaining valence electron for either isomer has the symmetry of a $2p_z$ orbital with its charge-density lobes perpendicular to the plane defined by the other three. It is this orbital which causes the peculiar physical properties of polyacetylene. The sp^2 hybridization

(a)

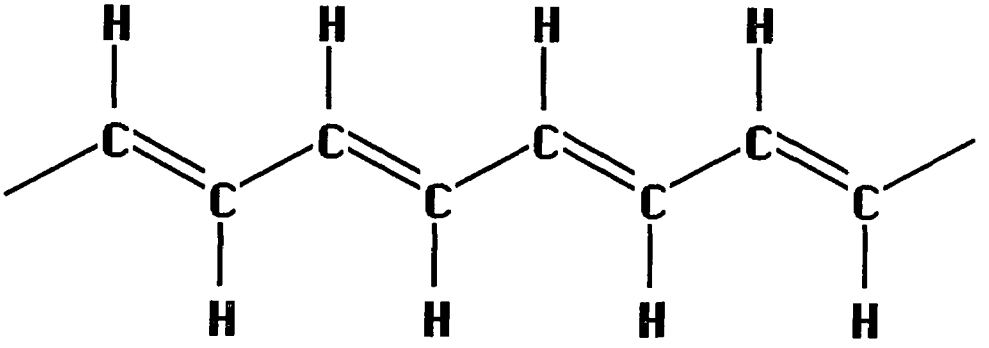

trans

(b)

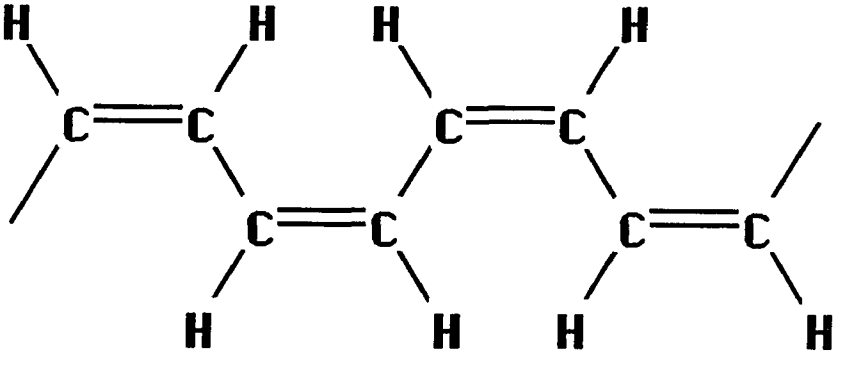

cis

Fig. 2.2-1: Structure diagram for polyacetylene
a) Trans-(PA) b) Cis-(PA)

leads to one unpaired electron ($2p_z$) per carbon atom. Hence, the chain symmetry determines the electronic structure (ie. the size and type of the repeat unit), with the result that polyacetylene can exhibit semiconductor or even metallic properties with the band half filled. Because of the strong intrachain bonding (and weak interchain coupling), the π electrons tend to delocalize along the polymer chain. Therefore, these systems are basically one dimensional.

An early consideration by Peierls[6], has shown that a one-dimensional system is energetically more favorable to distort spontaneously such that the spacing between successive atoms along the chain is modulated with a period of 2k, where $k = \pi/2a$ is the Fermi wave number and a is the lattice constant. When the band is half-filled, the tendency toward spontaneous symmetry breaking is particularly strong, and the distortion leads to a pairing of consecutive sites along the chain, or dimerization (Fig.2.2-2). This dimerization (the pairing of p_z orbitals thru π bonding) opens an energy gap at the Fermi surface, thereby lowering the energy of the occupied states and stabilizing the distortion. The competition between the lowering of the electronic energy and the increase of the elastic energy of the polymer leads to an equilibrium, a Peierls-dimerized ground state. Thus, the lattice instability removes the high density state at the Fermi surface. And since the electronic properties are governed by the gap near the Fermi energy, the system is a semiconductor as opposed to the metallic behavior expected of three dimensional systems with half filled bands.

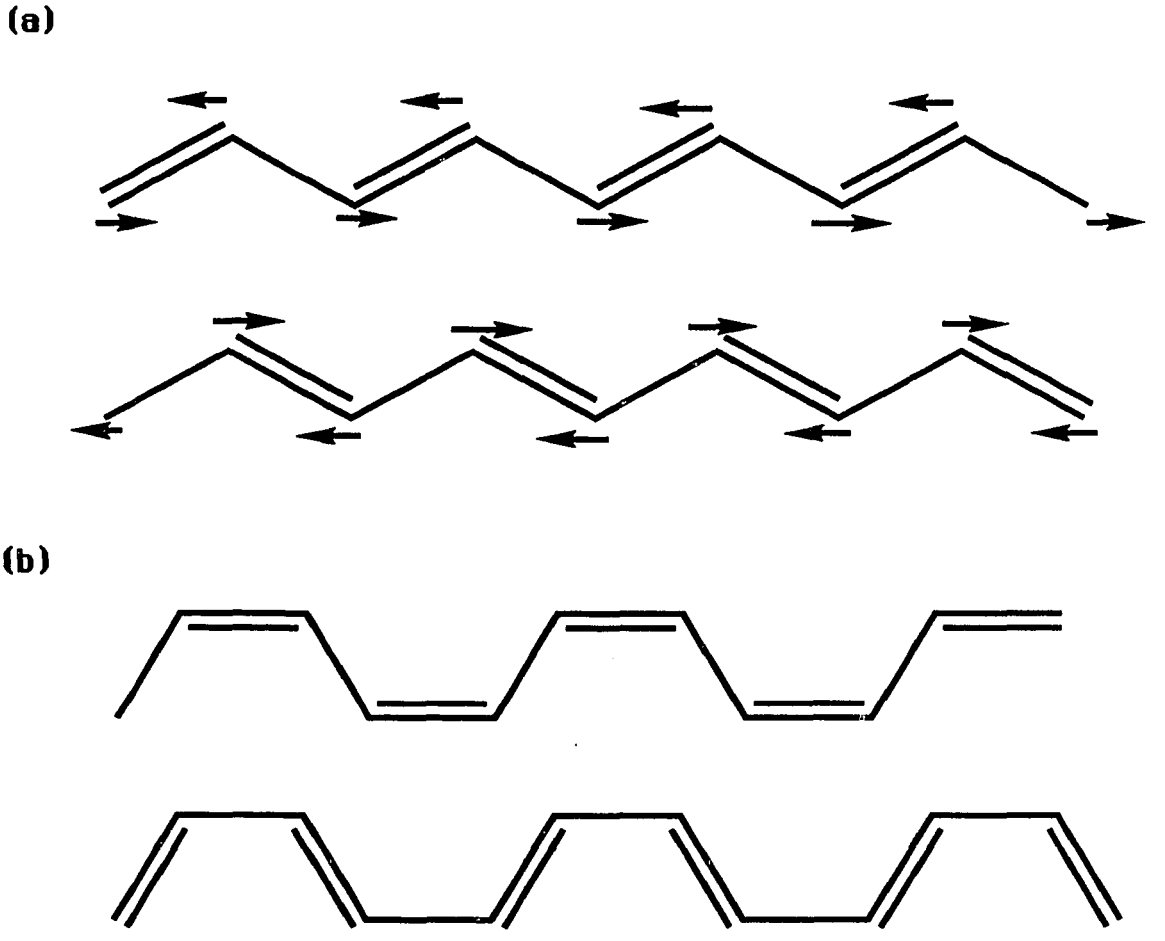

Fig. 2.2-2: a) The two degenerate ground states of trans-(PA).
b) The two nondegenerate ground states of cis-(PA).

Chemically speaking, polyacetylene is an unsaturated polymer chain with conjugated double bonds.

The dimerized trans-polyacetylene has two dimerization patterns or degenerate ground states (Fig. 2.2-2(a)) which allow the formation of defects in such a way that the chain approximates one ground state on one end and the other ground state on the opposite end (Fig. 2.2-3). These bond alternations have many names such as, Pople Walmsley[7] defects, misfits[8,9], domain walls, kinks or solitons. We will use the word solitons to describe these defects, which arise from the dangling bonds of the electronic p_z orbitals. The degenerate ground state is essential for solitons to arise. In cis-(PA), no such symmetry relates the two possible dimerization patterns (Fig. 2.2-2(b)), since the ground state is nondegenerative.

2.3) Su Schrieffer and Heeger (SSH) Model

i) Soliton Excitation

It was the prediction of Su and Schrieffer[10], of soliton photogeneration that stimulated the work on photoexcited (PA). We wish to give a brief description of this calculation, which serves as a framework for subsequent work, both theoretical and experimental. We have already acquainted the reader with the ground-state structure of (PA), in section 2.2. Illustrated in Fig. 2.3-1a is an alternate representation of the isolated segment of a perfectly dimerized chain of the trans isomer of (PA) shown in Fig. 2.2-1(a). The chain consist of a "zig zag" array of carbon atoms which are

(a)

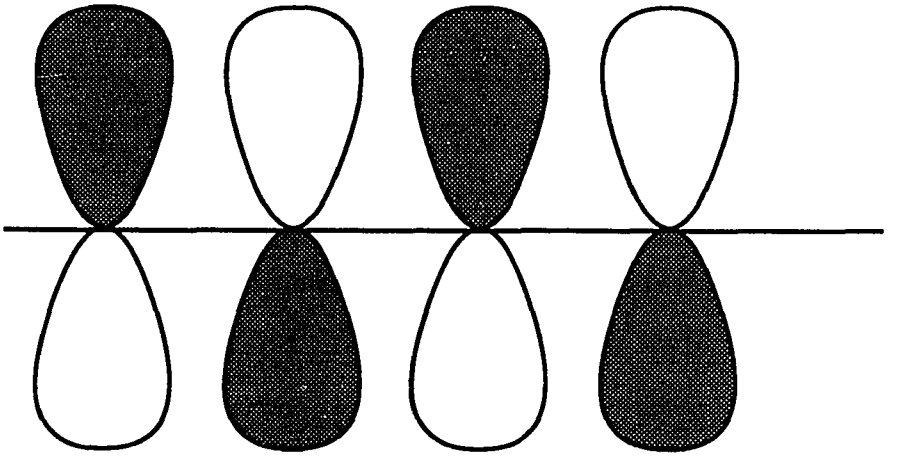

(b)

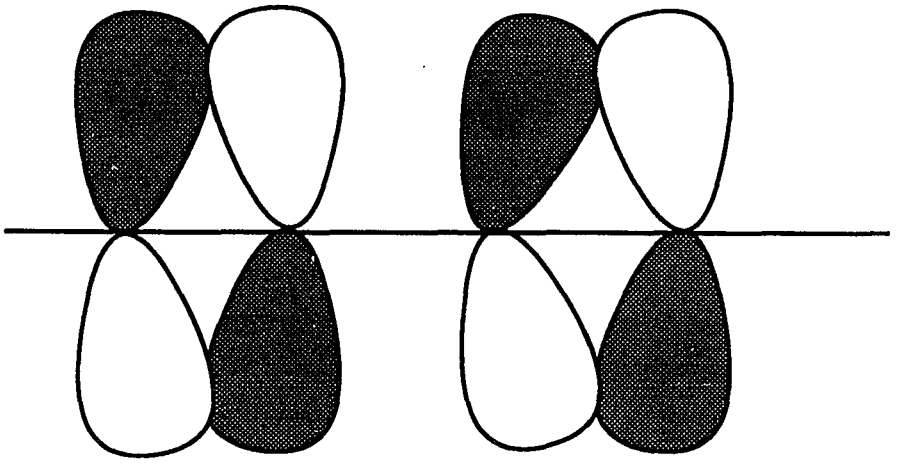

Fig. 2.2-3: 2pz orbitals of the C atoms a) in a metallic structure (e.g. benzene) b) in a structure dimerized by π bonds (Peierls insulator)

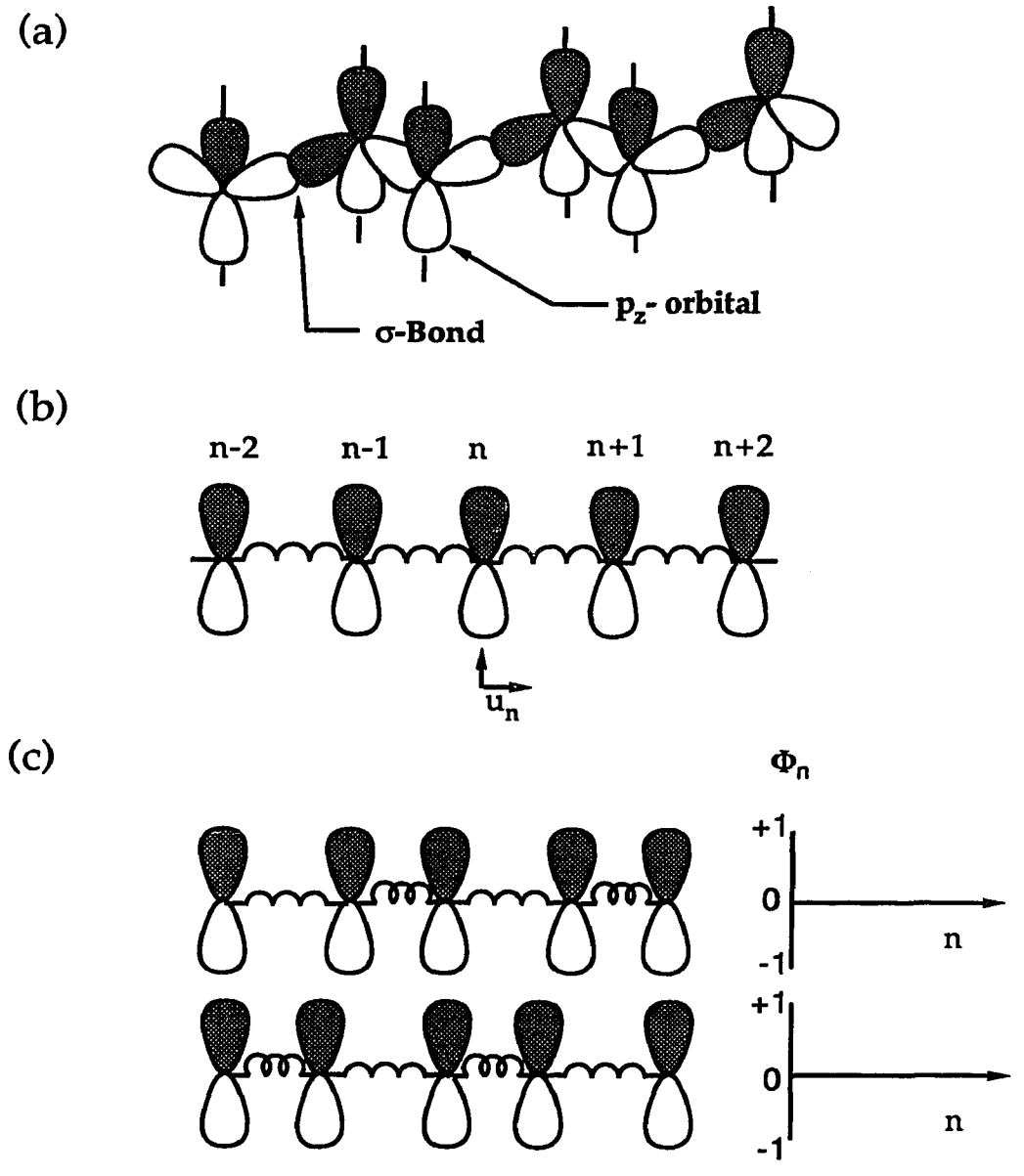

Fig. 2.3-1: a) Sketch of the planar "zigzag" structure of a chain of trans-(PA). b) Idealization of the structure shown in a). The zigzag array is replaced by a linear chain in which the σ bonds are conceived of as springs of force constant K. In this uniform chain the springs have lenghth a. c) Ground state structure of the electron-phonon coupled chain. The uniform chain spontaneously distorts to form a "dimerized" structure in which the springs become alternately stretched and compressed (Orenstein, J.)

connected by strong s bonds which lies in the plane. In addition, each carbon atom is bonded to a hydrogen which also lies in the plane, but has been omitted for clarity. And finally as stated in section 2.2, associated with each carbon is a p_z orbital which projects normal to the plane of the zig zag. For neutral undoped (PA) there is one electron for each p_z orbital. Theorist have preferred to work with a further idealized model, ignoring the zig zagging of the structure as illustrated in Fig. 2.3 -1(b). In this model the planar structure is replaced by a linear chain. This is justified only when the carbon atoms occupy equivalent sites. To describe the ground state and the low lying excitations of the chain, only the weakly bound π electrons are considered. For these electrons move readily along the chain by tunneling between nearest-neighbor p_z orbitals. The tightly bound s electrons form strong bonds between adjacent carbons which are conceived of in this model as springs of force constant K. A hamiltonian to describe this system was proposed by Su, Schrieffer and Heeger[5,11,12]. It consist of two terms

$$H_{SSH} = \sum_n t_{n,n+1}(a_n^+ a_{n+1} + C.C.) + \frac{1}{2}\sum_n K(u_{n+1} - u_n)^2 \qquad (2.3\text{-}1)$$

where $t_{n,n+1}$, is the intersite transfer matrix element, and a_n^+ creates an electron on the nth site. The first term describes nearest-neighbor tunneling of the π electrons, and the second the elastic energy of the springs. The coordinate u_n measures the displacement of the nth C atom from its position on a uniform (equal bond length) chain. The utility of this Hamiltonian is that the coupling of the electron motion to the vibrational dynamics of the chain can be incorporated in a

simple yet realistic way by allowing the $t_{n,n+1}$ to depend upon the intersite separation as

$$t_{n,n+1} = t_0 - a(u_{n+1} - u_n) \qquad (2.3\text{-}2)$$

The major assumptions in the model is that the electron-phonon interaction dominates the physics and that electron-electron repulsion can be taken into account by simply adjusting the parameters in H_{SSH}. Equation (2.3-1) describes a one-dimensional electron-phonon coupled system. Illustrated in Fig 2.3-1(c) is the ground-state structure of the electron-phonon coupled chain. The uniform chain spontaneously distorts (Peierls effect) to form a dimerized structure (with a degenerate ground state) in which the springs become alternately stretched and compressed lowering the total energy of the system. Solutions of the ground state of H_{SSH} are consistent with these general ideas. An useful representation of the chain structure is through an order parameter ϕ_n defined by $\phi_n = (-1)^n(u_n/u_0)$, where u_0 is the amplitude of the displacement in the ground state[5,10,11]. The two degenerate ground states then correspond to $\phi_n = -1$ or $+1$ for all n.

For a long chain, a soliton (anti-soliton) corresponds to a phonon field configuration that approaches the $\phi_n = -1$ phase as N goes to $-\alpha$, approaches $\phi_n = +1$ phase as N goes to $+\alpha$, and minimizes the total energy, where N is the number of monomers in the chain. Illustrated in Fig. 2.3-2 is such a configuration. The width of the soliton is dictated by the competition of two effects. 1) If ϕ_n should

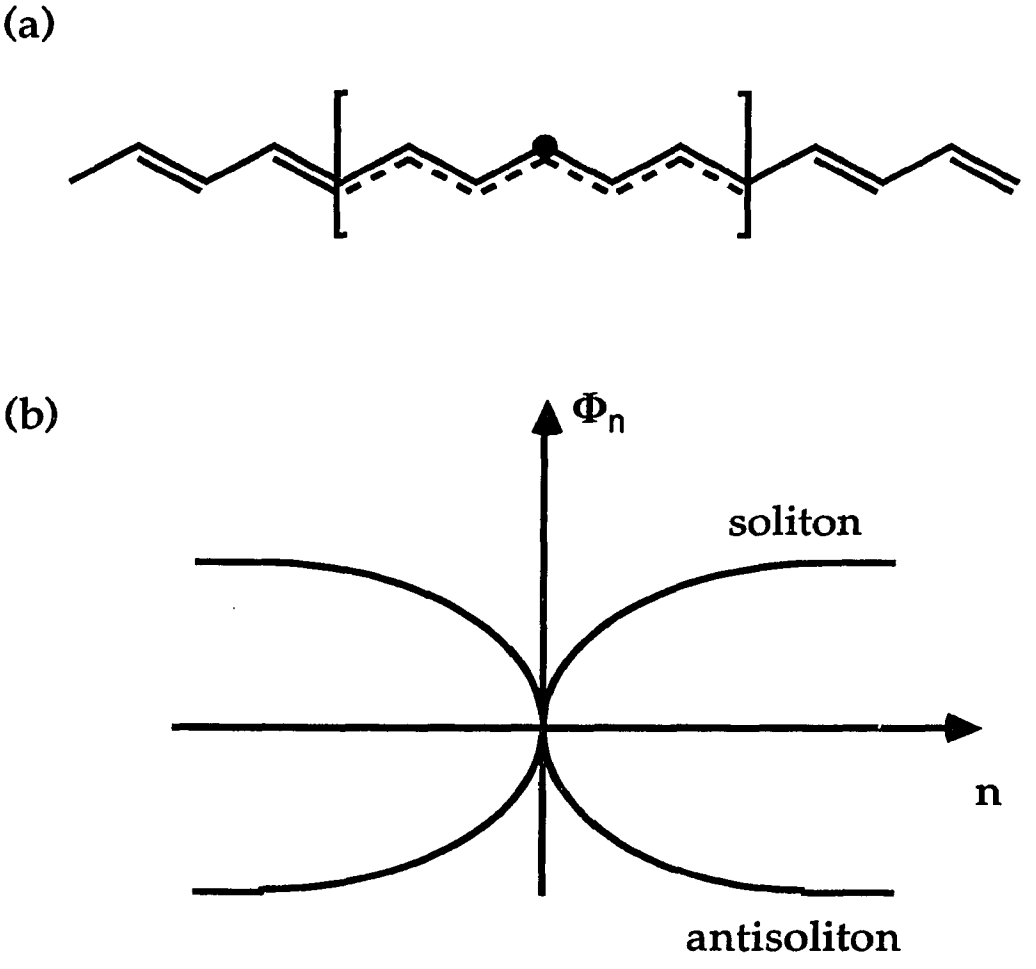

Fig. 2.3-2: Soliton or bond-alternation domain walls in (PA): a) Schematic form of a neutral soliton on a trans-(PA) chain. b) The order parameter for a soliton and antisoliton.

abruptly change from -1 to +1, for example at n = 0, the electronic energy will be very large due to the uncertainty principle. 2) If ϕ_n should change very slowly from -1 to +1, there will be a large region surrounding n = 0 where the energy per site is greatly reduced, again raising the energy. Hence there is an optimal width ξ of the soliton that minimizes the total energy. Numerical calculations[5,11] show that the form of ϕ_n that minimizes the adiabatic energy with these boundary conditions is

$$\phi_n \cong u_0 \tanh\left[(n - n_0)a/\xi\right] \qquad (2.3\text{-}3)$$

where ξ is approximately 7a for the SSH set of parameters, and n_0 is the location of the soliton center. With the above parameters (assuming an energy gap, 2Δ, is 1.4 eV.), the energy to create a soliton at rest (E_s) is approximately 0.42 eV, which is less than one half the assumed single-particle gap Δ. Since the chemical potential is midgap for the undoped material, this result shows that a soliton is less costly to create than either an electron or hole. It is for this reason that solitons spontaneously produced when electrons and/or holes are injected by doping, by thermal generation or by photoexcitation. Using the the same parameters, but interchanging the dimerization phase of the lattice, the form of ϕ_n becomes

$$\phi_n \cong - u_0 \tanh\left[na/\xi\right] \qquad (2.3\text{-}3)$$

representing an anti-soliton.

Su and Schrieffer performed a numerical integration of the SSH Hamiltonian (equ. 2.3-1) to describe the dynamical response

of the trans-(PA) chain to the injection of an electron/hole pair. Illustrated in Fig. 2.3-3 is a pictorial representation of the results of this calculation. Shown on the left is the response of the ID lattice in terms of the order parameter ϕ_n, on the right is the corresponding change in the electronic energy levels. Their simulation begins with the promotion of an electron from the highest occupied state to the lowest unoccupied one at time t = 0, as shown in Fig. 2.3-3 (a). Assume that initially the chain is in one of its degenerate ground states, for example $\phi_n = +1$. Within one vibrational period, Ω_0^{-1}, approximately 10^{-13} sec, the lattice will distort in the manner illustrated on the left in Fig 2.3-3(b). Associated with the localized distortion is a pair of electronic states which begin to split off symmetrically from the valence and conduction bands. At times, $t >> \Omega_0^{-1}$, the localized distortion develops into a pair of !D domain boundaries, or solitons, which separate the two degenerate structural ground states with $\phi_n = +1/-1$. This is shown in Fig. 2.3-3(c). In the electron energy state diagram of the chain, which now contains a soliton/anti-soliton S/$\underline{S}$ pair, there are two mid-gap states, ψ_s and $\psi_{\underline{s}}$, spatially localized at the position of the solitons. These two states combine to form a pair of states on opposite sides of the midgap, approaching it as S and $\underline{S}$ separate to distance d large compared to ξ. Each level can accommodate 0, 1, or 2 electrons due to spin degeneracy, corresponding to a net charge of +1, 0, or -1, respectively, for the soliton. As first pointed out by Ball et al.[13], the electronic state depicted in Fig. 2.3-3(c), when projected onto these site basis states, can be written as

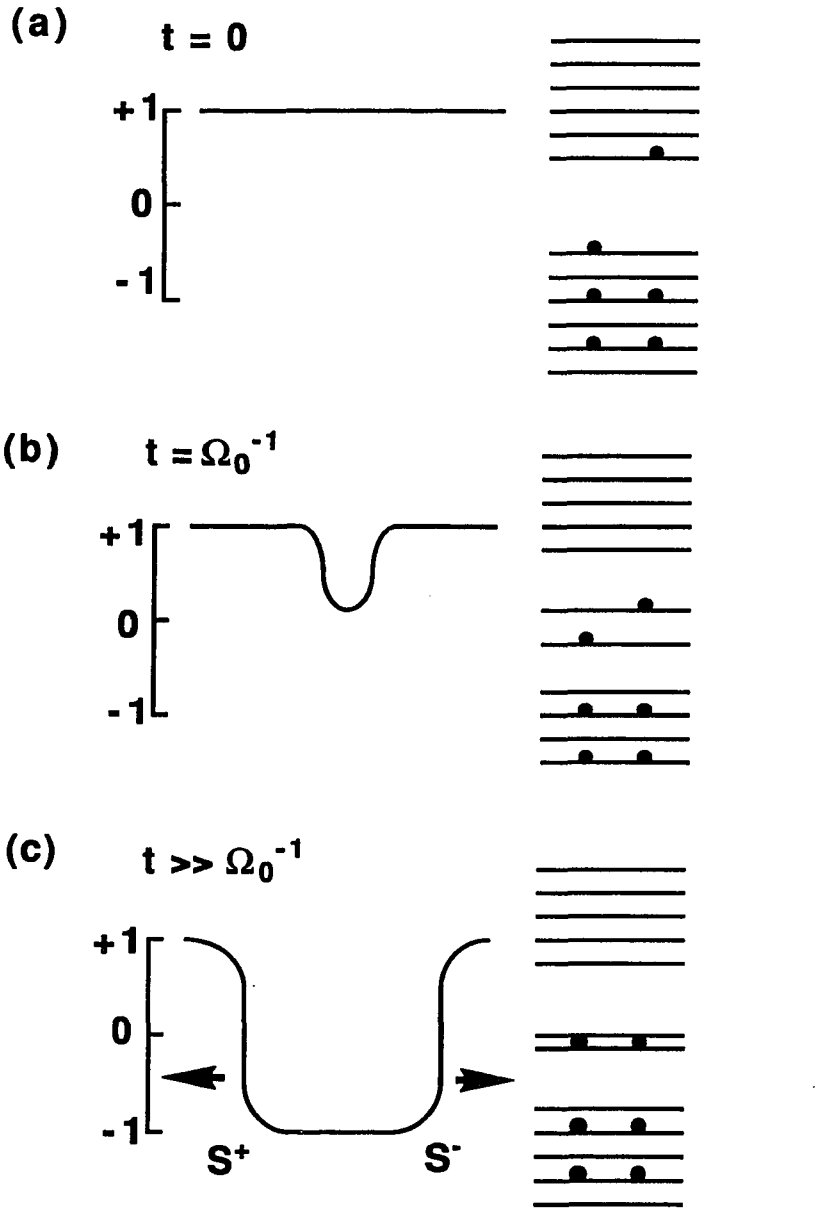

Fig. 2.3-3: Response of trans-(PA) to the creation of an electron-hole pair, showing the dynamics of soliton formation. a), b), and c) are snapshots of the system at t = 0, t = W_0^{-1}, and t >> W_0^{-1}, respectively. The left-hand side illustrates the structural relaxation of the 1-d lattice in terms of the order parameter F_n defined in the text; on the right-hand side the corresponding changes in the electronic level spectrum are sketched. (Orenstein, J.)

$$\psi(1,2,...,N) = \sum_{P}(-1)^{P}\left[\psi_{S}(1)\,\psi_{S}(2) - \psi_{\underline{S}}(1)\,\psi_{\underline{S}}(2)\right] \times \left\{\begin{matrix}\text{filled valence band} \\ \text{(N - 2 electrons)}\end{matrix}\right\} \qquad (2.3\text{-}5)$$

where P is the permutation operator and N is the total number of CH units in the chain. This wave function is a linear combination of states in which two electrons reside in the either ψ_s or $\psi_{\underline{s}}$; there is zero amplitude for one electron to be in each of the two localized states. Therefore photoexcitation, in this model, leads to the generation of a pair of spinless charged solitons, either $\underline{S}^{+}/S^{-}$ or $\underline{S}^{-}/S^{+}$. The SSH model of (PA) predicts a type of photocarrier which is entirely new to solid-state physics.

The charge spin states of the soliton are shown in Fig 2.3-4 along with the localized chemical-bond representation. The neutral spin-1/2 soliton is analogous to a neutral free radical, and the charged species $S^{-/+}$ may be viewed as spinless "ions". However the solitons move freely unless pinned, unlike the chemical analogs. An important point to note, is that the soliton has reverse spin-charge relations when compared with conventional electron hole carriers, i.e., charged solitons $S^{-/+}$ are spinless, while electrons and holes have spin 1/2. Moreover, the neutral solitons S^{0} have spin 1/2. Another important property of a soliton is its mass M_s. If the soliton is slowly translating M_s is approximately $6m_e$ for the SSH parameters, with m_e the electronic mass. The smallness of the mass arises from the width of the soliton ($2\xi >> a$) and the smallness of the

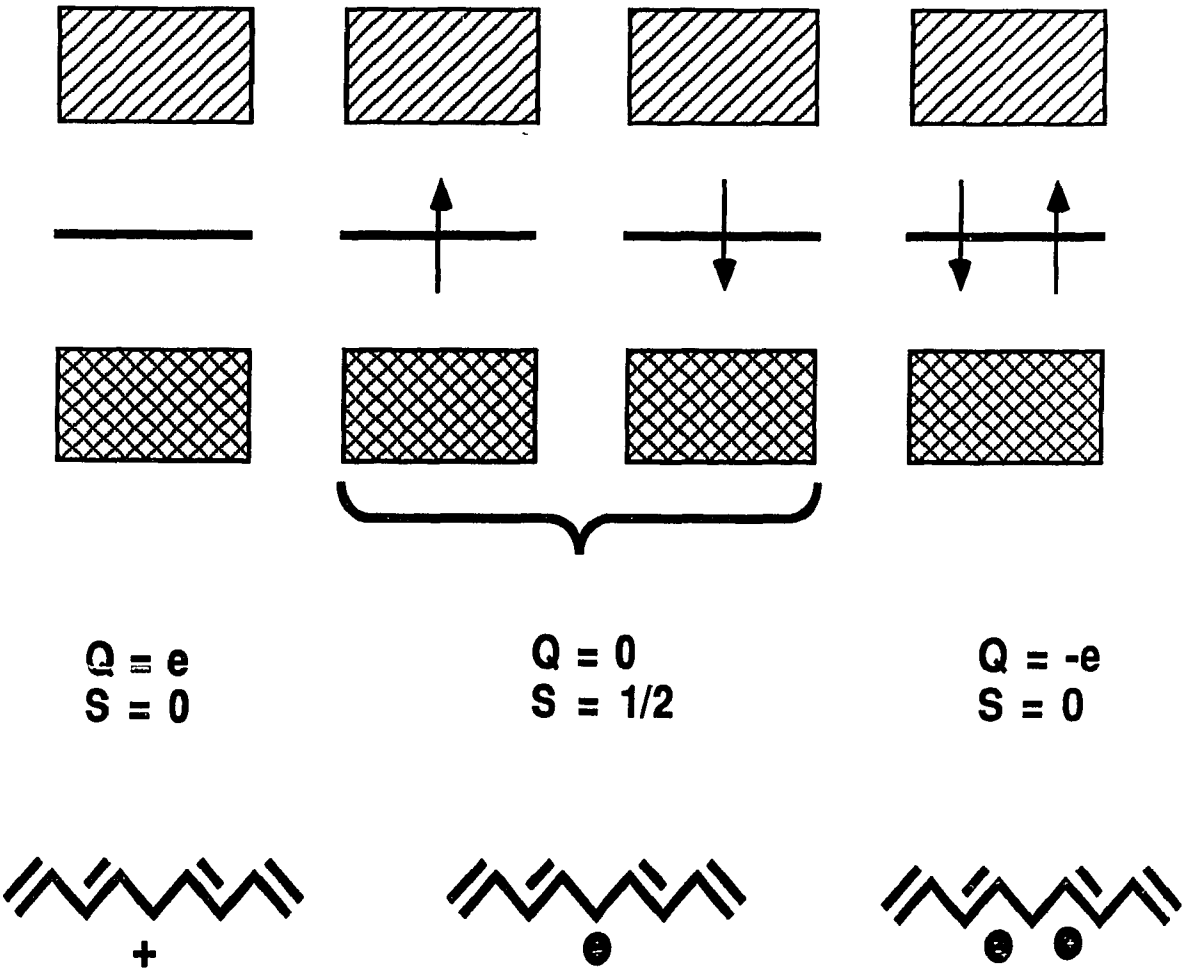

Fig. 2.3-4: The electronic structure leading to various charge and spin states of a soliton. A schematic representation of these localized structures. (Heeger et al. Rev. Mod. 60 July 1988)

nuclear displacements (u_0 compared to the lattice spacing a), so that the nuclei gain little kinetic energy as a soliton passes.

ii) Polaron Excitations

The photogeneration of solitons depends a great deal on the degenerate ground-state property of trans-(PA); however most conjugated polymers lack this property. These polymers have a lower symmetry structure than the zigzag in which the C atoms do not occupy equivalent sites. The other isomer of polyacetylene, cis-(PA), typifies this class of polymers The structures of cis- and trans-(PA) are compared in valence bond diagrams shown in Fig. 2.3-5. In the cis-(PA) structure adjacent C atoms, for example, those labeled α and β, occupy unequal sites. Looking to the left, one can see that the relative position of the third nearest neighbor is different for α and β.

Brazovskii and Kirov[14] have extended the SSH model to include the broad class of polymers typified by cis-(PA). In their theory the effect of the lower-symmetry backbone is impose by an external potential, Δ_{ext}, which has spatial wavelength 2a. The external potential acts together with the Peierls instability to determine the amplitude of dimerization in cis-(PA). Most importantly, the presence of Δ_{ext} lifts the degeneracy between the ϕ_n = +/- 1 structures, as illustrated in Fig. 2.3-5. Changing the phase of the bond alternation pattern by 180^0 now requires a large energy, of tenths of an electron-volt per monomer unit[15].

The photoexcited state predicted for cis-(PA) by Brazovskii and Kirova can be understood by again referring to Fig.

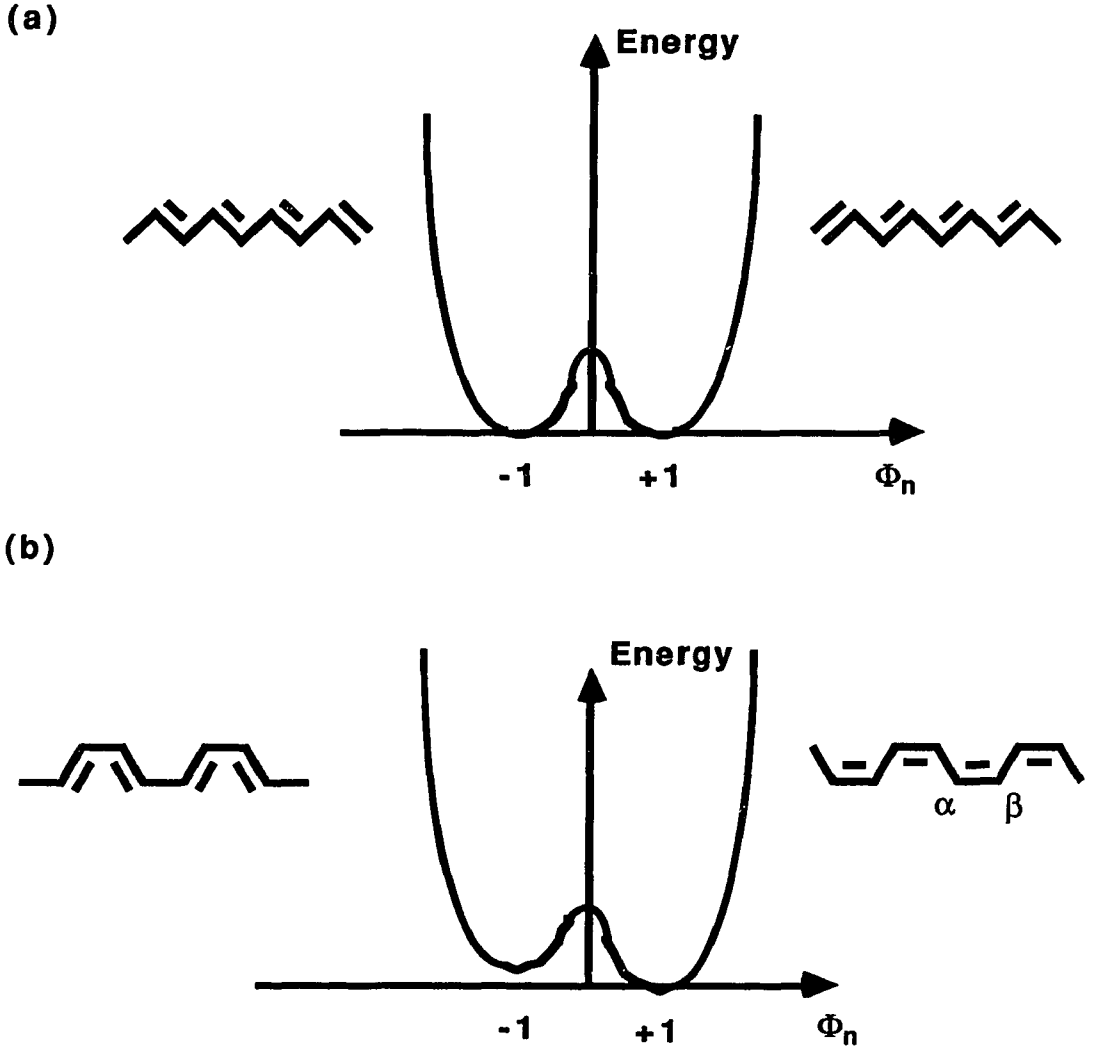

Fig. 2.3-5: The structures of trans- and cis-(PA) compared in conventional valence bond diagrams. Also shown is a sketch of the total energy of the electron-phonon coupled system as a funtion of Φ_n. a) The zigzag trans structure, in which all sites are equivalent, has a two-fold degenerate ground state. b) In cis-(PA) nearest neighbors, for example, a and b differ in the relative position of their third nearest neighbors. This lifts the degeneracy of the Φ_n = +/-1 structures. (Orenstein, J.

2.3-3. Just as for trans-(PA), a localized lattice deformation occurs within approximately Ω_0^{-1} following the creation of an electron-hole pair. However, in chains with a nondegenerate ground state the S-S pair cannot separate because of the energy required to extend a segment with the wrong structure, $\phi_n = -1$, between them. Instead, the pair reaches an equilibrium separation with a final lattice deformation and electronic level spectrum as in Fig 2.3-3(b). The equilibrium separation of the S-S pair is determined by the energy difference between the $\phi_n = +1$ and -1 structures. For example, a large difference would lead to a strong confinement of the S-S pair, a small amplitude deformation of the lattice, and energy levels which are only slightly displaced from the band edges.

The prediction of this model is that photogeneration of charge carriers on a single chain is absolutely unique to degenerate ground-state structures like trans-(PA). For all other conjugated polymer systems the photogenerated charges are bound in an overall neutral excited state. It is important to note that the binding is not due to coulombic forces as in conventional exciton pictures, but instead, results from the effects of electron-phonon coupling in one dimension.

Up this point we have only discussed the ideal case of the photoexcitation of a single isolated chain of (PA). Real (PA) polymers do not consist of isolated chains. Rather, they consist of chains packed in a crystalline array in which the distance between neighbors is approximately 4.25 angstroms. Excitation of this crystal with photons of sufficient energy can transfer electrons between chains. To describe the final state of the system we have to consider

the response of a neutral (PA) chain to the addition not of an electron/hole pair, but instead to a single electron or hole.

It was observed in early molecular dynamics studies by Su and Schrieffer [10] that the injection of a single electron or a single hole leads to the formation of a polaron. This nontopological excitation corresponds to the order parameter $\phi_p(x)$ with a dip at its center but not changing sign (in contrast with the order parameter $\phi_s(x)$ of a kink or soliton), as shown in Fig.2.3-6. Thus one has the symmetries

$$\phi_p(-[x - x_0]) = \phi_p(x - x_0), \qquad (2.3\text{-}6a)$$

$$\phi_s(-[x - x_0) = -\phi_s(x - x_0). \qquad (2.3\text{-}6b)$$

Polarons are well known in polar insulators and in semiconducting materials, acting as quasi-particles arising from phonon dressing of an electron or a hole.

Independent of the molecular dynamics studies of Su and Schrieffer [10], polaron solutions by Brazovskii and Kirova [14] in 1981 and Campbell and Bishop [16, 17] in 1981 and 1982 were discovered using the relation of the mean-field approximation to the continuum model and the Gross-Neveu model [18] of quantum field theory. In the continuum limit, the order parameter $\phi_p(x)$ describing the polaron centered at the origin is given by

$$\phi_p(x) = u_0 + (u_0/\,2^{1/2})\{\tanh[(x - x_0)/\sqrt{2}\xi] - \tanh[(x + x_0)/\sqrt{2}\xi]\} \qquad (2.3\text{-}7)$$

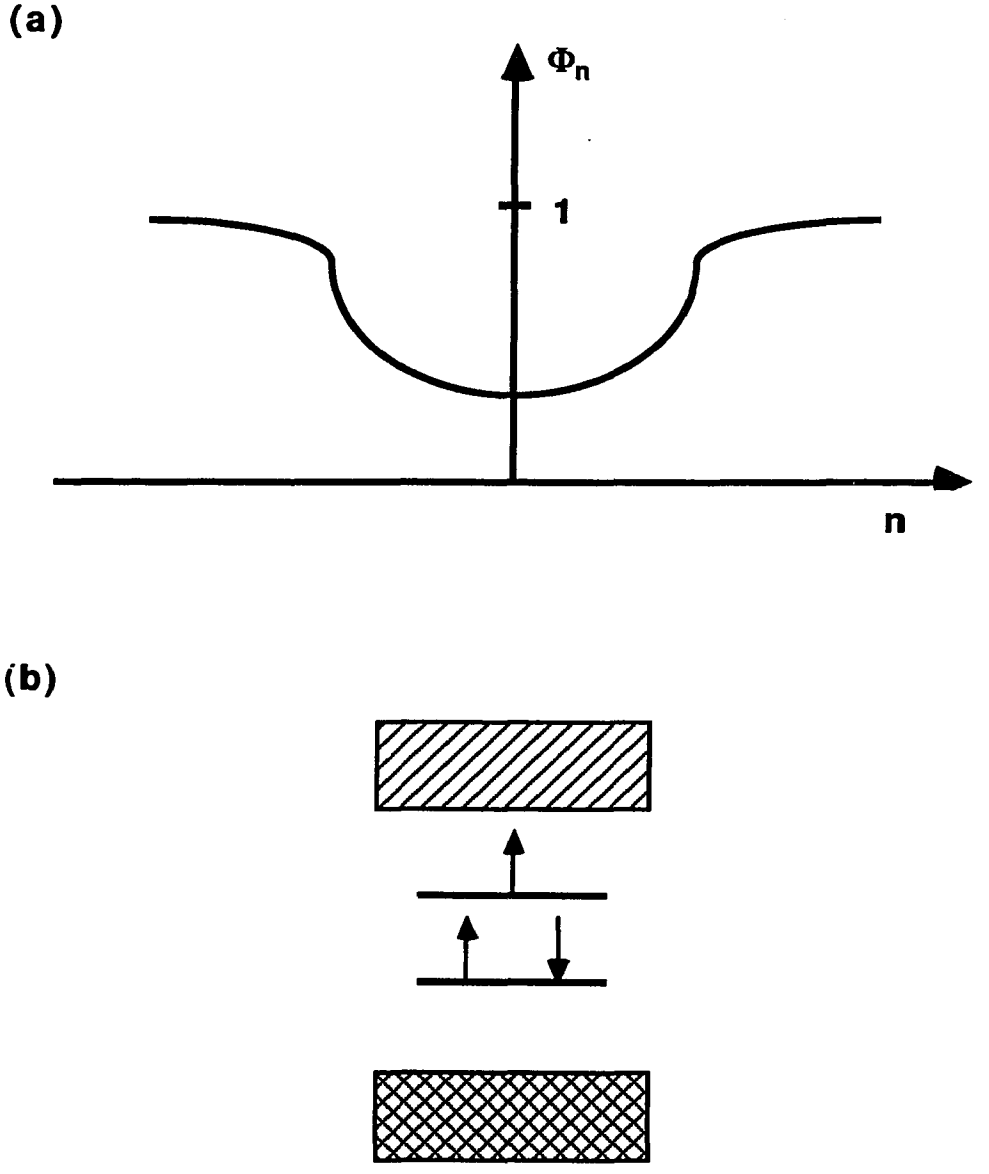

Fig. 2.3-6: Order parameter and band diagram for a polaron: a) the staggered order parameter Φ_n as afunction of n for a polaron; b) two states symmetrically split off from the band edges for a polaron. An electron is missing from the upper state for an electron polaron, and only a single electron occupies the lower state for a hole polaron. (Orenstein, J.)

where $x_0 = (\xi/2^{1/2})\ln(1 + 2^{1/2})$ which equals approx. 0.623ξ. Since a soliton located at y_0 is described by

$$\phi_s(x) = u_0 \tanh\left[(x - y_0)/\xi\right] \qquad (2.3\text{-}8)$$

one can roughly describe the electron or hole polaron as a bound soliton-antisoliton pair (one charged and one neutral) with centers separated by $2x_0 = \xi$. The factor $2^{-1/2}$ in Eq. (2.3-8) implies that, due to the interaction between two solitons, their width is somewhat greater than at infinite separation.

The Su and Schrieffer calculation is illustrated in Fig. 2.3-7. At time t = 0 a single electron is added to a neutral trans-(PA) chain. In response, the lattice distorts by locally diminishing the difference between single and double bond lengths, as in Fig. 2.3-3. Notice that in Fig. 2.3-7b the occupancy of the localized levels is different than in Fig 2.3-3b; the level which splits off from the valence band is now doubly occupied. It is clear that a structural distortion which proceeds further towards a S^+-$\underline{S}^0$ pair well raise the total energy. As the incipient S^+-$\underline{S}^0$ pair separates and the levels move toward mid-gap, two electrons are raised in energy, while only one is lowered. Instead of a separated S^+-$\underline{S}^0$ pair, the lowest energy state is the bound-pair configuration shown in Fig. 2.3-7c.

While the soliton has a single bound state associated with it, the polaron has two bound states split off from the continuum. Each of these states can accommodate one electron of each spin orientation. Starting from the charge-neutral case in which

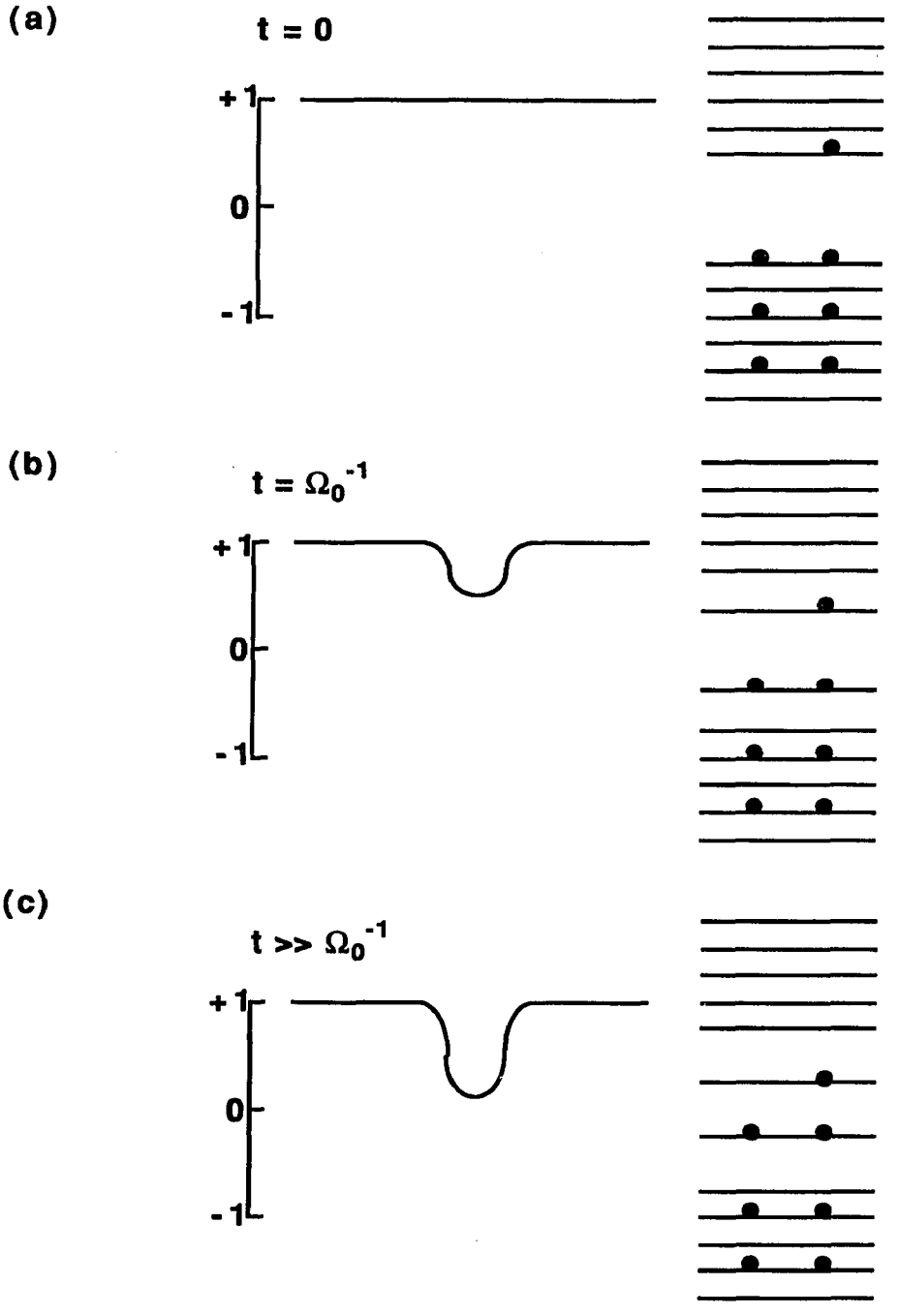

Fig. 2.3-7: Response of trans-(PA) in its ground state to the addition of an electron, illustrating the dynamics of polaron formation. In contrast to soliton formation, polarons are expected in systems with a nondegenerate ground state. (Orenstein, J.)

the lower state is filled, $n_- = 2$, and the upper state is empty, $n_+ = 0$, the conventional polarons are as follows:

electron polaron	$n_- = 2$,	$n_+ = 1$
hole polaron	$n_- = 1$	$n_+ = 0$

The spin of the charge-neutral case is zero, since all states, both continuum and localized, are doubly filled. Therefore the electron and hole polarons each carry spin 1/2, and the spin-charge relation is the conventional one.

The total energy calculations show that only the electron and hole polarons are stable. If one adds, for example, a second electron to an electron polaron, the resulting "bipolaron" lowers its energy by increasing the soliton-antisoliton spacing $2x_0$ until a free kink-antikink pair evolves at large separation. Thus, on doping, the first injected electron forms a polaron; the second injected electron breaks apart the polaron to form two negatively charged kinks. Note, however that when the precise ground-state degeneracy of the polymer is lifted (as in cis-(PA)), the resulting confinement of the solitons leads to stable bipolarons.

2.4) Fabrication and Isomerization

Polyacetylene was first produced in powder form by Natta et al.[19]. Subsequently free-standing films of PA were obtained by Ito, Shirakawa and Ikeda[20]. Electron microscopy studies[21] of

Shirakawa PA, show that the as-grown film consist of randomly oriented fibrils, of varying diameters depending on the polymerization condition. The films can be stretch oriented in excess of three times their original length, with concurrent partial alignment of the fibrils[22 23]. Stretched Shirakawa films displayed a low anisotropy when observed by x-ray diffraction[24].

The highly oriented trans-polyacetylene (HOPA) films used in this study were prepared (by Assoreni and Research Lab., Italy) using the Ziegler-Natta polymerization procedure and a Ti-base catalyst[25]. The as-synthesized cis- rich (sample having 85% cis units) film shows a metallic grey-greenish luster and exhibits a fibrillar morphology. Its overall density (ca. 0.9 g/cm^3) is higher than that of PA prepared according to the Shirakawa method. The films were stretched up to 7-8 times their original length. After drawing the material is characterized by a relatively large density (1.0-1.1 g/cm^3) approaching that of the theoretical[26] crystallographic (1.15 g/cm^3), and were 10-40 μm thick with a metallic lustre darker than the unstretched film.

The HOPA is then thermally isomerized from the cis-rich form to the all-trans configuration. This was accomplished by clamping the film between two micro slides and placing this unit inside a glass tube (refer to Fig.2.4-1) containing a nitrogen

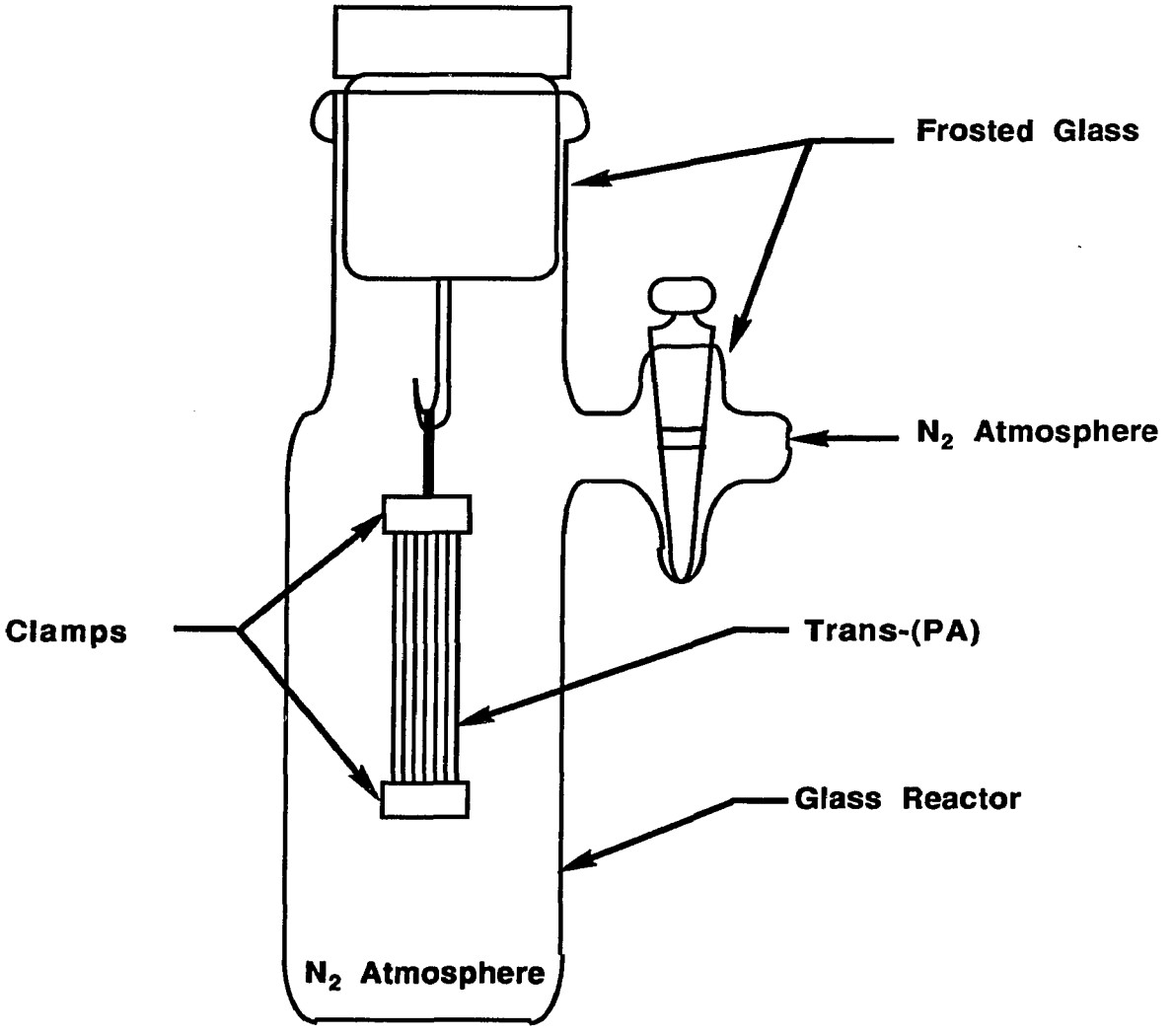

Fig. 2.4-1: Glass reactor used to thermally isomerize the HOPA from the cis- rich form to the all trans- configuration.

atmosphere. The sample was removed from its original ampule and placed inside the glass tube in a dry-box also containing a nitrogen atmosphere to avoid exposure to oxygen. The glass tube was then placed in a bath of cutting oil and heated to 200° C for 6-8 minutes. Ridges were formed along the length of the film as the isomerization process took place. X-ray diffraction patterns of similarly prepared samples have shown a very high degree of preferred orientation of the crystallites with the chain axis parallel to the stretching direction[27]. The orientation of the sample is slightly improved during the isomerization process, with an average misalignment angle of $\phi=5°$, as determined from the X-ray azimuthal profile. Similar to the Shirakawa-type films, both HOPA and the corresponding as-grown film are almost completely crystalline polymers independent of the cis-trans content. Shown in Fig. 2.4-2 is a scanning electron microscope picture of PA in each of its three forms; as grown, cis-rich and trans-rich.

Durham polyacetylene, a synthesis developed at Durham University [28, 29] uses a soluble prepolymer that is converted to polyacetylene as a final stage. The Durham polyacetylene can be stretched oriented simultaneously with isomerization into crystalline highly anisotropic free-standing films [30, 31]. Durham polyacetylene does not possess the fibrillar morphology and visible microstructure (by electron microscopy) of Shirakawa PA or the HOPA used in this study.

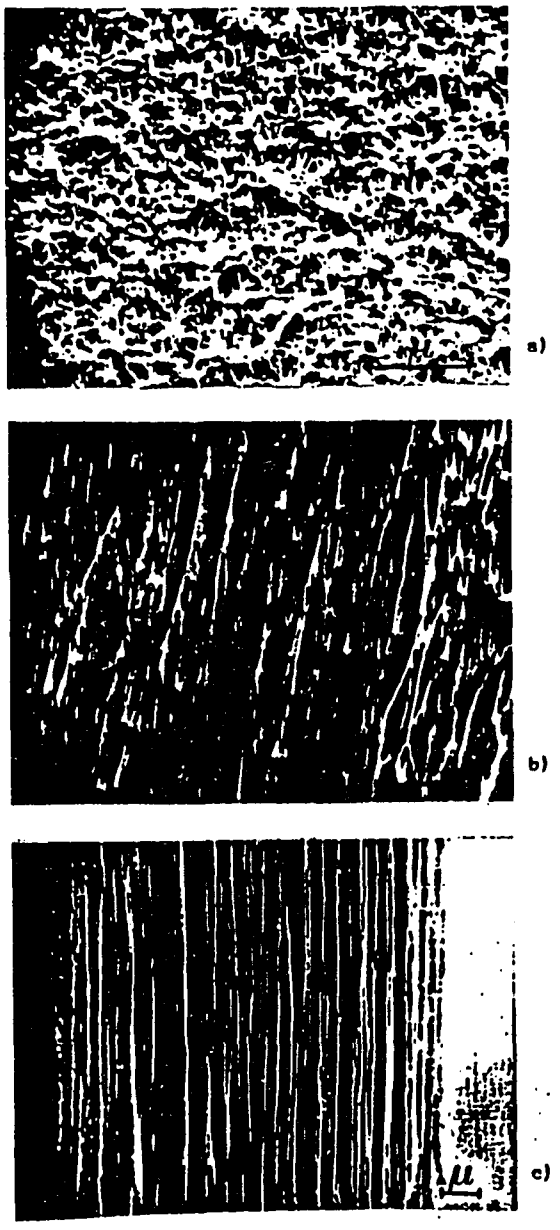

2.4-2: Scanning electron picture of (a) as-grown PA, (b) surface of cis-rich HOPA (α=6.5), (c) HOPA (α=7) isomerization at 200° C over 5 min, longitudinal section (from Lugli et al. J. Polym. Sci. Polym. Ed., 23, 129 (1985))

2.5) Previous Experimental Observations

Numerous experiments have been devised and performed in an effort to test the theoretical models of PA. In this section we will discuss several of them and their results.

i) Neutral Solitons

Imperfections in the polymer chains of polyacetylene produce neutral solitons. As polyacetylene transform from the cis- to the trans- configuration during the isomerization process neutral solitons are formed. The unpaired spin present in these defects makes possible the use of magnetic resonance studies, which enable the determination of important properties such as, the magnetic susceptibility and its temperature dependence, the spatial extent of the wave function and the motion and dynamics of the neutral soliton defects.

Initially these unpaired spins (spin-1/2) were characterized as extended π-electron defects, approximately one per 3000 carbon atoms in trans-(PA) chain [32, 33]. The magnetic susceptibility followed Curie's law (s 1/T) which is indicative of localized spins and the line width was narrow implying motion.

To determine whether or not the spin 1/2 species are charged or neutral, trans-(PA) was doped. After compensation with ammonia, the electrical conductivity decreased by orders of magnitude, implying a corresponding decrease in charge carriers or in their

mobility, but the number of spins did not change [33]. The narrow linewidth (implying a mobile species) both before and after compensation ruled out the possibility of trapping thus indicating that the spin is associated with a neutral carrier. Furthermore, the infrared-active vibrational modes that are characteristic of charged configurations [34, 35, 36] are not observed in carefully prepared pristine samples. These experiments demonstrate that the spin-1/2 defects found in trans-(PA) are neutral, consistent with the reversed spin-charge relations predicted by the SSH model.

With the goal of determining in detail the wave function of the spin-1/2 species, electron-nuclear double resonance (ENDOR) studies were done [37, 38, 39,40, 41, 42]. The delocalized spin distribution was directly observed from the distribution of ENDOR frequencies. The ENDOR line shape was found to be consistent with the spin-density profile predicted by the soliton theory (SSH model) when supplemented to include a finite on-site Coulomb interaction [43, 44]. The width of the neutral solitons (ξ approximately 8-11a) found in the ENDOR experiments is in reasonable agreement with the value predicted theoretically (approximately 7a) by the SSH model and inferred from electron-spin resonance linewidth measurements mention above.

The confirmation of the mobile neutral soliton first inferred from motional narrowed ESR linewidth, came from a series of nuclear-spin relaxation measurements, interpreted in terms of one-dimensional motion of the neutral solitons [45, 46].

Definitive evidence of the mobility of neutral solitons was provide by dynamic nuclear polarization (DNP) studies [47, 48, 49, 50],

placing a lower limit on the time necessary for the bond-alternation domain wall to diffuse a distance equal to its width. DNP has been used as a microscopic probe of soliton motion: if the solitons are fixed (trapped) or moving very slowly, the DNP occurs via the solid state effect, whereas, if the mobility is high, DNP occurs via the Overhauser effect [47]. DNP studies of Trans-(PA) showed that the neutral soliton are trapped at low temperatures, and are very mobile at high temperatures, and that there is a gradual conversion from trapped to mobile bond-alternation domain walls over a temperature range $10\ K < T > 100\ K$.

Finally, by comparing not only the ESR linewidth but all aspects of the magnetic resonance, it was concluded that the spin dynamics are determine by a combination of one-dimensional diffusion fo the solitons and soliton-soliton spin exchange.

ii) Charged Solitons

As mentioned earlier, solitons can be generated in two ways: charge transfer doping and photoexcitation. There are three distinctive signatures of charged solitons for which there exist both theoretical analysis and experimental evidence:

1) The formation of localized structural distortions with associated localized vibrational modes (localized phonons). These soliton induced characteristic infrared active vibrational modes (IRAV modes) can be observed in the mid infrared frequency range, which is typical for molecular vibrations.

2) The generation of the midgap state and the associated electronic transitions. This soliton induced transition can be observed in the near infrared range.

3) The reverse spin charge relations, i.e., charge storage in spinless solitons. This can be verified through electron spin resonance experiments. The key signature is that the ratio $N_S/N_{ch} << 1$, where N_S is the number of spins and N_{ch} is the number of charges.

Below we will briefly discuss several of the important experiments performed and presented as evidence for the existence of charge solitons induced by doping and photoexcitation.

A. Solitons induced by doping

1. infrared active vibrational modes

Doping induced IRAV modes were discovered in the first infrared studies of polyacetylene at dilute doping concentrations [34] [51, 36]. The principal doping induced IRAV modes are approximately at frequencies 900, 1260, and 1370 cm^{-1}, with a weaker mode at 1215 cm^{-1}. These doping induced absorptions are intense and isotope sensitive [36, 52]. The doping induced IRAV modes for trans-$(CH)_x$ and trans-$(CD)_x$ are shown in Fig. 2.5-1.

The intensity of the observed modes are proportional to the dopant concentration[53, 35, 36] but are essentially independent of the dopant type. The absorption is parallel to the polymer backbone, as verified

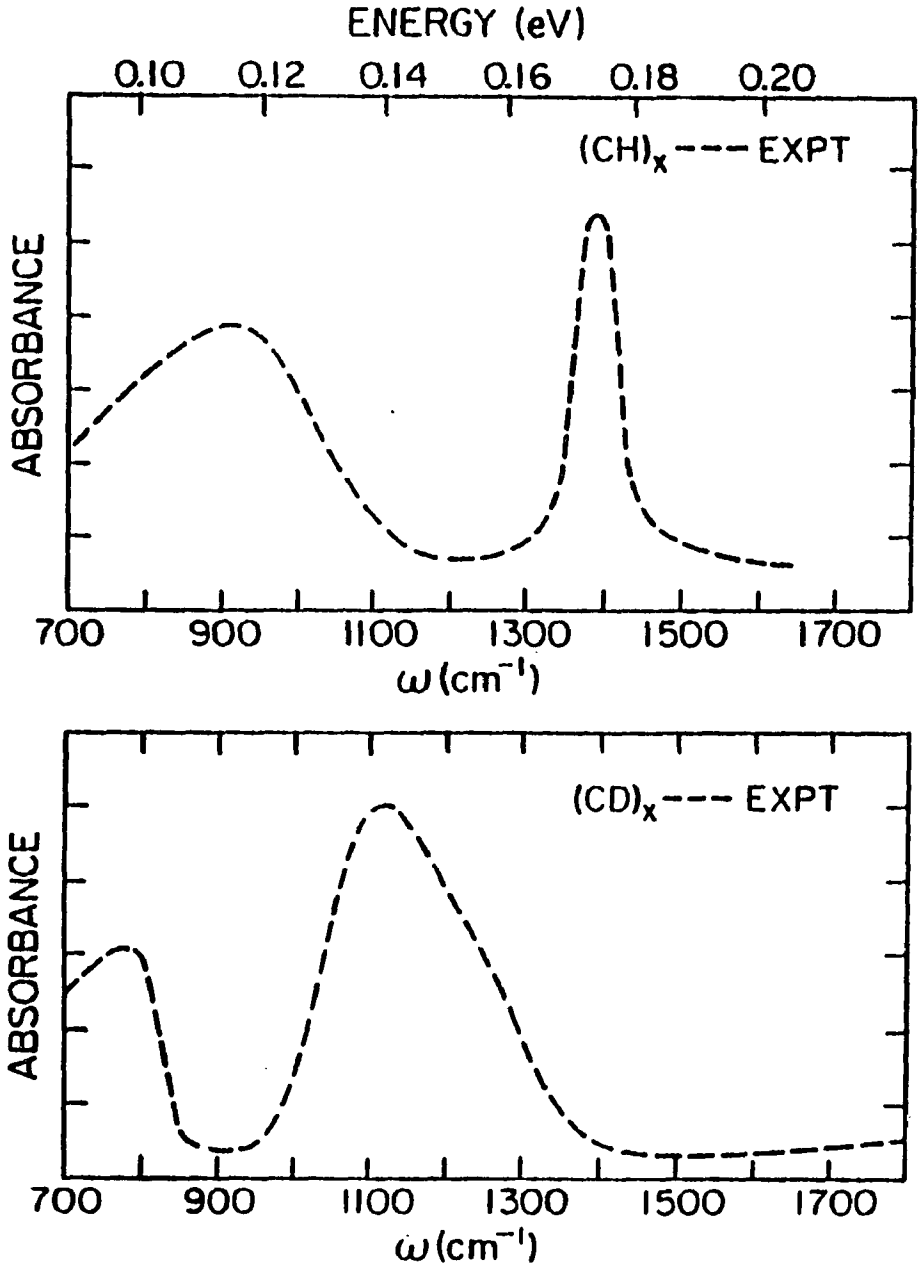

Fig. 2.5-1 : Doping-induced infrared-active vibrational modes for trans-(PA) : a) trans-(CH)x; b) trans-(CD)x. (from Etemad, et al. 1981)

by experiments on highly oriented samples [34 54 55]. Thus the doping induced ir modes are characteristic of the doped polyacetylene chains. They demonstrate that charged particles with associated distortions are generated upon doping. As predicted there is one localized phonon for each of the phonon branches of trans-(PA) (as observed through Raman scattering). The broad and intense absorption at 900 cm^{-1} is presumably the Goldstone mode (the zero frequency phonon mode), shifted up from zero frequency by pinning due to Coulomb binding of the charged soliton to the oppositely charged ion. The assignment of the 900 cm^{-1} as the pinned Goldstone mode is consistent with the observation that this mode appears at approximately 500 cm^{-1} in photoexcitation measurements; weaker pinning would be expected for photoexcitation, since the Coulomb field of the counter ion is absent.

2. Absorption of midgap states

The absorption of midgap states is a typical characteristic of doped polyacetylene[56 57 58]. Dopant induced near ir electronic transitions are observed to be independent of the type of dopant and of whether that dopant is a donor (n-type doping) or an acceptor (p-type doping). Illustrated in Fig. 2.5-2 is the results of in situ experiments, performed during electrochemical doping, on the visible-ir absorption in trans-(PA). As doping proceeds, the midgap absorption appears, centered near 0.65-0.75 eV. with an intensity

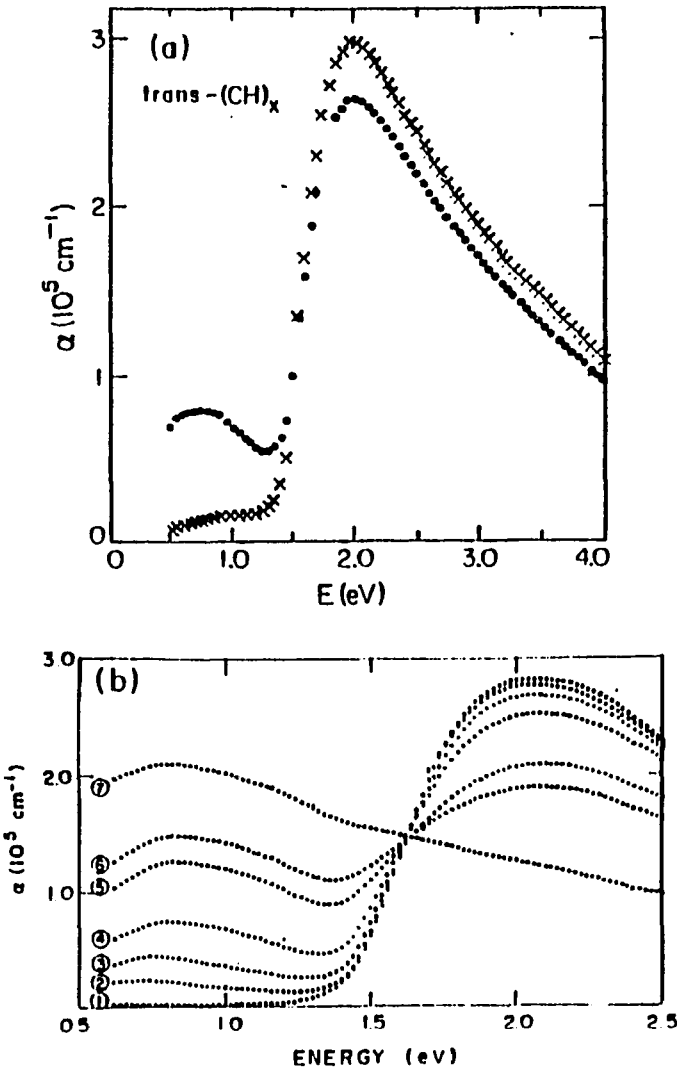

Fig. 2.5-2. Absorption spectra for neutral and doped trans-(PA). a) Absorption coefficient of trans-(PA): x, before doping; •, after doping with a fraction of a percent by exposure to AsF_5 vapor (from Suzuki et al. 1980). b) In situ absorption with (ClO_4)-. The applied cell voltages and corresponding concentra- tions are as follows: 1] 2.2 V (y=0); 2] 3.28 V (y=0.003); 3] 3.37 V (y=0.0065); 4] 3.46 V (y=0.012); 5] 3.57 V (y=0.027); 6] 3.64 V (y=0.047) 7] 3.73 V (y=0.078). (From Feldblum et al., 1982)

that increases monotonically in proportion with the dopant concentration. Simultaneously, the strength of the interband transition decreases preserving the overall oscillator strength. From the intensity of the dopant induced absorption and the magnitude of the associated bleaching of the interband transition, the width of the self-localized charged particle (ξ) can be inferred to be approximately 7a, in good agreement with theory.

3 Reversed Spin-charge relations

Initially spin resonance experiments (performed to detect spinless carriers) were carried out on p-type samples that used a vapor-phase doping technic. However, the interpretation of the results of these experiments lead to controversy[59 60], owing to the possibility of nonuniform doping, the use of thick films and the complex chemistry of AsF_5 doping. To circumvent such problems, subsequent work utilized in situ ESR measurements on thin films (thickness of order1 μm or less), performed during either chemical [58] or electrochemical doping[61 62]. With the electrochemical technique, the electrochemical potential and not the dopant concentration is the controlled variable, and the thin-film doped samples are at equilibrium. Experiments with both n-type $[Na^{+}_{y}\ (CH)^{-y}]_x$ [61, 62] and p-type $[(CH)^{+y}(CLO_4^{-})_y]$ [63] doping have been performed to investigate the presence of spinless charge carriers in polyacetylene. These measurements clearly demonstrated the spinless character of the doping induced charge carriers at dilute concentrations and, established the reverse spin-charge relation for solitons in trans-(PA).

B Optical properties of polyacetylene

The band structure of polyacetylene has been investigated by a combination of optical-absorption and reflection measurements in the frequency range from the middle ir (0.1 eV) through the visible (4.0 eV)[64].

This study provides a more complete understanding of the electronic structure of polyacetylene. The samples were prepared using the standard Shirakawa technic. Visible absorption measurements utilized thin films (0.1 μm) polymerized on the inner surface of a glass reactor. The reflection measurements were carried out on free standing films (typically 0.05-0.1 μm). Orientation was achieved by stretching as mentioned above.

Illustrated in Fig. 2.5-3 is the absorption data for undoped trans-polyacetylene. The absorption coefficient begins a slow increase around 1.0 eV rising sharply at 1.4 eV. to a peak at approximately 1.9 eV. The magnitude of the absorption coefficient ($3x10^{-5}$ cm^{-1}) at the peak is comparable with the peak value of a typical direct gap semiconductor. Shown in Fig. 2.5-4 is the polarized reflectance data from oriented films (l/l_o approximately 2.5 -3) of stretched trans-(PA), where l_o

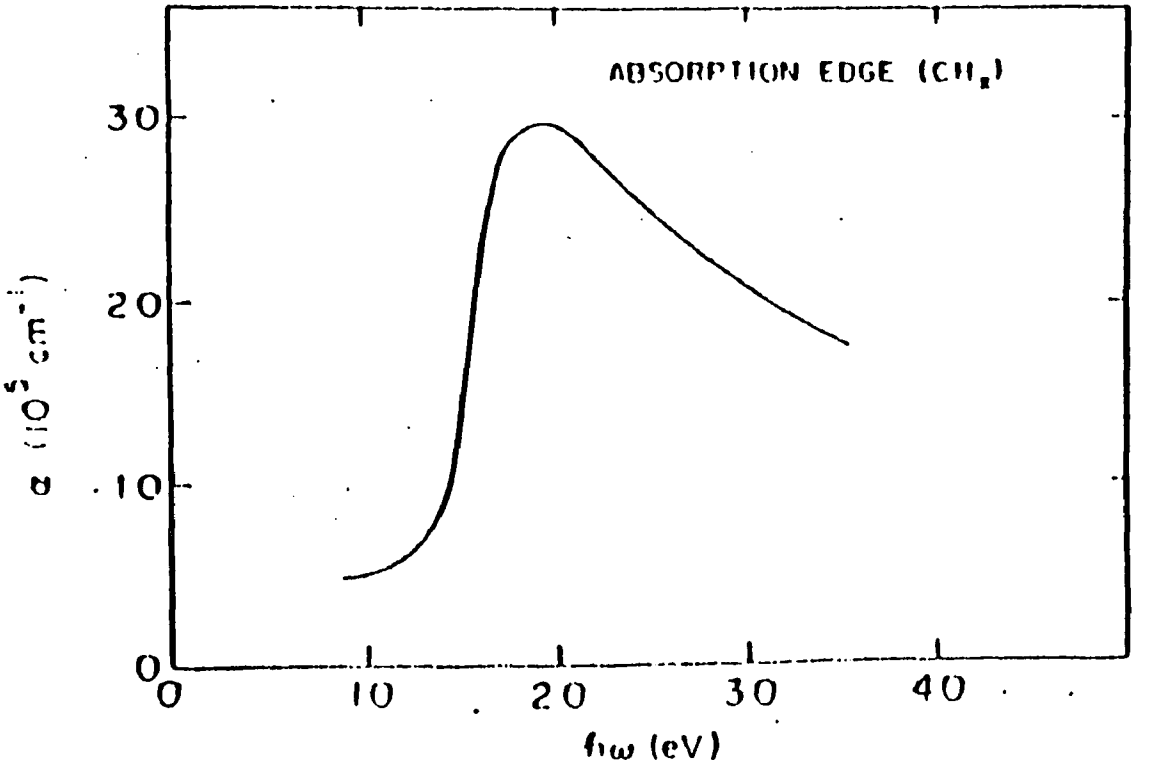

Fig. 2.5-3: Absorption coefficient as a function of frequency for unoriented Trans-(PA). (from Fincher et al. Phys. Rev. B 20, 1589 (1979))

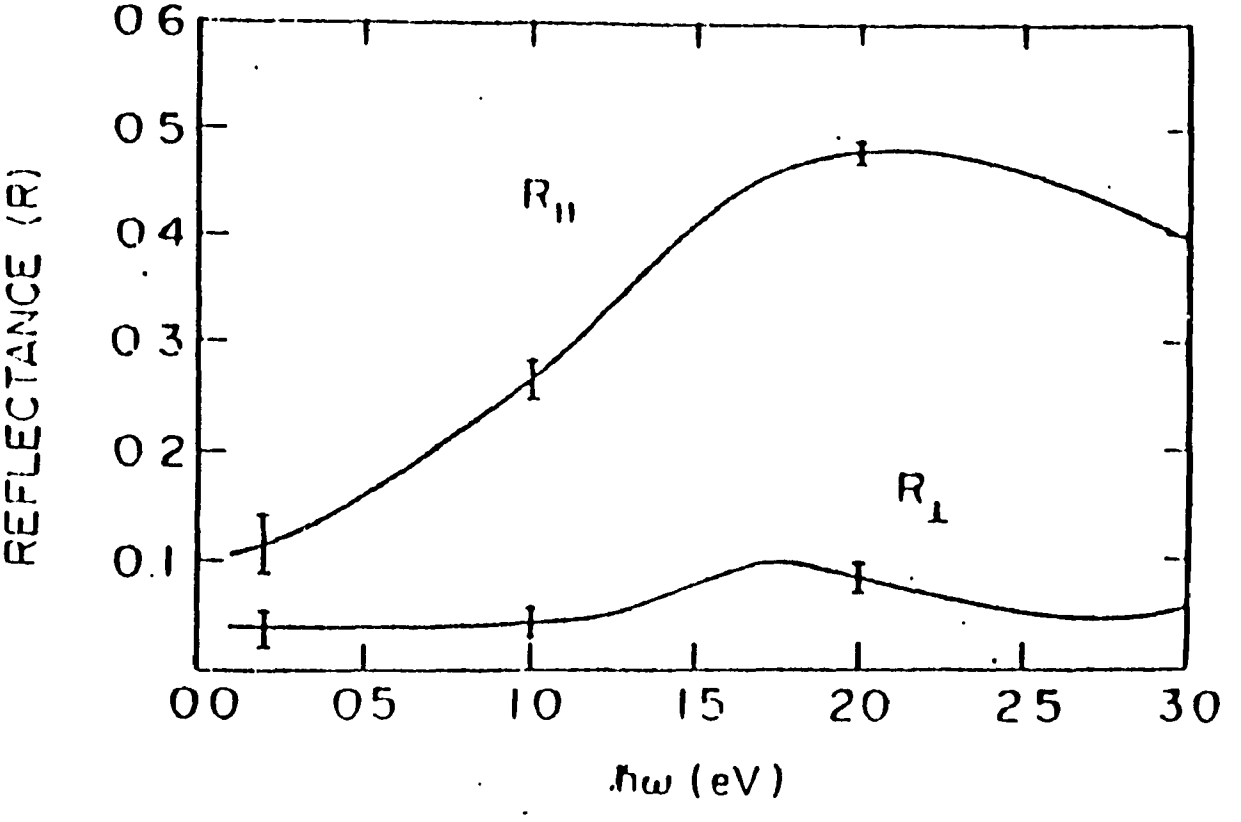

Fig. 2.5-4: Polarized reflectance as a function of frequency from partially oriented (CH)x. $R_{||}$ and $R_{\perp}$ refer to light polarization parallel and perpendicular to the orientation direction. (from Fincher et al. Phys. Rev. B 20, 1589 (1979)

and l are the unstretched and stretched lengths, respectively. The large optical anisotropy induced by orientation is evident. The interband transition apparent in the parallel reflectance (R) in the region of 2 eV with the reflectance decreasing to a low frequency value of approximately 0.1. The perpendicular reflectance is small throughout the measured range characteristic of quasi-one-dimensional behavior and relatively weak interchain coupling.

The optical absorption measurements for oriented polyacetylene prepared under grapho-epitaxial[65] and shear flow[66] polymerization conditions are illustrated in Fig. 2.5-5 and 2.5-6 respectively[67]. The former shows a pronounce optical anisotropy whereas the latter does not. This result is correlated with the orientation of the chain axis relative to the fibre axis, which is preferentially parallel in grapho-epitaxially grown films. The absorption coefficients in the infrared and visible spectrum were determine from transmission spectra and a reflectivity which was assumed to be wavelength independent and calculated from the known long wavelength index of refraction. The sample thickness (500 A to 2000 A) was determine by a scanning electron microscope.

The method of fabrication used to synthesize polyacetylene strongly influences its band structure and optical properties.

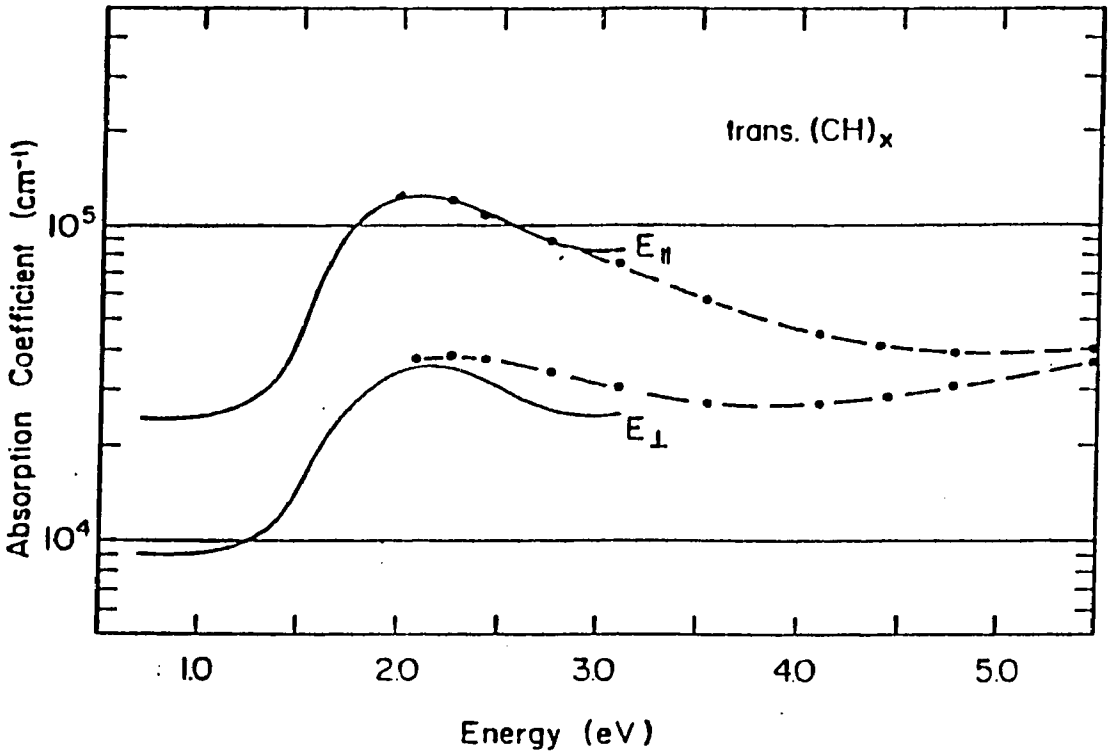

Fig. 2.5-5: Absorption coefficient as a function of energy for light parallel and perpendicular to the fibre axis. (from Kiess et al. Mol, Crst. Lig. Cryst. 77, 147 (1981)

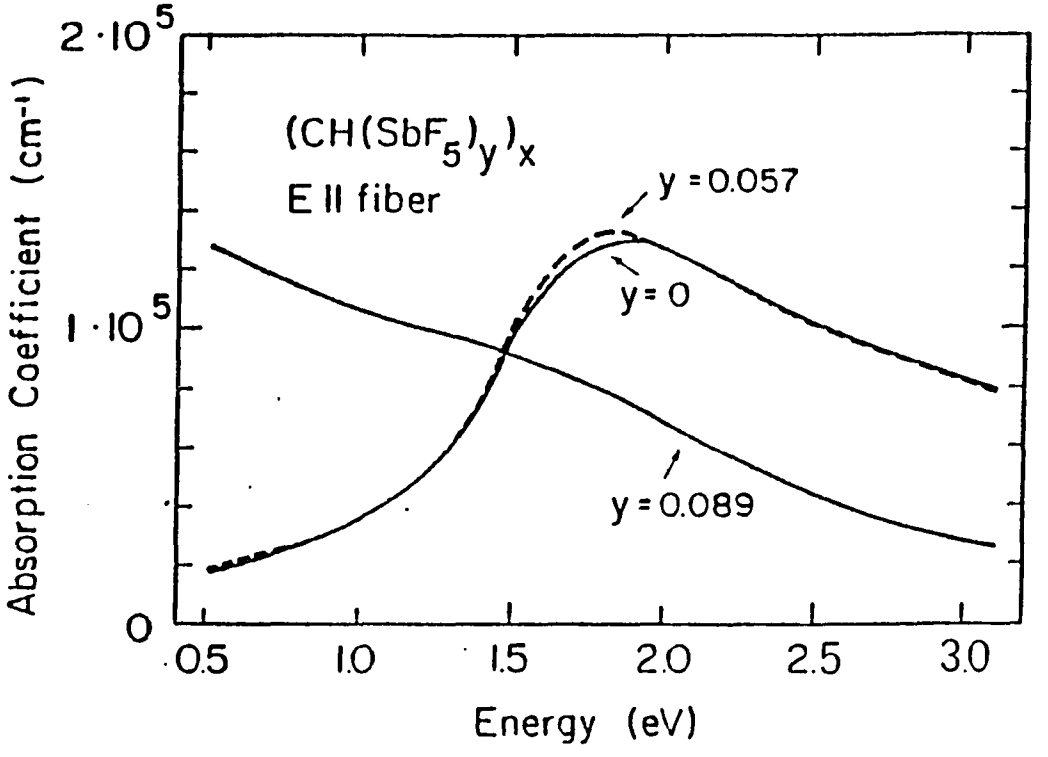

Fig. 2.5-6: Absorption coefficient of a shear-flow polymerized film for various doping levels. (from Kiess et al. Mol, Crst. Lig. Cryst. 77, 147 (1981)

C Raman Spectroscopy

Raman spectroscopy has been used extensively to study the vibrational modes and structure of polyacetylene. The expected zone center modes have been observed at frequencies that are in agreement with the calculated values[68, 69, 70, 38, 71, 72, 73, 74].

The Raman spectra of conductive polyacetylene-iodine complexes and their parent polymers have been studied[75]. The high electrical conductivity of iodine doped polyacetylene provoked such a study. Structural information on these materials is needed to understand the mechanism of such high conductivities. The trans-rich polyacetylene film contains trans segments of various lengths while the cis-rich polyacetylene film is composed of relatively long cis sequences making it difficult to obtain a clear-cut conclusion concerning their structure. It is because of this mixture of components in polyacetylene, that Resonance Raman spectroscopy is suited to problems of this kind, in that it affords selective information on a component provided the light source is properly chosen. The C=C ($\nu_{C=C}$) and C-C (ν_{C-C}) stretching vibrations found in polyacetylene, especially the former, are known to be sensitive to the number of conjugated bonds ($N_{C=C}$)[76 77]. The I-I (ν_{I-I}) stretching vibration of various compounds containing iodine have been shown to be sensitive to the state of iodine[78]. Hence, these vibrations are useful markers for studying the chain-length and the state of iodine.

Resonant Raman spectroscopy has also been used to probe the electronic energy gap. For laser wavelength 676 nm ($h\omega$ = 1.83 eV), three phonon lines are observed, as shown in Fig. 2.5-7. As the excitation frequency (energy) increases, the Raman sidebands exhibit dramatic line-shape changes[79, 69, 70, 71, 72, 73, 74]. Shoulders on the high-frequency side of the primary peaks eventually develop into secondary peaks at $h\omega_L$ = 2.71 eV. Attempts have been made to explain the unusual features.

One such attempt involves a distribution of conjugation chain lengths [69, 71, 72, 73, 74]. It is based on the well known fact that both the optical excitation threshold and the Raman-active C=C stretching frequency decrease with increasing chain length in finite polyenes. In this approach, the line-shape dispersion is interpreted as a resonance process in which the Raman cross section for short trans segments of a given sample are selectively resonantly enhanced for excitation energies above the gap. However, this is difficult to reconcile with the high conductivity observed in doped samples and with the evidence of extremely mobile solitons obtained from NMR and ESR analysis. Otherwise, the "short-chain" model seems to explain the dopant, polarization, history, and sample quality dependences of the Raman line shape.

Another model to describe the origin of the Raman dispersion, proposes a distribution in the elecron-phonon coupling constant λ, $p(\lambda)$, which is due to the disorder in the imperfect samples[80 81 82]. With all other parameters fixed, λ uniquely determines the energy

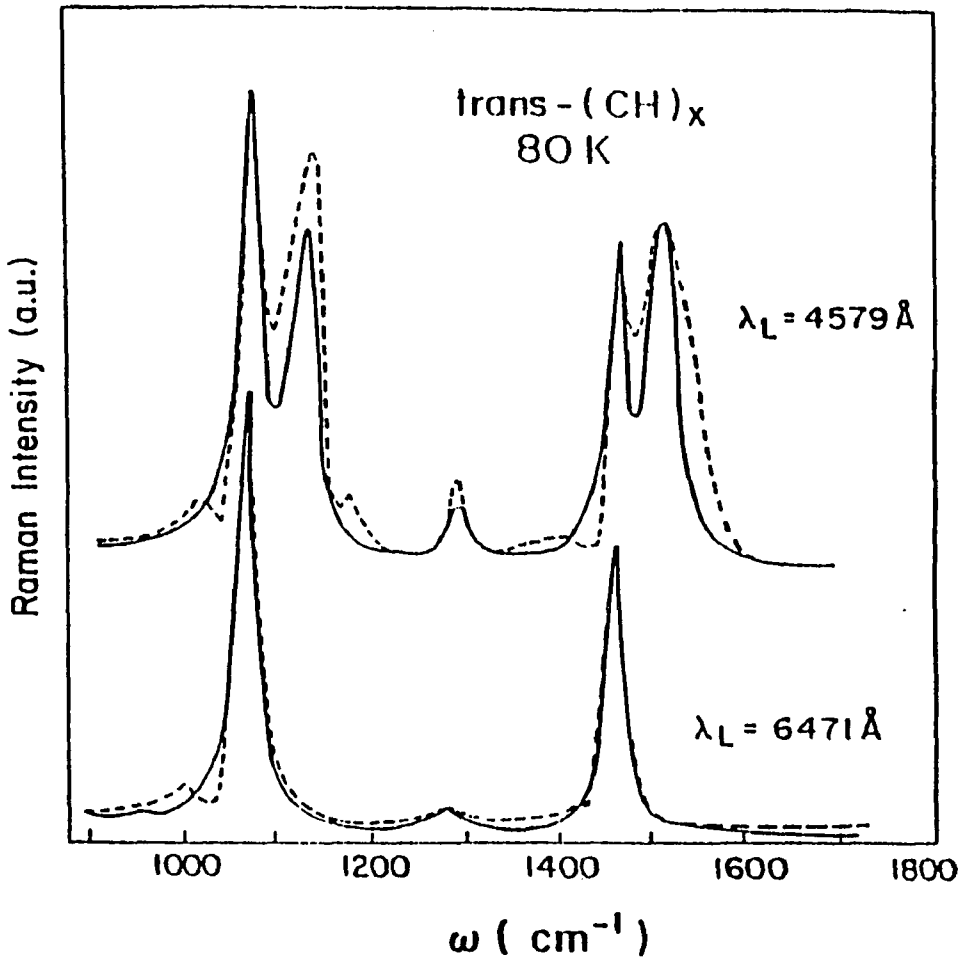

Fig. 2.5-7: Resonant Raman spectra from trans-(PA); dashed line, experimental data; solid line, theoretical fit (from Mulazzi et. al. (1985))

band gap $2\Delta(\lambda)$ and the phonon frequencies. In the analysis of Vardeny and co-workers, independent of ω_L, the primary peaks correspond to the maximum of $p(\lambda)$ at $\lambda=\lambda_o$, whereas the satellite peaks results from resonance condition $h\omega_L=2\Delta(\lambda) > 2\Delta(\lambda_o)$. With a very narrow Lorentzian distribution, it is possible to explain all aspects of the observed spectra in detail [80, 81, 82], including the sliced excitation profiles[83]. The latter were inconsistent with the "short-chain" model. The distribution in λ arises from finite localization lengths, which in turn are due to disorder. Thus the $p(\lambda)$ model can be viewed as a some-what more sophisticated attempt to include the "short-chain" effects. At present there is no concrete theoretical explanation of the origin of $p(\lambda)$.

Using the Shirakawa catalyst, and growing polyene chains into activated sites of polybutadiene, which act as a soluble carrier, Tubino et. al.[84] have been able to develop a novel form of polyacetylene partially soluble in conventional aromatic solvents[85]: Polyacetylene synthesized by traditional Shirakawa procedure is an insoluble polymer. In this novel material, because of special preparations, it is expected that interchain forces, as well as chain rigidity are strongly reduced compared to the solid form. This in turn permits the study of intrachain effects without interference from interchain interactions, cross-linking and the like there of. The availability of the polyene chains in solution can contribute to the solution of controversies regarding the structure and the properties of PA, namely the extent of interchain interaction, the cross-link formation, and the soliton dynamics in a truly one-dimensional system.

Illustrated in Fig. 2.5-8 is the optical absorption spectrum of soluble PA. It consists of a broad and asymmetric absorption band centered a 580 nm. The absorption maximum is blue shifted by 90 nm with respect to the maximum exhibited by the optical absorption spectrum of thin films [56] prepared by the conventional Shirakawa procedure.

Two conceivable explanations for the observed shift are: 1) The interchain interactions are probably far less effective in soluble PA than in the solid. It has been shown[86] that the introduction of three dimensional interactions through transverse hopping integrals has the effect of reducing the energy gap of a strictly one-dimensional chain. 2) It is well known that in polyenes the lowest optical absorption, shifts towards lower energies with increasing chain length[87]. The observed blue shift could be related to a reduction of the average conjugated chain length in the solution with respect to the film.

The absorption spectrum of the soluble trans(PA) exhibits phonon-assisted side bands, that are manifested in the form of the two peaks at 635 nm and 600 nm in Fig. 2.5-8. The presence of a resolved vibronic structure in the absorption spectrum of the dissolved polymer seems to indicate a sharper distribution of chain lengths and/or a reduction of the interchain interactions as expected [69, 88].

The emission spectrum of the soluble PA for an excitation at 488 nm si shown in Fig 2.5-9. The spectrum consist of two fundamental Raman vibrations centered at 1110 cm $^{-1}$ and 1490 cm^{-1}, followed by a weak second order scattering. The spectrum of the

solution is consistent with the emission spectrum of trans(PA) films reported by various authors [70, 89]. Therefore it is believed that the soluble PA consist mainly of polyene in the trans form.
The strong Raman lines observed at 1110 and 1490 cm^{-1} are assigned to the C-C and C=C A_g stretching vibrations respectively. Availability of soluble PA offers the unique opportunity of measuring the polarization properties of the scattered radiation in order to confirm the assignment. The observed depolarization ratio for both the two strong Raman lines shown in Fig. 2.5-9 is P_s=0.4, in agreement with the expected value for A_g modes under noncubic symmetry (C_{2h} point group).

The resonant secondary emission of the dissolved PA bears a very close similarity with the corresponding spectrum of the solid trans-PA. In the latter system the lack of a distinctive band-edge recombination luminescence peak and a strong multi-phonon Raman activity has been taken as evidence of the soliton formation due to an intrinsic instability of the photogenerated electron-hole pair [10]. These results seem to imply that PA should be able to support solitons even in solution.

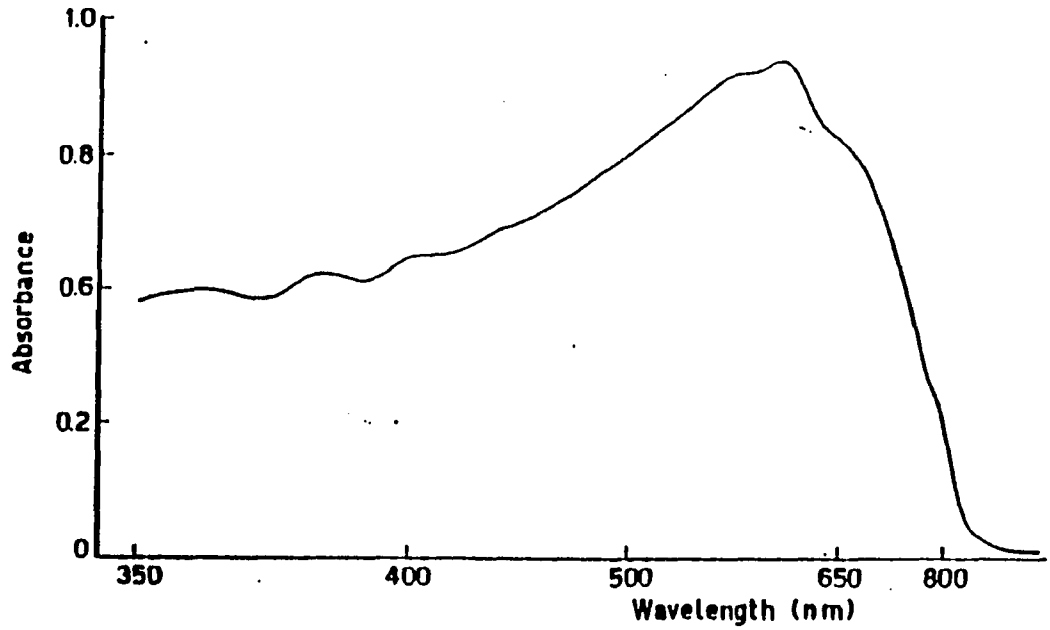

Fig. 2.5-8: Absorption spectrum (at room temperature) of soluble polyacetylene. (from Tubino et. al. Phys. Rev. B 30, 6601 (1984))

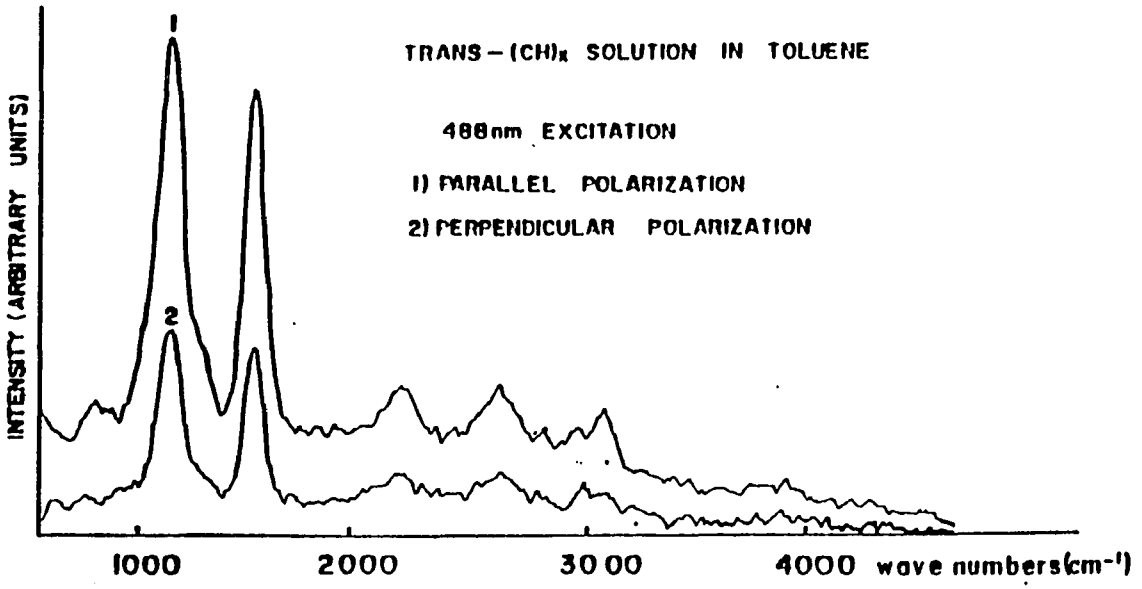

Fig. 2.5-9: Emission spectrum of soluble polyacetylene, excitation 488 nm. (1) Analyzer parallel to the polarization of the laser beam. (2) Analyzer perpendicular to the polarization of the laser beam. (from Tubino et. al. Phys. Rev. B 30, 6601 (1984))

D Photoexcitation Experiments

According to the Su, Schrieffer and Heeger mode [5, 10] a photoinduced electron hole pair evolves to a soliton-antisoliton pair in about 100 fsec. The pair is coupled to localized states at the gap center, and an important test of the existence of solitons in trans-PA should be the observation of the photoinduced absorption below the interband threshold. The absorption spectrum was predicted to change as oscillator strength shifts from $h\omega$ to $h\omega_s$ after photoexcitation. Studies of the infrared-active vibrational (IRAV) modes, midgap absorption, and electron-spin resonance following photoexcitation have confirmed the Su Schrieffer mechanism.

1) Infrared-active vibrational modes

Photoinduced absorption has been reported rising from infrared-active vibrational modes[90 91 92]. Three vibrational modes with large oscillator strength are observed. In Horovitz's "amplitude mode" formalism, these correspond to the coupling of the three lattice degrees of freedom of the polymer chain (that modulate the dimerization amplitude and thus, are resonantly enhanced in Raman scattering) to the zero-frequency uniform translational freedom of the charge. The existence of the photoinduced IRAV mode provides experimental proof that a localized lattice distortion is generated via photoexcitation. Moreover, the one-to-one correspondence between the principle IRAV modes, photoinduced [90, 91, 92] and doping-induced [34, 35, 36] indicates that the same charge carriers is produced

in both cases. The doping induced IRAV mode at 900 cm-1 was identified [90] as the "pinned" uniformed translation mode (or the Goldstone mode), the pinning being the result of the Coulomb attraction of the charged soliton to the charged counter ion. The large shift of the lowest-frequency IRAV mode upon photoexcitation, from 900 cm^{-1} [34] to 540 cm^{-1} [90]
is consistent with more weakly pinned photogenerated charges.

2) Photoinduced absorption and photoconductivity

A great effort has been devoted to the interpretation of the photoinduced infrared absorption and the photoconductivity in conventional isotropic Shirakawa films to elucidate the nature of photoinduced charge carriers. It has been shown theoretically that in PA mobile charged solitons can be photogenerated directly or indirectly after photoexcitation of an electron-hole pair. Time resolved spectroscopy[93] has been used to observed the predicted absorption due to photogenerated intrinsic gap states in trans-(PA). Orenstein and Baker initially observed two photoinduced absorption features (both in time resolved and steady state measurements), one at 0.5 eV and one at 1.34 eV. Vardeny et al. [91] and Blanchet et al.[94] later observed three photoinduced bands at 0.5, 0.17 and 0.06 eV. The 0.5 eV feature scales in every way with the characteristics of the IRAV mode (ie. same temperature and laser pump intensity dependence, etc.) It has been proposed that the 0.5 eV absorption originates from an electronic transition involving the mid-gap state associated with soliton [91, 94] whereas the 1.35 eV is associated with

neutral excitation. The origin of the low energy peak at 0.06 eV is controversial. Blanchet et al. [90] have assigned this peak to the pinned translational mode of the soliton, Rice[95] proposed that this peak originates from an oscillation of a bound pair of oppositely charged solitons. Sun et al.[96] have attributed this band to a vibrational mode of a polaron about its equilibrium configuration.

Dorsinville et. al.[97] were the first to report photoinduced absorption and photoconductivity measurements in highly stretched films of polyacetylene. The intensity of the "mid gap" absorption at 0.49 eV and the intensity of the cw photocurrent exhibit similar dependence on polarization of the laser beam. The measurement illustrated in Fig. 2.5-10 and Fig. 2.5-11 imply that the photoinduced cw anisotropy and the cw photoconductivity reach their maxima when the laser polarization is perpendicular to the chain direction in trans-(PA) although the transition moment of the lowest interband transition is along the chain. These data suggest that the intensity of the photoinduced near infrared absorption and the photoconductivity are strictly related as they exhibit the same dependence on the polarization of the inducing optical electric field with respect to the fiber orientation.

Studies using subpicosecond resolution have shown that the gap states and the associated interband bleaching are produced in less than 10^{-13} s[98 99 100]. Data showing subpicosecond photoinduced bleaching of the interband transition are shown in Fig. 2.5-12. Picosecond photoconductivity measurements by Sinclair et al.[101] and Bleier et al.[102] demonstrated the fast photoproduction of charged excitations with a relatively high quantum efficiency. Shown in Fig.

2.5-13 is the transient photoconductivity of unoriented trans-(PA) due to a 1μJ pulse at 2.1 eV with a bias field of 1.5 x 10^5 V/cm. The observed rise and fall time of the signal is approximately 50 ps and 300 ps respectively. The experimental demonstration that the photoconductivity and the photoinduced change in optical absorption, decay on the same time scale implies that the photogenerated charge carriers involve a major shift in oscillator strength, consistent with the proposed photogeneration of charge solitons.

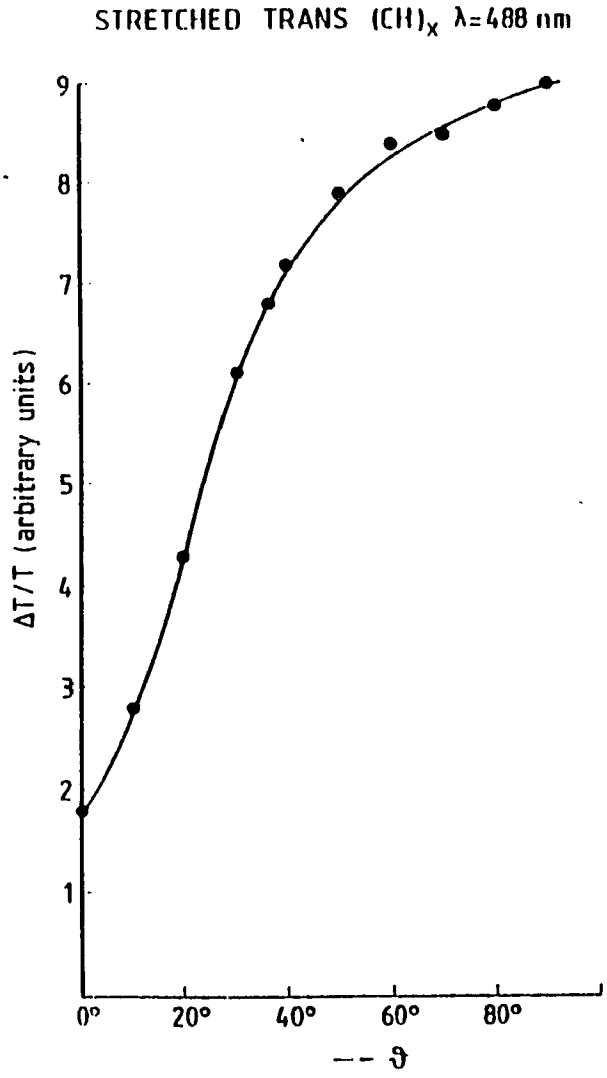

Fig. 2.5-10: Photoinduced absorption intensity of highly oriented trans-(PA) as a function of the angle θ between the polarization of the argon-ion laser and the stretching direction.(from Dorsinville et. al. Solid State Commun. 56, 857 (1985))

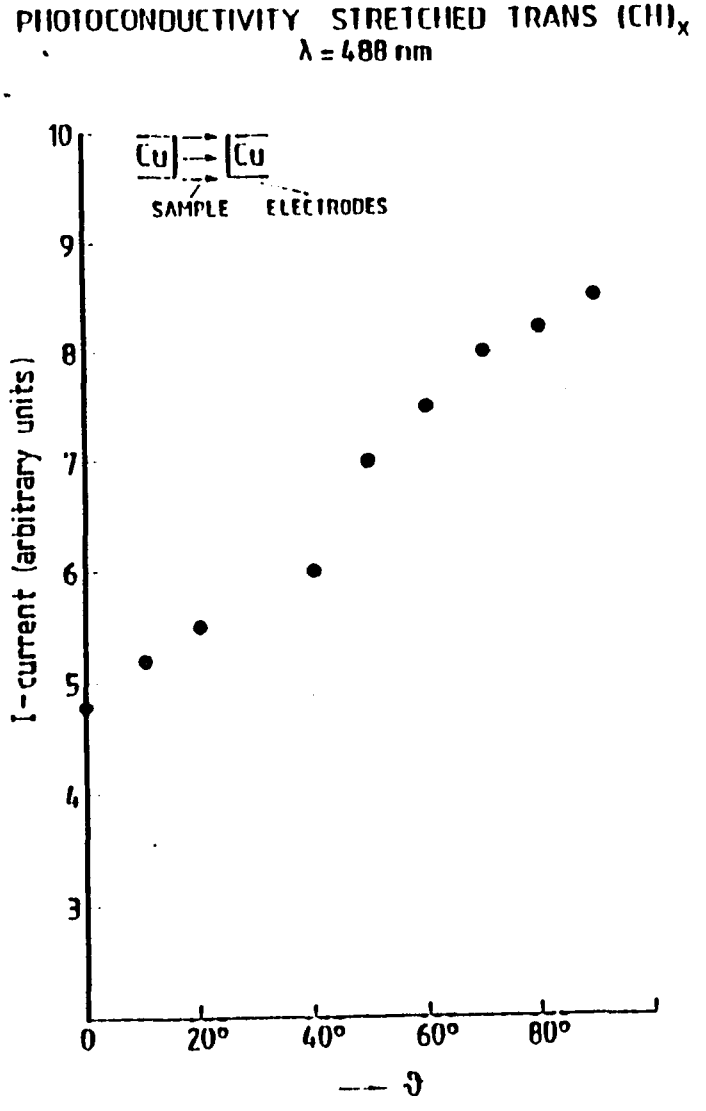

Fig. 2.5-11: Parallel component of the photoconductivity of highly oriented trans-(PA) as a function of the angle θ. λ = 488 nm (from Dorsinville et. al. Solid State Commun. 56, 857 (1985))

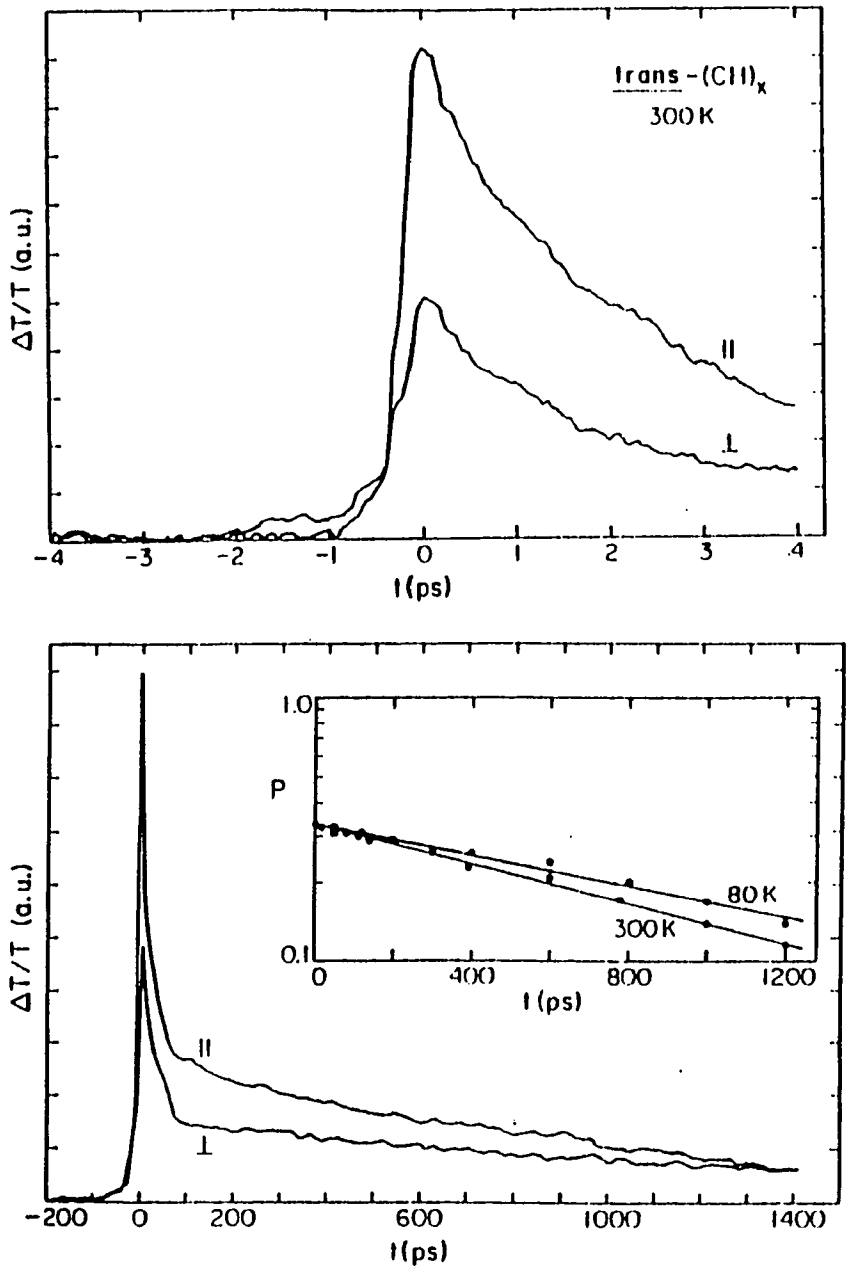

Fig. 2.5-12: Transient (picosecond) photoinduced bleaching of the interband transition in trans-(PA); the oscillator strength shifts from the interband transition into the midgap transition (from Vardeny et al., 1982)

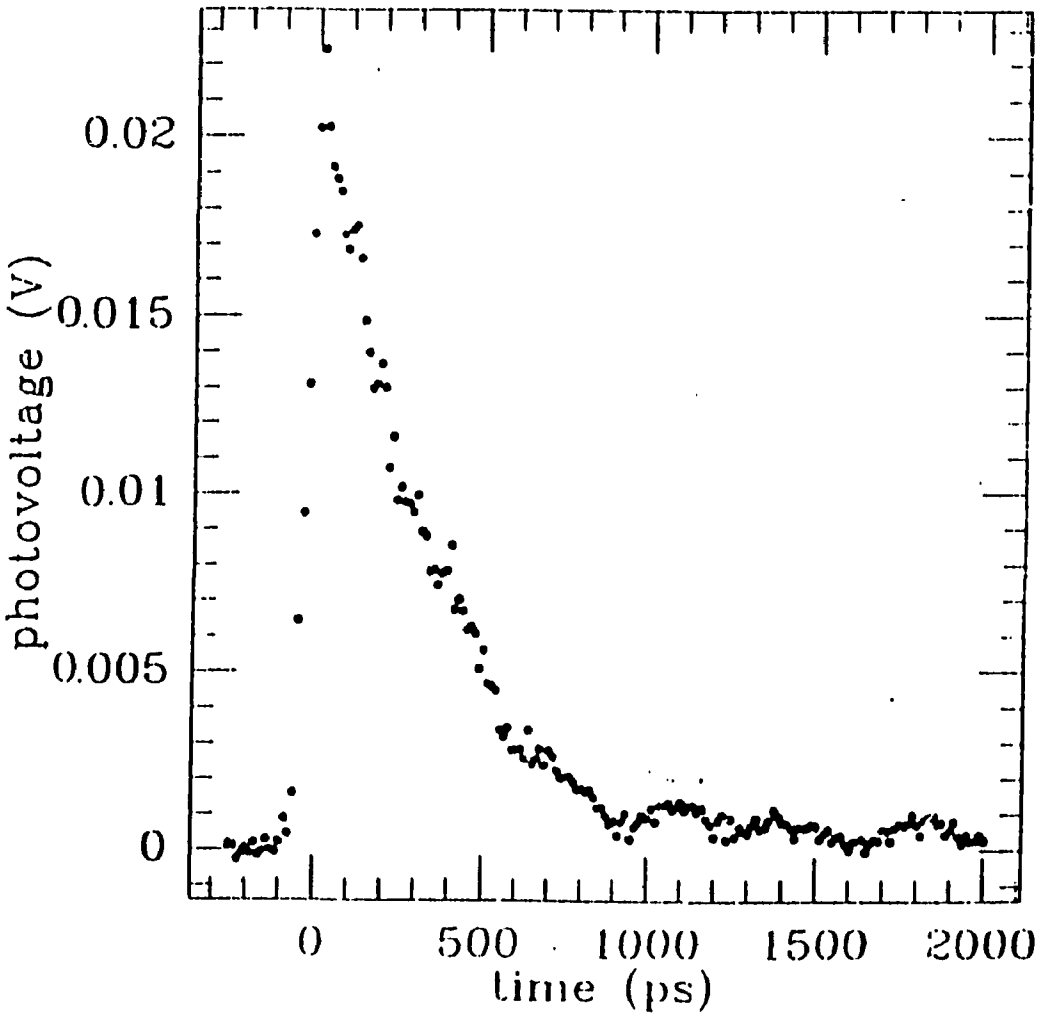

Fig. 2.5-13: Transient photovoltage across 50 Ω of trans-(PA) in the Auston switch configuration. The peak value corresponds to a current density in excess of 10^3 A/cm^2 and a photoconductivity of approx. 0.3 S/cm (from Sinclair et al. 1986)

Rothberg et al. [100] have time resolved the photoinduced absorption associated with the mid gap transition, by pumping at 2.1 eV. and probing the photoinduced absorption at 0.3-0.55 eV, the results are shown in Fig. 2.5-14. In this experiment, the intrachain photogeneration of intrinsic charged solitons in trans-(PA) was observed and information about their absorption spectrum and decay dynamics on the picosecond time scale was obtained. The intrachain soliton pairs can be distinguished from the charged solitons produced via an interchain absorption process (presumably leading to charged polarons on different chains); the latter are formed at later times either by neutral-to-charge soliton conversion or by the reaction $P^+ + P^+$ to $2S^+$ (or the compliment) when two polarons of like charge diffuse onto a single chain.

A scenario that is consistent with all the above mentioned experiments has been developed[103, 101] . The initial absorption is principally intrachain. The mid gap absorption due to charged solitons (0.45 eV), band-edge absorption (1.4 eV), and bleaching of the interband absorption all decay on similar picosecond time scales. A reasonable description is that the soliton-antisoliton pairs are directly photogenerated within 10^{-13} s and begin to decay into neutral soliton pairs (that absorb at 1.4 eV) in several femtoseconds. The neutral soliton in turn decay rapidly to phonons.

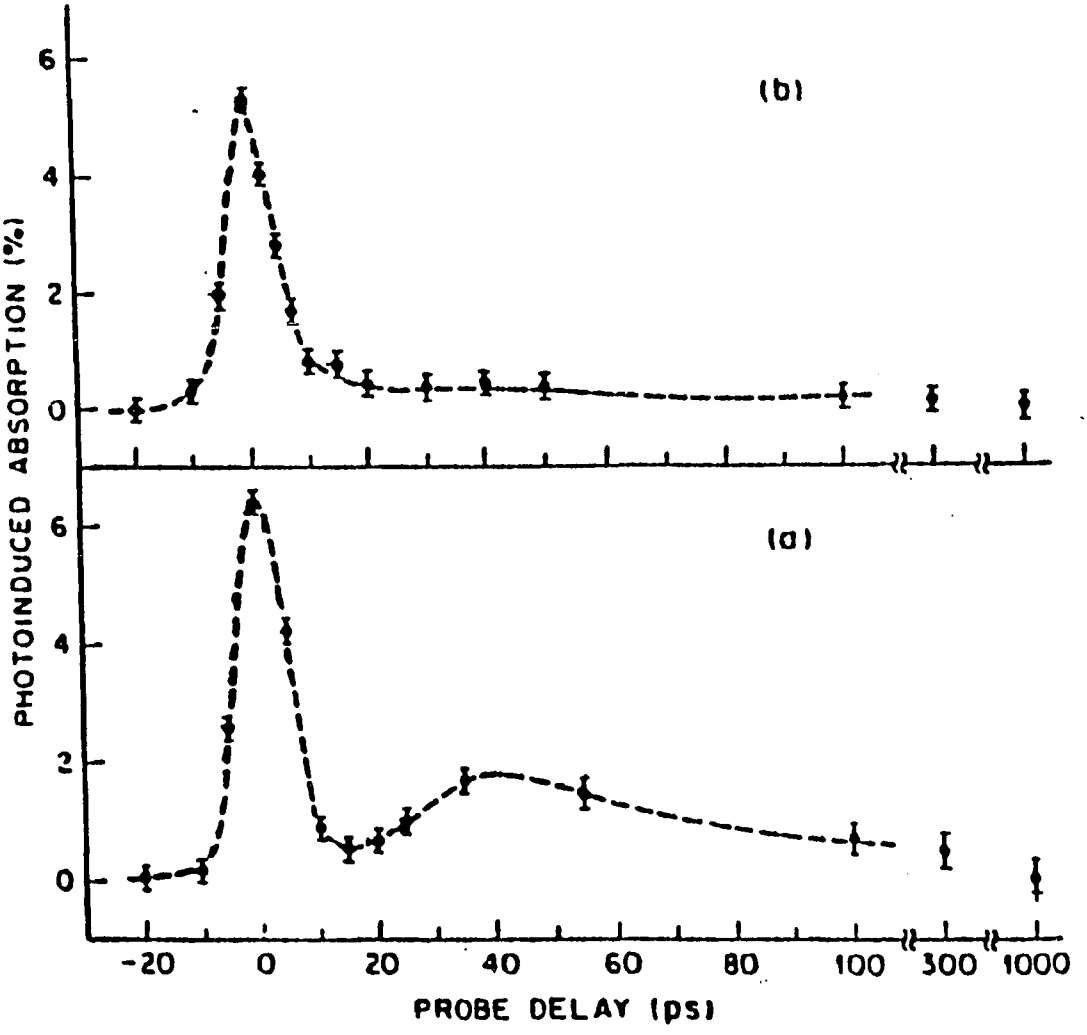

Fig. 2.5-14: Time-resolved photoinduced absorption of trans-(PA) in the midgap spectral range: (a) 25 K, (b) 300 K. Dashed lines are to guide the eyes. (Rothberg et al. 1986)

3) Reverse Spin Charge Relation

The results of light-induced ESR experiments[104 105] (i.e., electron-spin resonance experiments carried out during photoexcitation, LESR) have demonstrated that photogenerated excitations in trans-(PA) are spinless and confirm the reverse spin-charge relation of solitons.

The objective of such an experiment is to determine the number of photogenerated spins directly from quantitative ESR measurements during photoexcitation and determine the number of photogenerated charges from the strength of the photoinduced IRAV mode and the photoinduced 0.45 eV mid gap absorption, these photoinduced infrared features being calibrated through direct comparison with the corresponding doping-induced spectral features (where the doping concentration is known). LESR experiments have set an upper limit of 3×10^{-7} of photogenerated spins per carbon for a pump power of 20 mW/cm^2. Two independent calibrations of the intensity of the IRAV mode as a function of doping concentration [34 106] and a separate experiment calibrating the mid gap transition [57] has been performed. Using these data, the strength of the photoinduced infrared signatures set limits on the concentration of photogenerated charges between 10^{-4} and 5×10^{-4}. Thus, even using the smallest number for the photogenerated charge density the ratio

of the spin density to charge density is 3 x 10^{-3}, indicating that the photogenerated charge carriers are spinless.

The following sections describe the results and analysis of the work performed for this thesis.

III Experimental Technique and Apparatus

3.1) Introduction

This section will focus on the main equipment used in the experiments performed for this thesis. A description of the laser and a brief discussion on picosecond photoconductivity and the geometry of the optical switch will take place here. Peripheral equipment like, a real time scope (approximately 250 psec resolution), a sampling scope (appox. 90 psec resolution), photodiodes, RF amplifiers, box car averager, and glass Dewar were available.

3.2) Laser

The laser source used in all experiments was the commercially available Quantel Nd:YAG laser (YAG denotes yttrium-aluminum-garnet), which is both passively and actively mode locked. The operation of this laser system is described below (refer to Fig. 3.2-1). The laser rod which is cut at Brewsters angle, is pumped by two Xenon flash lamps. Lasing occurs with p polarization. Mode locking is initiated by both an acousto-optical crystal (active mode locking) and a saturable absorber dye (passive mode locking) placed inside the laser cavity. The acousto-optic crystal modulates the lasing florescence. The modulated florescence has random noise bursts and fluctuations which are amplified by the laser rod. As the light

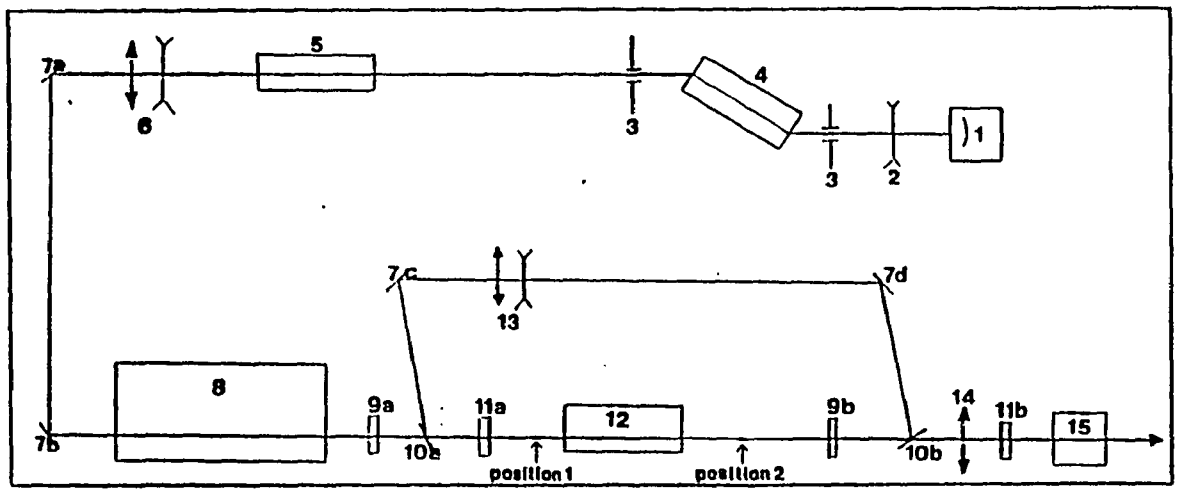

LEGEND

75mJ MODE

1) MS400 mode-locking dye cell
2) Diverging lens
3) Pinhole
4) SF408-07 Brewster/Brewster oscillator
5) AML-1 (Acousto-optic mode-locker)
6) Beam expanding telescope, +155, -92
7) 45° turning mirror
8) PF302 pulse slicer
9) $\lambda/2$ plate
10) Dielectric polarizer
11) $\lambda/4$ plate
12) SF410-09 2°/2° amplifier head
13) Beam expanding telescope, +155, -104
14) Converging lens
15) Second Harmonic Generator (SHG)

Fig. 3.2-1: Passive and active mode lock Nd:YAG laser system schematic.

passes through the saturable absorber, the larger noise bursts are preferentially selected, while the weaker noise bursts are absorbed. After several round trips through the cavity, a well defined single pulse develops with a duration of 35 psec at the lasing wavelength of 1.06 μm.

The acouto-optic crystal is electrically modulated by a radio frequency signal. This modulation frequency is equal to the round trip time of the laser cavity 2L/c, where L is the cavity length and c is the speed of light. This creates sidebands or additional frequency components on each side of the allowed longitudinal frequency components of the laser cavity. The saturable absorber and acousto-optic mode locker compliment each other in the sense that the newly created sidebands of a particular longitudinal frequency component is exactly equal to the next higher and lower longitudinal cavity frequencies. This action couples all the allowed longitudinal modes of the laser cavity. The combined action of the saturable absorber and the acousto-optic modulator allows the production of 35 psec pulses at 1.06 μm in a gaussian envelope of approximately 10-12 pulses in the train. The total energy in the train is about 7 mJ. The saturable absorber has the greatest effect on decreasing the pulse duration, while the acousto-optic modulator has the greatest effect on the shot to shot stability. This stability can be checked by using a slow photodetector and a Tektronix 7934 storage oscilloscope.

As stated above, the output from the laser cavity is a train of pulses at 1.06 μm, where each pulse has a duration of approximately 35 psec. A train is emitted because for each round

trip in side the laser cavity, a portion of the laser pulse is transmitted through the output mirror. The envelope impressed upon the train of pulses corresponds to the gain envelope of the laser medium during the time of population inversion. The train of pulses is then directed into a Pockel cell pulse slicer. This device essentially consist of an electro-optic crystal and polarizing optics. A laser pulse can be selected from the laser pulse train, by applying a well define voltage pulse across the electro-optic crystal, which rotates the plane of polarization of one of the optical pulses in the train, allowing it to pass through two cross polarizers. The well define bias voltage across the electro-optic crystal must be synchronous with the lasing process for selection of a single optical pulse. The rejected or unwanted train of pulses can be observed by using a fast photodiode connected to a Tektronix 7104 oscilloscope, this will allow monitoring of the pulse selection process. The two types of photodiodes used were the S-1 detector biased by a 1.5kV. and a Motorola MRD 510 photodiode connected in a RC circuit biased with 20 volts. The pulse ejected from the pulse slicer is s polarized.

Pockel cell alignment is obtain by diffusing the incoming 1.06 μm optical pulse with lense tissue. The diffused light is then permitted to pass through the Pockel cell and a cross polarizer. The standard Maltese cross pattern which indicates the crystalline optic axis is observed. The crystal is then adjusted such that the optical path of the 1.06 μm pulse is through the center of the Maltese cross pattern. Once this is accomplished the Pockel cell is properly aligned.

After the pulse slicer has selected a single pulse from the pulse train, it is then amplified by a double pass ring amplifier. Using

a half wave plate, polarizer, and polarizing beam splitters, the single laser pulse can be amplified to 75 mj. A Scientech calorimeter energy power meter (model number 362) is used to measure the energy of the laser pulse. The transverse mode of the pulse is multi-mode after amplification.

A more detail description of the ring amplifier is as follows (refer to Fig. 3.2-1). After the pulse slicer, the selected s polarized laser pulse passes through a half wave plate, which converts its optical orientation to p polarization. After its first past through the amplifier rod the amplified pulse passes through another half wave plate which converts its optical orientation to s polarization. The amplified pulse is reflected from a polarizing beam splitter and begin its second pass through the amplifier system. After the second pass through the amplifier rod, the s polarized amplified pulse passes through the second half wave plate for a second time. This second pass converts the optical orientation of the s polarized amplified pulse to p polarization once again. With this polarization, the amplified pulse passes through the polarizing beam splitter. The amplified pulse has a duration of approximately 35 psec, which can be measured using second harmonic autocorrelation techniques or by two-photon florescence in Rhodamine 6G.

The procedures for aligning the Nd:YAG laser system requires the use of a HeNe laser and several pinholes which reference the optical beam path. The oscillator cavity is aligned, by having the back reflections from both the front and rear mirrors, retrace their original beam paths back to the HeNe laser output port. The double pass amplifier is aligned using two reference pinholes,

one on each side of the amplifier rod. Burn paper is used to make sure that the first pass is properly centered in the amplifying rod. The first passed amplified pulse is then redirected into the amplifying rod, making sure that the second pass amplified pulse cross section is concentric with the first pass.

Finally the amplified pulse passes through a type I second harmonic generator crystal (KDP). This crystal converts up to thirty percent (30%) of the incident 1.06 μm (the fundamental frequency of the laser) light to the second harmonic frequency of 0.532 μm. The pulse duration of the second harmonic laser pulse is approximately 25-30 psec. with a s polarization optical orientation. The pulse width of the second harmonic output of the Nd:YAG laser can be measured by similar techniques used to measure the fundamental output. Alternatively, the streak camera can be used to obtain real time single shot measurements of the second harmonic output pulse.

3.3) Picosecond Photoconductivity

3.3-1) History

Over the past 15 years a new field has emerged, namely, picosecond optoelectronics. With the availability of femtosecond laser pulses, such a device may have a subpicosecond time response. The picosecond devices discussed in this section are based upon the picosecond photoconductivity effect (The carrier generation by photoexcitation with picosecond optical pulses usually caused by the transition of electrons from the valence band to the conduction

band.). They consist of a bulk photoconductor used in conjunction with a picosecond laser. The field of picosecond photoconductivity refers to the study of photoconductivity effect with picosecond optical pulses. The first observation of the picosecond photoconductivity effect was reported by Jayaraman and Lee in 1972[107]. They compared the response of a Cr:GaAs photoconductor to the Q-switched nanosecond pulses with that to the mode-locked picosecond pulses. It was obvious from this experiment that the photoconductivity signal responds rapidly to the laser pulses. This showed that picosecond electrical pulses can be generated by the picosecond photoconductivity effect. Utilizing the almost instant response of the photoconductor to picosecond optical pulses, Auston[108] demonstrated the switching, gating, and sampling of voltage pulses in a microstrip line using Si photoconductors. The most unique feature of this switch is the lack of jitter. Lawton and Scavannec[109] used Cr:GaAs as a microstrip line structure for detecting picosecond optical pulses from a mode-locked dye laser, exploiting the characteristically short photoconductive lifetime of the charge carriers in this material. Because of its high dark resistivity (108 Ω cm), GaAs could be dc biased to 15 kV[110] with a switching efficiency of 90-95%. Other materials have been used as switches. They include Fe:InP[111] $CdS_{0.5}Se_{0.5}$[36], amorphous silicon[112], germanium[113], GaP[114], CdCrSe[115], diamond[116] and polycrystalline OMVPE GaAs/SiO_2 films[117].

The applications of picosecond photoconductor are numerous based on their unique characteristics, i.e., extremely high speed, large dynamic range, scalable, and jitter-free response. In

general there are two major categories of applications: low voltage and high voltage (kilovolts). In the former case it is high speed that is the most important characteristic of the device. The switching efficiency is not of major concern. In fact one may sacrifice mobility for the sake of getting the shortest possible carrier life time. In the latter case the device must deliver as much power as possible to the load. The switch transfer efficiency should be near 100%. Speed is not crucial, but, the mobility of the material should remain at a reasonable value. One basic function of all these devices is electronic switching and gating[34]. Other applications include sampling [118, 119, 120], jitter-free streak camera operation[121], picosecond active pulse shaping[122, 123], wave form generation[124], microwave modulation[125, 126], generation of microwave burst[127], optical detection [128, 37, 38], particle detection[129]. All these applications utilize the conductive mode property of the photoconductor.

Much of the work in the past on photoconductive switches have been device oriented; concentrating on making them faster and more efficient. This is not the objective of this study. Here we wish to use the picosecond photoconductive switch as a tool for material studies.

3.3-2) Picosecond Switch

A standard photodetector consist of two parallel plates. This geometry produces a rather large capacitance lumped at the plate surfaces, which causes the detector to respond sluggishly to photoexcitation. In order to observe a picosecond transient, the

bandwidth of the detector must be increased by reducing its capacitance. To reduce the capacitance and thereby increased the speed of response, a 50 Ω microstrip transmission line[130, 131] geometry was used. The capacitance is reduced because it is distributed along the transmission line. A typical picosecond photoconducting switch is illustrated in Fig. 3.3-2-1.

A sheet of dielectric material, sandwiched between two sheets of copper (copper cladding, 3M Cu Clad 250) and a 3M Brand Microwave Design Aid kit was used to construct the microstrip line geometry. The kit consist of transferable copper foils backed by an adhesive which can be used to build working microstrip and stripline circuits. The copper cladding surfaces must first be prepared for application of the photoresist. Its surfaces were cleaned with warm water and a small amount of abrasive copper cleanser and thoroughly rinsed. From this point on, the board was held by it edges to prevent dirt and oil from the fingers from contaminating the surfaces, which would prevent photoresist adhesion. Photoresist adhere better to surfaces which are acidic. To accomplish this, the board was dipped into a dilute bath of HCL (10% by volume) then rinsed under running water. The board is thoroughly dried and now its ready for coating. Because photoresists are sensitive to ultraviolet

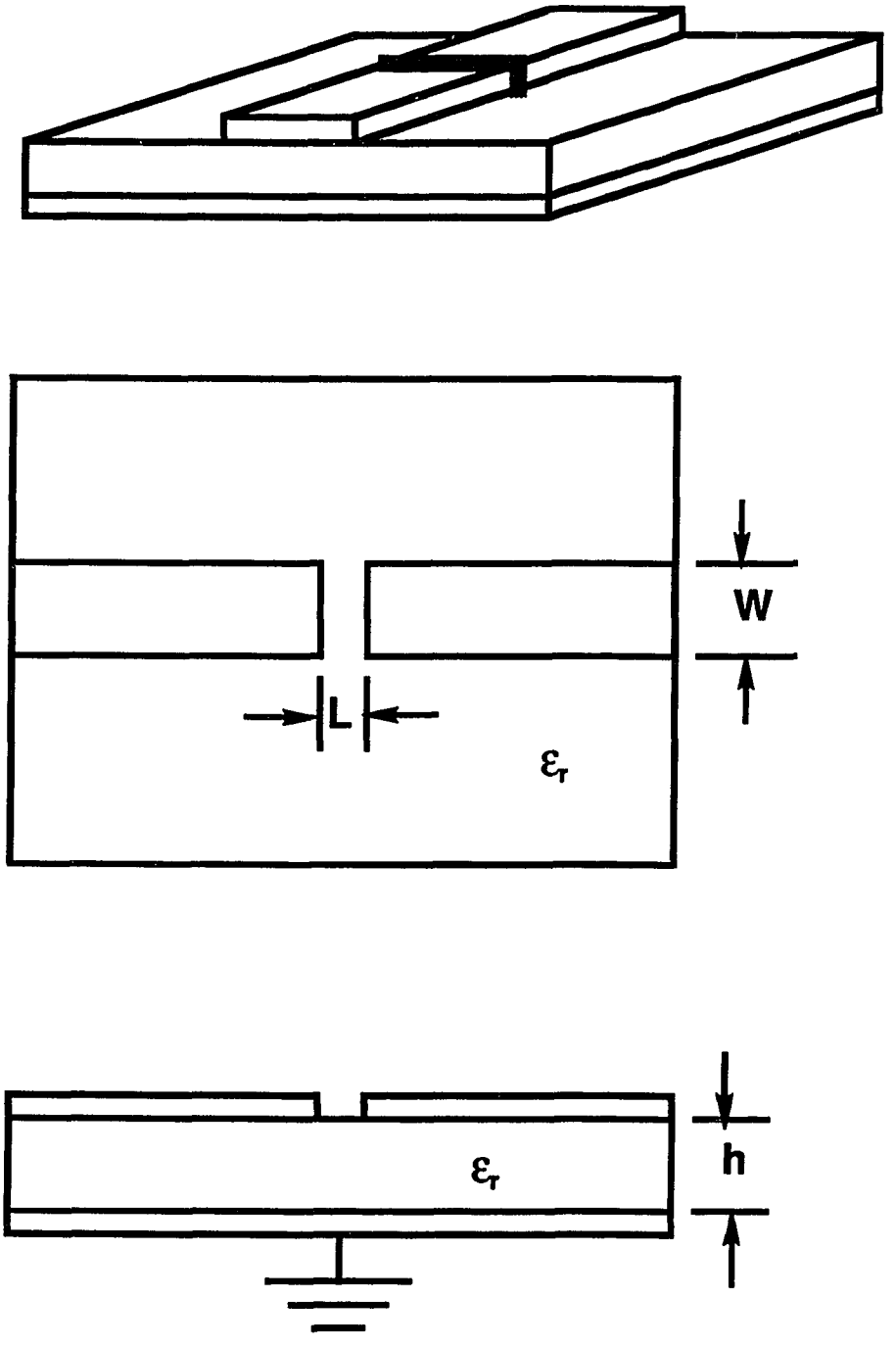

Fig. 3.3-2-1: Schematic diagram of a high-speed microstrip transmission line. The active region is the gap in the top electrode at which the light is focused.

radiation, steps were taken to provide "safelight" conditions in which the resist was handled. White fluorescent tubes wrapped with KODAGRAPH Sheeting, (orange), can be used.

A small amount of photoresist was poured with a pipette into the middle of the board. The board was then tilted in various directions until one side was entirely covered, making sure the resist did not coat the other side of the cladding. The excess resist was drained from the corners and then the board was stood in a near vertical position until the resist had dried. This took about 6 hours. The removal of residual solvents from the photoresist is important. Retention of the solvents in the photoresist could reduce photosensitivity. If the resist is not dry, the response to ultraviolet radiation is low and adequate exposure cannot take place. The resist coating must be exposed to a light source rich in ultraviolet radiation. This was accomplished by using a mercury-vapor lamp. The coated side of the board was exposed to the ultraviolet light source for approximately 2 to 3 hours to assure curing, after which, the board was ready for etching. Either ferric chloride, cupric chloride, or ammonium persulfate was used as an etchant. The board was placed in a glass container with the etchant and heated to approximately 49° C (120° F). Heating accelerates the etching processes. An important factor in good etching is constant agitation. This is necessary to carry away reaction products and provide fresh etchant to carry on the process. Occasionally the board was removed to check the progress of the copper removal. The etching continued until all the unwanted copper was removed. The board was then rinsed in running water to remove any excess etchant. The remaining

photoresist had to be removed before the board could be used. If this was not done, contact problems with the remaining copper could develop. So, the board was thoroughly scrubbed with warm water and a small amount of pumice until the remaining resist was removed. It was then rinsed and dried and ready for use.

The use of the 3M Brand Microwave Design Aid kit allowed the foregoing of the lengthy and rather tedious process of photomasking, image developing, and a number of other steps used in microwave circuit fabrication. A strip of copper foil of the appropriate dimension is secured to the dielectric substrate completing the transmission line. The microstrip line is interrupted by a 0.5 mm gap. This gap forms the active region of the optical switch. The stretched polymer film was attached by pressure to the copper electrodes of the microstrip across the gap. This geometry is referred to as a gap or planar configuration. The characteristic impedance, Z_o of the microstrip transmission line is determined by the relative dielectric constant, ε_r, and the height, h, of the substrate and the width of the copper microstrip. The closed form expressions for Z_o and ε_r have been reported by Wheeler[132, 133], Schneider[57], and Hammerstad[134]. The expressions for W/h in terms of Z_o and ε_r are as follows:

For $A > 1.52$

$$W/h = \frac{8\exp(A)}{\exp(2A) - 2} \qquad (4.3\text{-}2\text{-}1a)$$

For A< 1.52

$$W/h = \frac{2}{\pi}\left\{ B - 1 - \ln(2B - 1) + \frac{\varepsilon_r - 1}{2\varepsilon_r}\left[\ln(B - 1) + 0.39 - \frac{0.61}{\varepsilon_r}\right]\right\} \qquad (4.3\text{-}2\text{-}1b)$$

where

$$A = \frac{Z_o}{60}\left(\frac{\varepsilon_r + 1}{2}\right)^{1/2} + \frac{\varepsilon_r - 1}{\varepsilon_r + 1}\left(0.23 + \frac{0.11}{\varepsilon_r}\right) \qquad (4.3\text{-}2\text{-}1c)$$

and

$$B = \frac{60\pi^2}{Z_o\sqrt{\varepsilon_r}} \qquad (4.3\text{-}2\text{-}1d)$$

These expressions provide an accuracy of better than two percent. For a nominal characteristic impedance Z_0 of 50 Ω and a relative dielectric constant ε_r of 2.5 the following parameters were obtained: W = 2.16 mm, and h = 0.76 mm. A schematic drawing of the photodetector geometry is illustrated in Fig. 3.3-2-2.

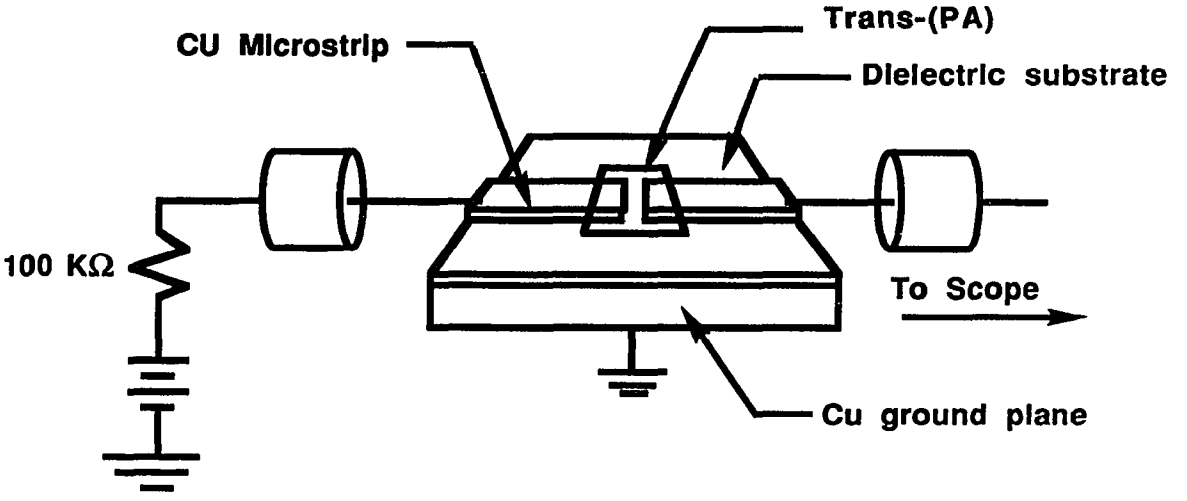

Fig. 3.3-2-2: Schematic drawing of photodetector geometry. The end-on electrodes form a 50 Ω microstrip transmission line. A small gap in the center is the active region of the switch.

In order to make electrical contact with the optical switch, it was necessary to mount the entire unit on a copper block with silver paste (which act as a continuation of the switches ground plate). Electrical contact was made with either Omni-Spectra OSM (18 GHz) or OSSM (40 GHz) coaxial-to-micostrip connectors or SMA strip-line launchers. The switch was biased on one side by a charged coaxial transmission line and on the other side the output signal was transmitted through a semi-rigid coaxial cable (18 GHz) and a 10 db Comlinear wide bandwidth amplifier to the different measuring devices (i.e. Sampling scope, Box car integrator, etc.). The biasing circuit consisted of a d.c. power supply and a blocking resistor. The blocking resistor (typically 100 KΩ) is standard and served the purpose of controlling the amount of current entering the optical switch. The blocking resistor also served as a precautionary device. The maximum signal that the sampling head could handle was plus/minus 5 V. Voltages as high as 600 V were utilized. The magnitude of the blocking resistor was chosen such that most of the voltage drop would be across it in case a short developed in the switch.

The picosecond optical switch was placed inside a liquid nitrogen Dewar that was fitted with high speed semi-rigid coaxial cable and feedthroughs. The Dewar served two purposes: 1) It protected the sample from oxidation by the atmosphere and 2) it permitted the measuring of the temperature dependence of the picosecond photocurrent of the HOPA sample. A copper-constantan thermal-couple was used to measure the temperature of the sample.

IV Picosecond Photoconductivity Above Gap Excitation

4.1) Introduction

Polyacetylene is a quasi one-dimensional system which is expected to show highly anisotropic optical and transport properties. Most of the experimental investigations carried out on trans-polyacetylene have used isotropic Shirakawa films and were unable to detect any anisotropy. It is now widely accepted that in conducting polymers excess charge carries created either by doping or by photon absorption, strongly interact with the lattice, giving rise to charged excitations which carry along a charge distortion. In the case of a polymeric chain with a degenerate ground state such as trans-polyacetylene, the localization of the carrier is predicted to give rise to topological, highly mobile solitons, which are believed to control the electrical transport properties of this polymeric semiconductor. Since this kind of excitation can only exist in pairs, the bond alternating kink cannot be carried along when the electron is transferred to a neighboring chain, and a polaron is formed in this case[135]. According to various authors[136, 102, 100] direct photoproduction of polarons is also possible when the exciting radiation is polarized perpendicular to the chain direction. In this case, because of interchain coupling[137, 138] a weak perpendicular absorption occurs and each absorbed photon creates an electron and a hole in different chains, preventing their 1D recombination. Again in this case individual electrons and holes cannot relax into a soliton

state. It is therefore concluded that both solitons and polarons can be charged carriers in polyacetylene[139].

There appears to be two relevant time regimes for the photoexcitation and decay process in trans-(PA): the picosecond time regime during which the intrachain charged photoexcitations are produced and undergo initial rapid decay and the long-time behavior ($t > 10^{-9}$ s), where the residual excitations are trapped and slowly decay. After 10^{-9} s, only a few percent of the initial photoexcitations remain. It is these trapped long-lived excitations that are observed in the steady-state photoinduced absorption and LESR experiments and that are responsible for the long-time tail in photoconductivity.

In addition to the intrachain photoexcitation processes, photoexcitation of electron-hole pairs on neighboring chains (an interchain process) form polarons as was previously mention. Although the magnetic properties expected for photogenerated polarons are not observed [105] such interchain excitations may play a transient role in the formation of the charged solitons which are observed at long times. As these polarons diffuse along and between chains, they will form solitons in two ways: (a) two polarons with the same charge on a single chain will lead to a pair of metastable charged solitons; (b) a polaron on a chain with preexisting neutral defects will convert the neutral soliton into a charged soliton. The first process appears to be dominant; it involves no change in the net number of spins and therefore is consistent with LESR data [104] [105].

Steady state[140] [141] [142] [143] [144] and pulsed photoconductivity of unoriented Shirakawa polyacetylene films have been studied by several groups as mentioned above. Dorsinville et al. have studied

the anisotropy of the cw [97] photoinduced absorption and the cw photoconductivity in highly oriented trans-polyacetylene (HOTPA). Photoconductivity measurements have also been carried out on polyacetylene obtained from a stretched prepolymer [102] showing an anisotropy behavior for an applied external electric field parallel and perpendicular to the chain direction as well as for different polarization angles of the incident light.

Tubino et al.[145] have investigated the cw photoresponse of HOTPA as a function of the applied electric field, of the temperature, and of the direction of the current flow with respect to the stretching direction. These measurements show that as in the case of single crystals of polydiacetylene,[146] [147] HOTPA appears to be capable of exhibiting either one- or three-dimensional behavior of the motion of the charge carriers depending on the direction of the current flow with respect to the carbon skeleton of the polymer.

The existence of at least two different transport processes in polyacetylene is suggested by the temperature dependence of the photoconductive response in unoriented polyacetylene reported by Sinclair et al. [101] and by Roth and Bleir[148]. These authors found that the fast component of the photoconductivity was temperature independent while the slow component was temperature dependent. Roth and Bleir concluded that the two components were due to different transport processes.

In this section we will study the temperature T and electric field E dependence of the fast photoconductive response of HOPA for above gap excitation. We will compare the temperature dependence of the picosecond current for the 1D and 3D

configurations. The 1D configuration is when the electrodes of the switch and the applied electric field are parallel to the chains of the polymer as shown in Fig. 4.1-1a. The 3D configuration is when the electrodes of the switch and the applied electric field are perpendicular to the chains of the polymer as shown in Fig. 4.1-1b. Our objective in this section, is to show that the character of the charged carriers in HOPA not only evolves in time, but, depends on the direction of the current flow relative to the chain direction. Onsager's dissociation theory qualitatively accounts for the influence of dimensionality on the charge transport. We will compare the temperature dependence of both the transient and steady state photoconductive response of HOTP.

4.2) Experimental Setup

The experimental setup for measuring the picosecond photocurrent is shown schematically in Fig. 4.2-1. For this experiment the 25 psec pulses of a frequency-doubled actively-passively mode-locked Nd-YAG laser operating at 10 Hz with an excitation energy of 2.3 eV. was used. The energy per pulse was approximately 10 μJ. The picosecond photocurrent signal was amplified with a 10 db Comlinear wide bandwidth amplifier and recorded by an EG&G Princeton Applied Research 4400 boxcar system (4420 boxcar averager, 4421 sampled integrator, and a 4402 signal processor) fitted with a Tektronix S4 sampling head (with a response time of 25 psec.). The jitter of the unit limits its response

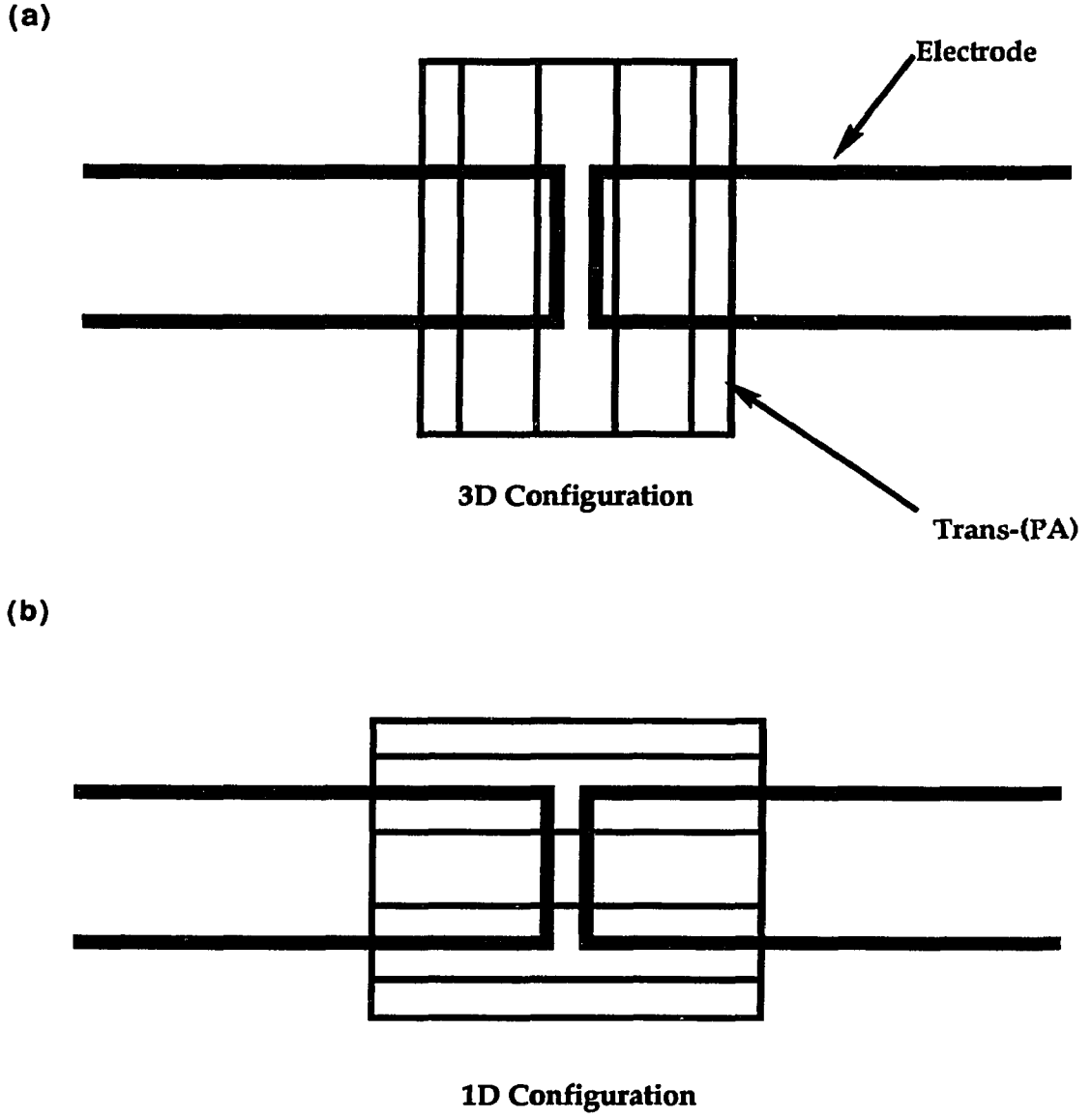

Fig. 4.1-1: Schematic representation of the a) 3D configuration (electrodes and applied electric field perpendicular to polymer chains) and b) 1D configuration (electrodes and applied electric field parallel to the polymer chains

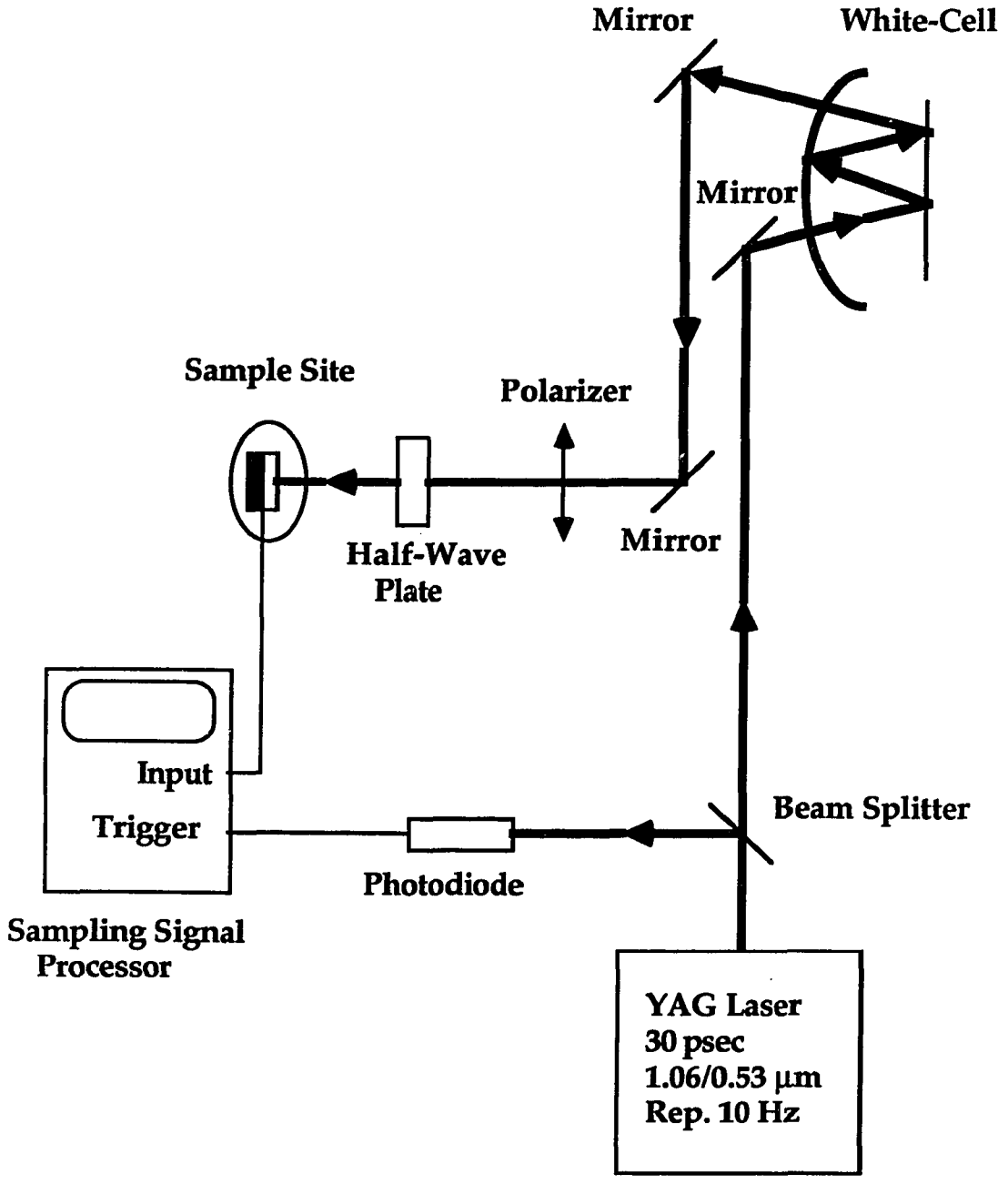

Fig. 4.2-1: Schematic diagram of experimental set-up for picosecond photoconductivity measurements.

time to approximately 90 psec. This sampling signal processor allows the acquisition of data, for signals that occur at repetition rates below 1 KHz, as compared to more conventional sampling scopes that need signal repetition rates of 1 KHz and greater.

As can be seen in Fig 4.2-1, the laser output passed through a glass slide which acted as a beam splitter (B.S.), reflecting 4% of the laser energy to a photodiode that externally triggered the sampling signal processor. The transmitted portion of the beam was delayed with respect to the triggering optical pulse by making several round trips through a white-cell. The delaying of the transmitted beam, was necessary to compensate for the trigger lag time, which is inherit in any electronic device such as the sampling scope. The beam then passed through a polarizer, and a half-wave plate and focused onto the sample site with a 7cm lens. The polarizer made sure that the beam remained linearly polarized after traveling through the directing optics. The half-wave plate was used to rotate the polarization of the incident beam.

A similar setup was used for the cw measurements. The photoexcitation in this case was achieved by a cw argon-ion laser. The maximum total incident light power was 15 mW.

4.3) Experimental Results

Illustrated in Fig. 4.3-1 is the linear I-V relationship (characteristic of ohmic contacts) of the dark current in the 3D configuration. The conductivity was found to be in the 10^{-6} - 10^{-7} $(\Omega\ cm)^{-1}$ range for both the 1D and 3D configurations. Figure 4.3-2

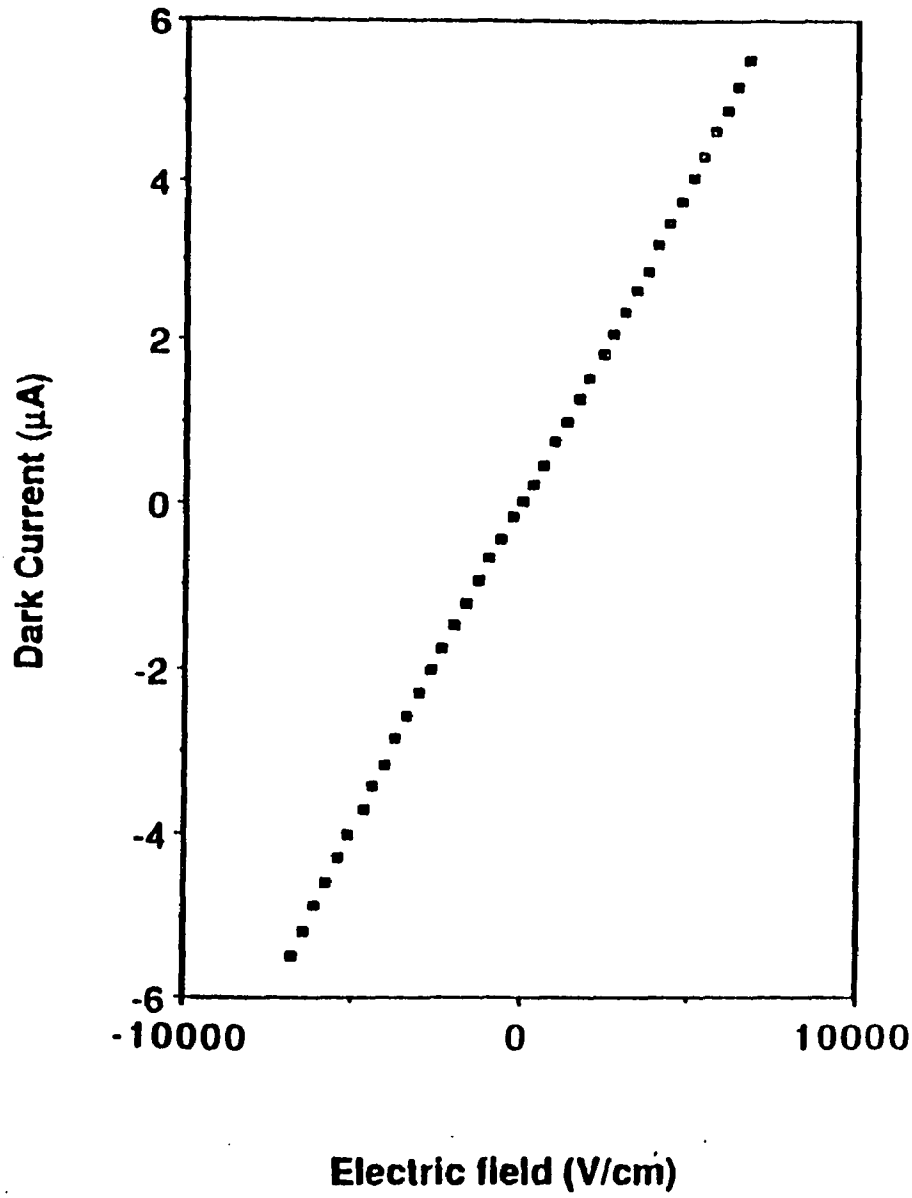

Fig. 4.3-1: Linear I-V relationship (characteristic of ohmic contacts) of the dark current of Trans-(PA) in the 3D configuration.

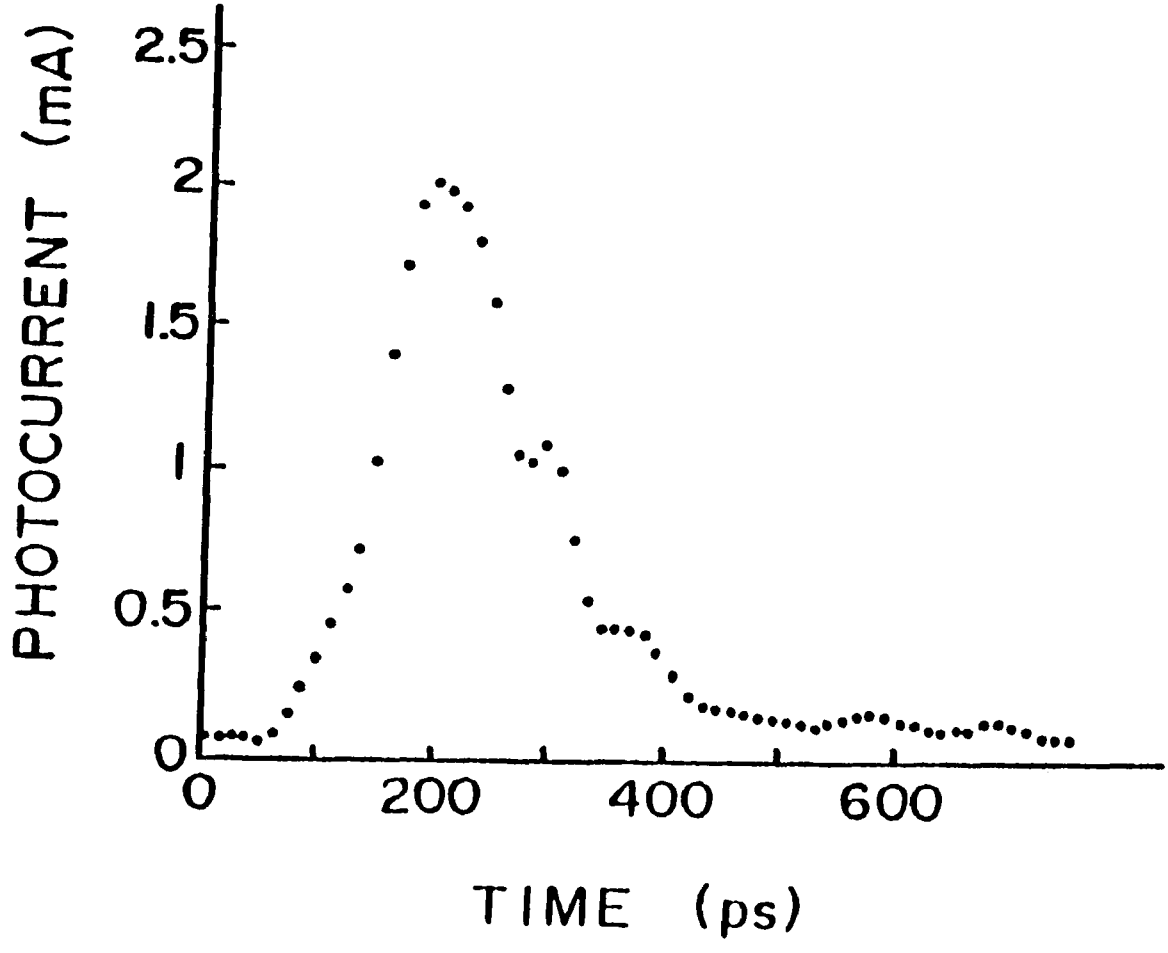

Fig. 4.3-2: Time dependence of the fast photocurrent in oriented trans-polyacetylene for the applied field parallel to the fibrils

shows the transient photoconductive response of HOTPA at room temperature. The sample was oriented according to the 1D configuration and the excitation pulse was polarized perpendicular to the stretching direction. The curve shows a fast risetime (approximately 80 ps) followed by a double exponential decay: a fast initial decay with a time constant of about 100 psec followed by a slower 400psec decay which includes the tail of the photoresponse. The photocurrent at the maximum of the experimental curve was about 0.2-0.25 mA (taking into account the 10 db amplifier) yielding a conductivity of approximately 0.04 S/cm. This value is two orders of magnitude smaller than the value found by Sinclair *et al.* in isotropic samples.

A similar curve was obtained when the excitation pulse was polarized parallel to the stretching direction, but the photocurrent magnitude was about 2.5 times weaker. This was expected and consistent with the cw data obtained by Dorsinville et al. [97] and confirmed by other authors in later experiments[149, 102]. A plausible explanation of this anisotropy is the difference in bimolecular recombination for the two polarizations because of the difference in penetration depth. Other explanations[64, 65, 66, 71, 72] have also been considered and assume, as we have discussed in the introduction, a small electronic transition moment perpendicular to the chains which gives rise to long-lived carriers created in different chains. Bleier *et al.*[72] have shown that the anisotropy decreases with increasing laser intensity, probably indicating an increase of the dark current which monitors a local heating of the sample.

The picosecond photoconduction measurements were repeated in the 3D configuration. The temporal shape of the photocurrent was identical to the 1D case with a peak value about 2 times smaller. The light polarization dependence was found to be similar to the 1D case.

Shown in figures 4.3-3 is the dependence of the picosecond photocurrent on the applied electric field for a sample of HOTPA in the 3D and 1D configurations for above-gap (2.34eV) excitation at an laser intensity of 54.6 MW/cm^2. There is a distinct difference in the field dependence of the 3D and 1D transient photoresponse. In the 3D configuration corresponding to a current flow perpendicular to the stretching direction (which is aligned with the polymer chains), the behavior of the picosecond photocurrent is linear becoming slightly superlinear at fields above 10 kV/cm. In the 1D configuration corresponding to current flow along the chains, the picosecond photocurrent appears to be superlinear from the start. The field dependence of the picosecond photoresponse of HOTPA in the 1D and 3D configurations for below-gap (1.17 eV) excitation at a laser intensity of 36.4 MW/cm^2, is similar to the above-gap response as is shown in Fig. 4.3-4. The below-gap photoconductive response of HOTPA will be dealt with in more detail later.

Figure 4.3-5 shows the temperature dependence of the photoconductivity for 1D and 3D configurations. The polarization of the excitation pulse was kept perpendicular to the stretching direction for both cases to keep the penetration depths identical and to get the strongest signal. In the 1D case (electric field parallel to chain) the fast photocurrent is practically independent of the

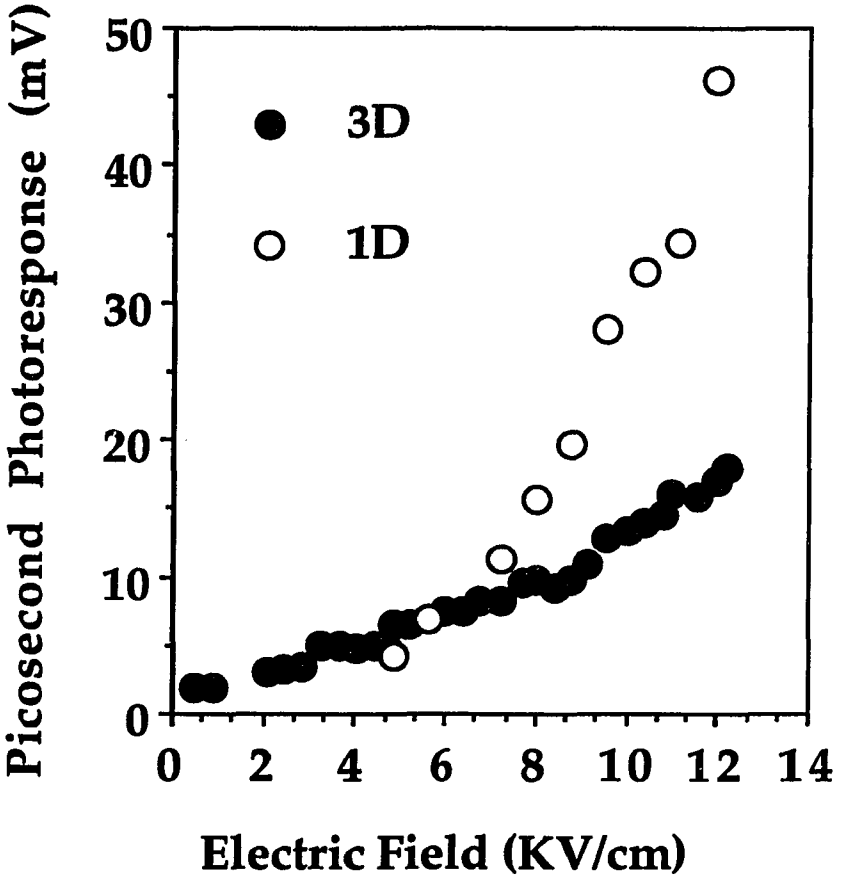

Fig. 4.3-3: Electric field dependence of the picosecond photocurrent of HOTPA in the 3D and 1D configurations for above-gap excitation (2.34 eV)

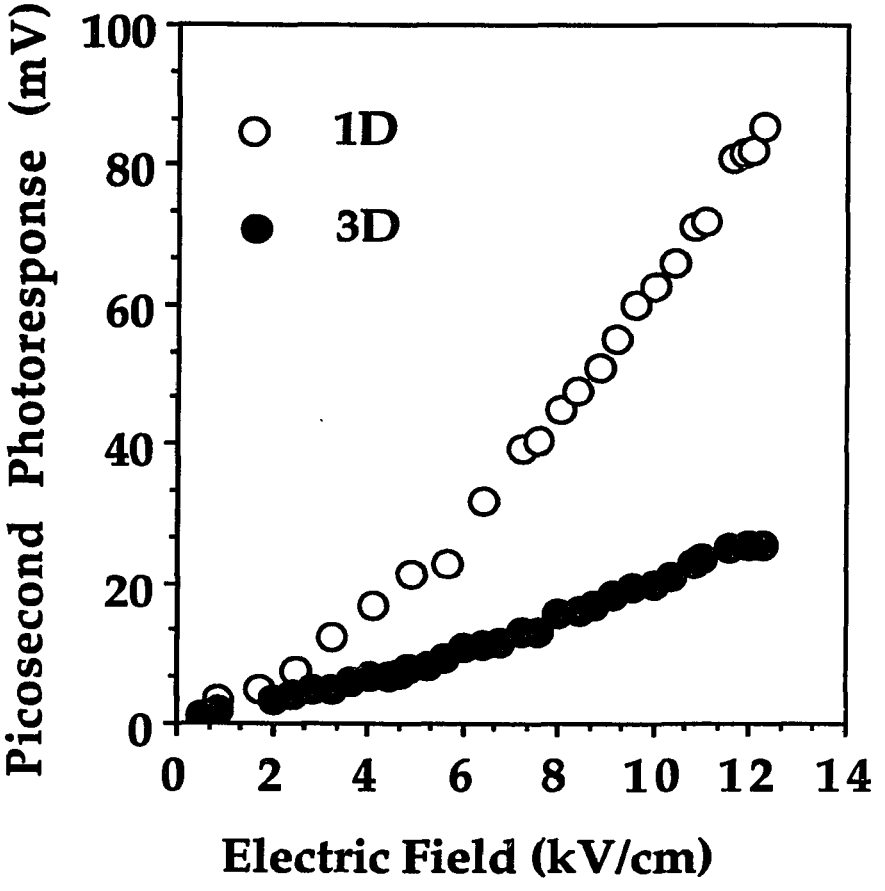

Fig. 4.3-4: Electric field dependence of the picosecond photocurrent of HOTPA in the 3D and 1D configurations for below-gap excitation (1.17 eV)

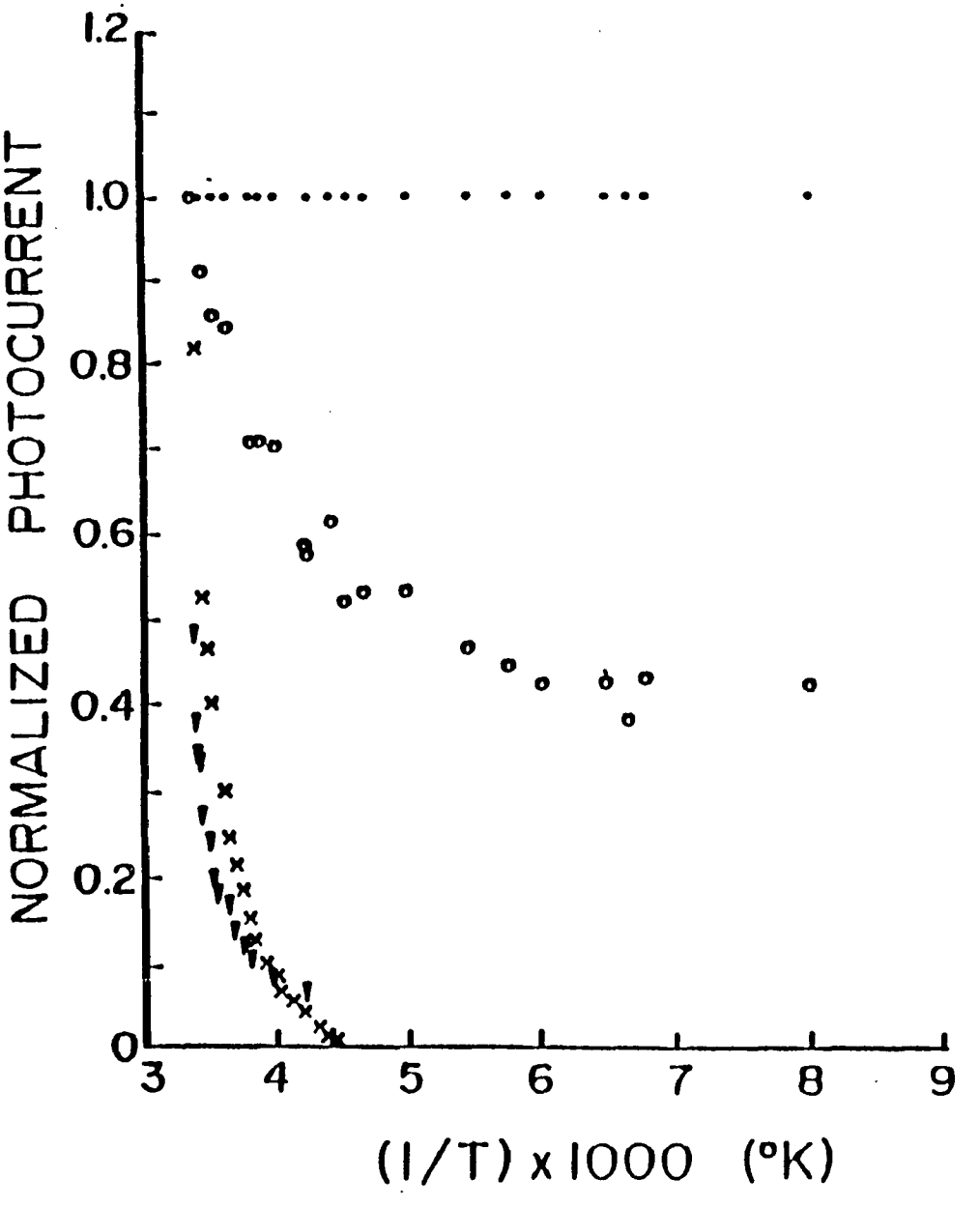

Fig. 4.3-5: Temperature dependence of the photocurrent in oriented trans-polyacetylene. [closed circle] 1D picosecond photocurrent, [open circle] 3D picosecond photocurrent, [x] 1D cw photocurrent, [triangle] 3D cw photocurrent.

temperature between 300 K and 100 K in agreement with both Sinclair *et al.*[68] and Bleier *et al.*[69] In the 3D case (electric field perpendicular to the chain) the fast photocurrent is temperature dependent between 300 and 200 K and reaches a constant background below 200 K. Laser heating effects, which could explain the lack of temperature dependence, can be ruled out for two reasons. One is that we still observe quite a large polarization anisotropy. The second indication that the sample is responding to the temperature changes, comes from the fact that only the 1D picosecond photocurrent is insensitive to the temperature, while the 3D picosecond photocurrent has a strong temperature dependence.

In figure 4.3-5 the magnitude of the steady state photocurrent as a function of temperature for the 1D and 3D configurations is plotted. These curves were obtained with cw excitation with a 30 mW Argon laser at 514 nm. The cw photocurrent shows a rapid decrease of the photocurrent with temperature, but the temperature dependence does not appreciably change upon switching the direction of the applied electric field.

Figure 4.3-6 shows a semi-logarithmic plot of the steady state and picosecond photoconductive response as a function of temperature for the 3D configuration. The low temperature constant background has been subtracted from the plot of the fast component. This background, which amounts to 20% of the fast 1D component, could be the result of the slight misalignment of the chains. Both picosecond and cw curves are linear with 1/T but with very different slopes. The activation energy in the steady state case was about 0.15 eV, and only 0.048 eV in the pulsed case.

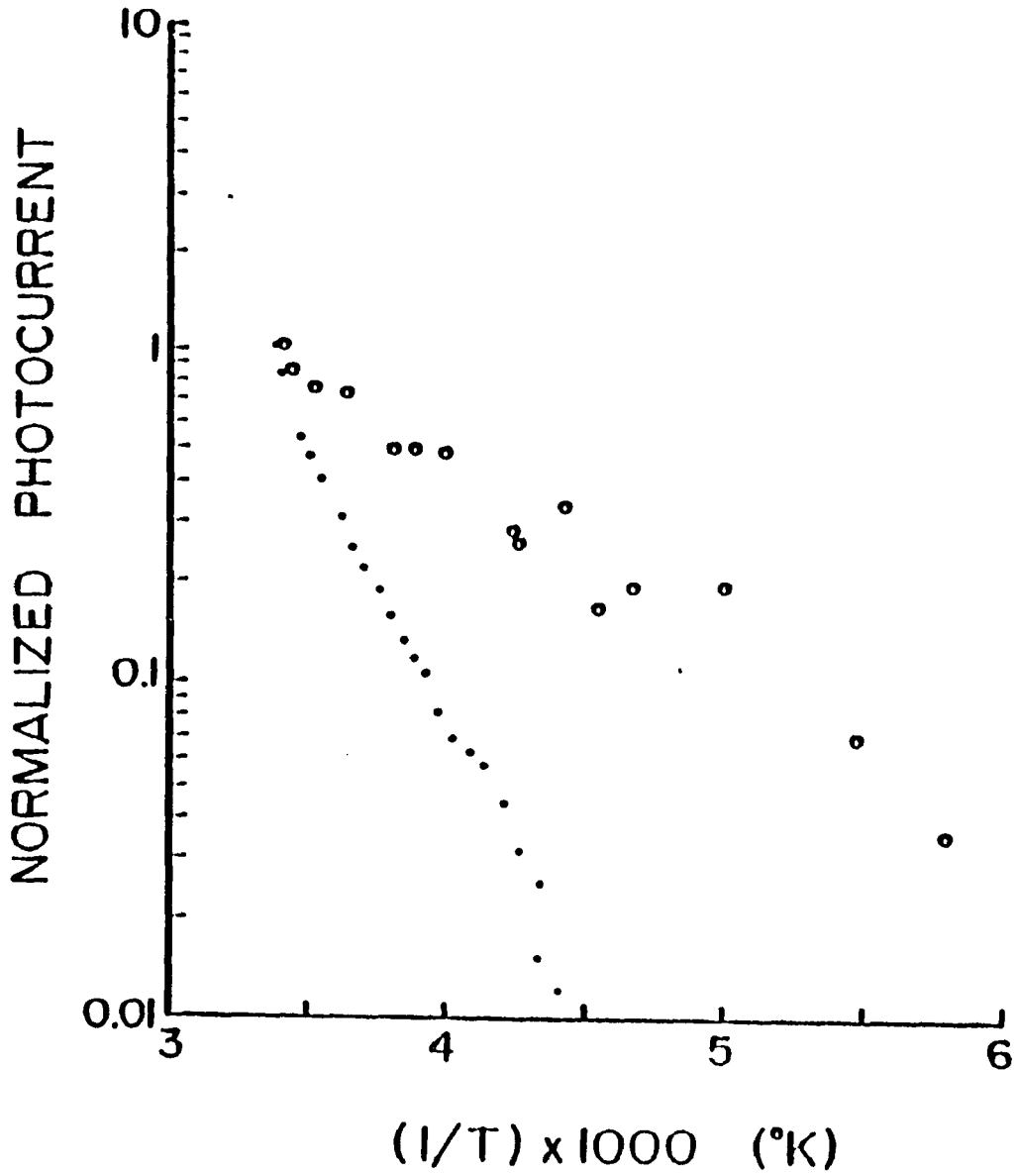

Fig. 4.3-6: Semilogarithmic plot of the temperature dependence of the photoconductivity [open circle] 3D picosecond photocurrent, [closed circle] 3D cw photocurrent.

4.4) Discussion

The discussion of the experimental results shall be presented in two parts, first we will look at the field dependence (I-V characterization) of the picosecond photoresponse and then the temperature dependence of both the picosecond and cw photocurrent. We will show that the picosecond photoconductive I-V characteristics for the 1D and 3D configurations can be modelled qualitatively by

$$\boxed{i_p \propto \eta \phi_{1D/3D}(r,E)E} ,$$

where η is the quantum efficiency for the conversion of each absorbed photon into an electron/hole pair, and $\phi_{1D/3D}$ which is dependent on the magnitude and direction (1D and 3D) of the applied electric field E, is the probability of the free charge carriers escaping geminate recombination.

Geminate recombination, is when a carrier recombines with the same partner it was originally liberated from (ie. an electron of an electron/hole pair recombining directly with the same hole).

i) 1D and 3D Picosecond I-V Characteristics

When a photon exceeding the energy band gap of HOTPA is absorbed, an electron-hole pair is formed, that is rapidly converted into a pair of oppositely charged solitons. Since the transition moment of the band-band transition is aligned with the chain

direction, most of the soliton-antisoliton pairs are created in the same chain. The photoconductive response depends on the free carrier lifetime, the mobility and the probability to escape geminate recombination. The latter two parameters should depend on the dimensionality of the carrier motion. In the following, we will show that the difference in the I-V characteristics for the 1D and 3D transport configurations can be accounted for, at least qualitatively, by considering the dimensionality (1D and 3D) dependence of the escape probability ϕ.

To account for the dependence of the escape probability on the direction of the applied field with respect to the chain direction, a model by Onsager[150 151] originally developed for electrolytic solutions (which are basically isotropic 3D), which studies the motion of oppositely charged carriers diffusing under the influence of an externally applied field, was used. This theory assumes that after each initial act of photoionization (photoexcitation), the positive and negative charge carriers thermalize rapidly, reaching during this process a certain initial separation (r_0). From there, a random walk is initiated under the influence of the mutual Coulomb field and the applied electric field, until the charge carriers either recombine (geminate recombination) or escape the Coulomb attraction, thus contributing to the photocurrent. An obvious limitation in the application of this model to polyacetylene is that it does not consider the coupling of the excess charge carriers with the lattice. However, the anisotropic version of Onsager's analysis has been proven effective in explaining the electric field, laser wavelength, and intensity dependence of the intrinsic steady state photocurrent in

polydiacetylenes [146], which are quasi-one-dimensional organic systems with similar properties. This suggested that the model could be used for a qualitative understanding of the photocurrent characteristics in polyacetylene.

On the basis that the theory of geminate (or initial) recombination reduces to the problem of Brownian motion of a particle in the presence of Coulomb attraction and the applied electric field, Onsager[150, 151, 152] has approached this problem by solving the equation of Brownian motion given by

$$\frac{df}{dt} = \frac{kT}{e}(\mu_1 + \mu_2)\, div\left[\exp\left(-\frac{U}{kT}\right) grad\, f \exp\left(\frac{U}{kT}\right)\right] \qquad (4.4\text{-}1)$$

where μ_1 and μ_2 are the mobilities of the two charge carriers, f is a probability function, and U is the Coulombic potential modified by the applied field and is given by

$$U = -\left(\frac{e^2}{4\pi\varepsilon r}\right) - eEr\cos\theta \qquad (4.4\text{-}2)$$

Using the boundary condition of zero initial separation between the electron and the positively charged center, the probability of

ionization under the steady state condition (df/dt=0) in the presence of the applied field is increased by ratio[153, 154]

$$\frac{P(E)}{P(0)} = \frac{J_1(j\alpha)}{j\alpha/2} = 1 + \frac{1}{2!}\left(\frac{\alpha}{4}^2\right) + \frac{1}{2!\,3!}\left(\frac{\alpha}{4}^2\right)^2 + \frac{1}{3!\,4!}\left(\frac{\alpha}{4}^2\right)^3 + \ldots \qquad (4.4\text{-}3)$$

where J_1 is the Bessel function of the first order and

$$\alpha = (e^3/\pi\varepsilon)^{1/2}\, E^{1/2}/kT \qquad (4.4\text{-}4)$$

If an initial separation between the electron and the positively charged center being ro rather than zero is used for the boundary condition, eq. (4.4-3) is modified to [153]

$$\frac{P(E)}{P(0)} = 1 + \frac{1}{2!}\left(\frac{\alpha}{4}^2\right) + \frac{1}{2!\,3!}\left(\frac{\alpha}{4}^2\right)^2\left(1 - \frac{2r_0}{r_c}\right) + \frac{1}{3!\,4!}\left(\frac{\alpha}{4}^2\right)^3\left(1 + 3!\,\frac{r_0^2}{r_c^2} - 3!\,\frac{r_0}{r_c}\right) + \ldots \qquad (4.4\text{-}5)$$

where r_c is the cut-off separation distance to separate the bound and the free carriers and is defined as the critical Onsager distance at which the Coulomb energy is equal to kT,

$$r_c = \frac{e^2}{4\pi\varepsilon kT} \qquad (4.4\text{-}6)$$

e being the electric charge, k the Boltzman constant, ε the dielectric constant of the medium, and T the absolute temperature.

Carriers which are within the separation distance $0 < r < r_c/2$ are bound charge carriers.

Onsager [150] has also calculated the probability $p(r,\theta,E)$. The expression is as follows[155, 156, 157, 153]

$$p(r, \theta, E) = \exp(-A)\exp(-B)\sum_{m=0}\sum_{n=0}\frac{A^m}{m!}\frac{B^{m+n}}{(m+n)!} \qquad (4.4\text{-}7)$$

where

$$A = \frac{e^2}{4\pi\varepsilon kTr} \quad , \qquad B = \left(\frac{eEr}{2kT}\right)(1+\cos\theta) \qquad (4.4\text{-}8)$$

Numerous investigators[158, 159, 160] have used the Onsager model to explain photoconduction and photogeneration processes in organic semiconductors. By defining ϕ_{po} as the ionization quantum yield (the efficiency of production of thermalized ion pairs per absorbed photon) and g(r,t) as the initial spatial distribution of thermalized pair configuration (separation between ions of each ion pair-or between electron and ionized donor), the carrier quantum yield (carrier generation efficiency) is given by

$$\phi_p(r_0, E) = \phi_{p0} \int p(r, \theta, E)\, g(r, \theta,)\, d^3 r \qquad (4.4\text{-}9)$$

By assuming ϕ_{po} is independent of the applied electric field and $g(r,\theta)$ is an isotropic delta function and is expressed as

$$g(r, \theta) = \left(\frac{1}{4\pi r_0^2}\right) \delta(r - r_0) \qquad (4.4\text{-}10)$$

substituting eqs. (4.4-7) and (4.4-10) in eq. (4.4-9) and carrying out the integration, the resulting expression for the escape efficiency of the charge carriers is given by [153]

$$\phi_p(r_0, E) = \phi_{p0}\left(\frac{kT}{eEr_0}\right)\exp(-A)\sum_{m=0}\frac{A^m}{m!}$$
$$x\sum_{n=0}\left[1 - \exp\left(\frac{-eEr_0}{kT}\right)\sum_{l=0}^{m+n}\left(\frac{eEr_0}{kT}\right)^l\frac{1}{l!}\right] \qquad (4.4\text{-}11)$$

The first few terms of equ. (4.4-11) can be written as

$$\phi_p(r_0, E) = \phi_{p0}\exp\left(-\frac{r_c}{r_0}\right)\left[\begin{array}{l} 1 + \left(\frac{e}{kT}\right)\frac{1}{2!}Er_c \\ \quad + \left(\frac{e}{kT}\right)^2\frac{1}{3!}E^2r_c\left(\frac{1}{2}r_c - r_0\right) \\ \quad + \left(\frac{e}{kT}\right)^3\frac{1}{4!}E^3r_c\left(r_0^2 - r_0r_c + \frac{1}{6}r_c^2\right) + \ldots \end{array}\right] \qquad (4.4\text{-}12)$$

Equation 4.4-12, is the all important expression for the probability of photoexcited carriers in the 3D configuration escaping geminate recombination.

Following Onsager's model, the probability that an absorbed photon creates a pair of free oppositely charged carriers is given by $\eta\phi$, where η is the probability of creation of a pair of hot carriers and ϕ is the probability of escaping geminate recombination. For

interband excitations, almost every absorbed photon creates a pair of thermalized carriers (thermalization distance r_0) bound by their mutual Coulomb attraction (η=1).

In the 3D configuration, assuming isotropic motion of the carriers in the lattice, the probability of escaping geminate recombination as a function of the electric field for a pair of carriers with a separation r_0 is given by equ. (4.4-12). This relation has been obtained under the assumption that the initial distribution of thermalized pairs is an isotropic function. Equ. (4.4-12) predicts that the escape probability is independent of the applied electric field for relatively high field values. But for sufficiently high applied electric fields, the escape probability increases first linearly and then saturates at the asymptotic value of 1. The source of this behavior is that at low fields, in the 3D case, the isotropic motion of the charge carriers is controlled by diffusion and there exist a finite probability that the carriers will escape geminate recombination, even in the absence of an electrical field.

This situation is quite the contrary when the carrier motion is restricted to one dimension. In this case, the probability of escape is zero in the absence of an applied electric field; as a diffusing carrier will always return to its origin and recombinate. For a better understanding of this point, consider the charge motion scheme of an electron/hole pair in a photoexcited 1D polymer illustrated in Fig. (4.4-1), where the parallel lines represent the chains of the highly oriented polymer. The X's represent recombination sites (ie. defects, trapped neutral solitons, etc.) in the polymer. The shaded area is the region enclosed by Onsager's radius (r_c). Photoexcited carriers

moving perpendicular to the parallel lines (polymer chains) are participating in 3D conduction, while those moving parallel to the lines (polymer chains) are involved in 1D conduction. Notice, in Fig. 4.4-1. there are two routes that a charge carrier can take: 1) The charge is captured by a recombination center thus escaping geminate recombination. 2) The motion resulting in geminate recombination. A photoexcited electron/hole pair can either recombine or be excited to where a diffusion of the electron along the the x-axis is possible. At $|x| > r_c/2$ electrons can be trapped by recombination centers or recombine directly with holes from other pairs (escaping geminate recombination). However, the presence of an applied field will greatly effect the probability of the photogenerated charge to escape geminate recombination. A 1D Onsager model for the photogeneration of charge carriers in molecular crystals with highly anisotropic, quasi-one-dimensional electronic conduction, has been worked out by Haberkon and Michel-Beyerle[161] (a similar model has been developed by Sokolic et al.[162]). These authors have consider the case of a one-dimensional random walk of carriers under the influence of an external field and an image force.

Under the double restriction $r_0 < r_c$ and $E < KT/er_c$, the escape probability for 1D takes the relatively simple form

$$\phi_{1D} = \frac{e r_0^2 E}{r_c kT} \exp\left(-\frac{r_c}{r_0}\right), \qquad r_0 < r_c, \qquad E < \frac{kT}{e r_c} \tag{4.4-13}$$

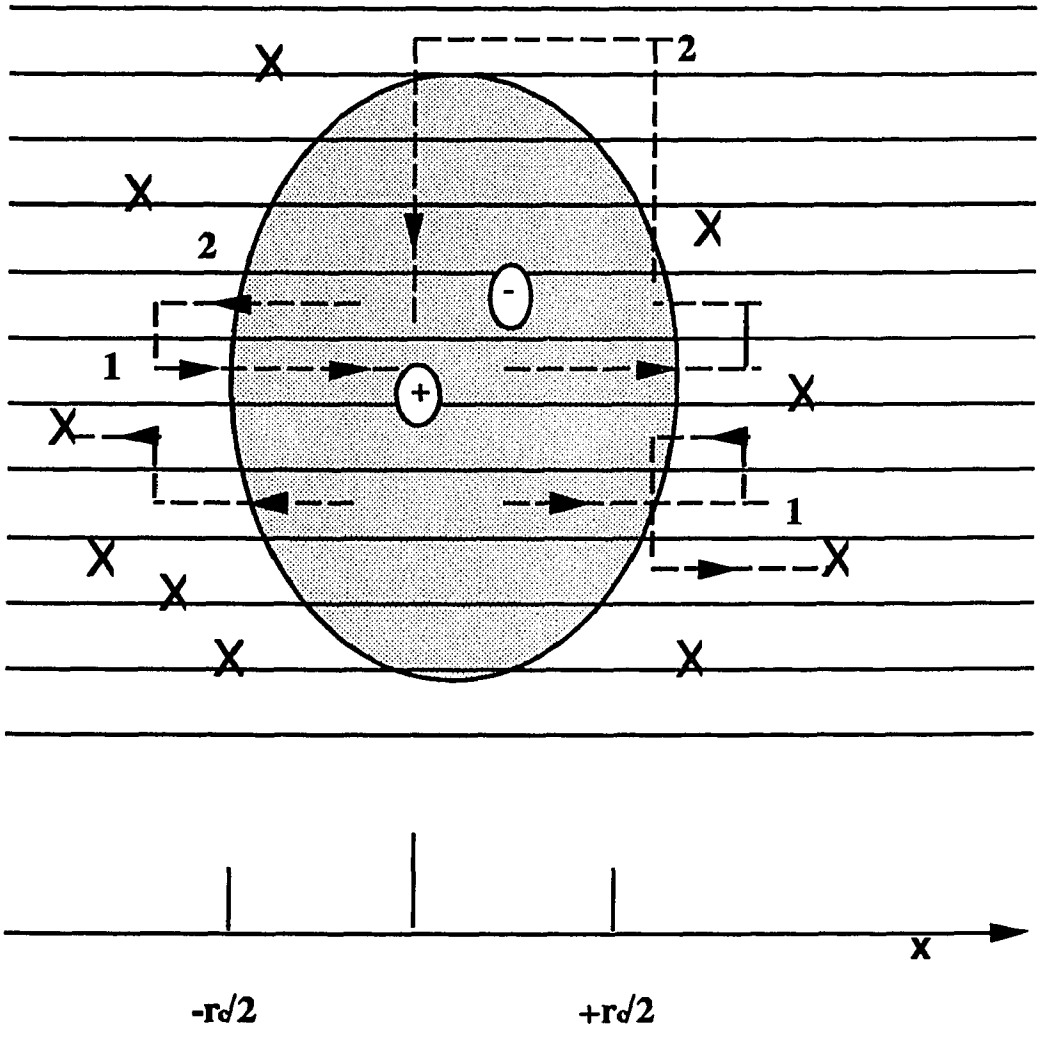

Fig. 4.4-1: Schematic representation of charge motion during initial separation in a quasi-one- dimensional system. Typical diffusion paths:1) charge is captured by a recombination center (X) thus escaping geminate recombination; 2) motion resulting in geminate recombination. Shaded area represents region enclosed by Onsager's radius. (I. A. Sokolik et al. Chem. Phys. Lett. 159, 113 (1989))

When the direction of the applied field (hence the direction of current flow) coincides with the stretching direction, the motion of the carriers can be considered essentially one dimensional and the escape probability is given by equ. (4.4-13) which varies linearly with E for low fields. When the applied field is perpendicular to the chains a more isotropic configuration is obtain and equ. (4.4-12) should be used. The distance r_0 of separation of the hot carriers in polyacetylene after thermalization for the isotropic case was evaluated following the treatment by Knights and Davies[163] for amorphous selenium.

The quantity

$$\Delta E = h\nu - E_g + e^2/4\pi\varepsilon r \qquad (4.4\text{-}14)$$

represents the excess kinetic energy of the hot carriers over the local potential. In equ. (4.4-14) E_g is the band-gap energy and r the initial electron-hole pair separation. This energy can be dissipated by electron-phonon scattering at a maximum rate given by $h\nu_p^2$. Assuming diffusive motion during thermalization, the electron-hole separation r_0 at the end of the thermalization process is given by the equation[164]

$$r_0^2/\Delta E = D/h\nu_p^2 \ , \qquad (4.4\text{-}15)$$

where D is the diffusion coefficient which can be evaluated from the mobility μ ($D = kT\mu/e$). Therefore, the parameters involved in the calculations are the mobility μ and the phonon frequency ν_p. For a

mobility μ estimated at 0.04 cm^2/V s and ν_p = 1000 cm^{-1} a value of 1.6 angstroms is obtain.

By inserting eq. (4.4-15) into eqs. (4.4-12) and (4.4-13) the dependence of the escape probability as a function of photon energy, applied field and temperature can be calculated. Fig. 4.4-2 shows the calculated dependence of the escape probability as a function of the applied electrical field in both the 1D and 3D configurations.

In a pulsed picosecond photoconductivity experiment the peak photocurrent i_p is given by[165]:

$$i_p = \eta\phi(1-R)(1-e^{-\alpha d})\frac{eV_b\mu P}{h\omega L^2} \qquad (4.4\text{-}16)$$

The important parameters are: ϕ which is the probability of escaping geminate recombination given by eqs. (4.4-12) (3D case) and (4.4-13) (1D case); η the quantum efficiency for the conversion of each absorbed photon into an electron hole pair; R the sample reflectivity; α the absorption coefficient; d the film thickness (for our sample $\alpha d \gg 1$); ω the photon frequency; $V_b = |E|L$ the bias voltage; L the distance between electrodes; E the applied electric field; P the pulse energy; and μ is the mobility. Eq. (4.4-16) predicts a linear dependence of the photocurrent versus the electric field when the escape probability is independent of the field such as in the 3D case and a superlinear dependence of the photoresponse for the 1D case.

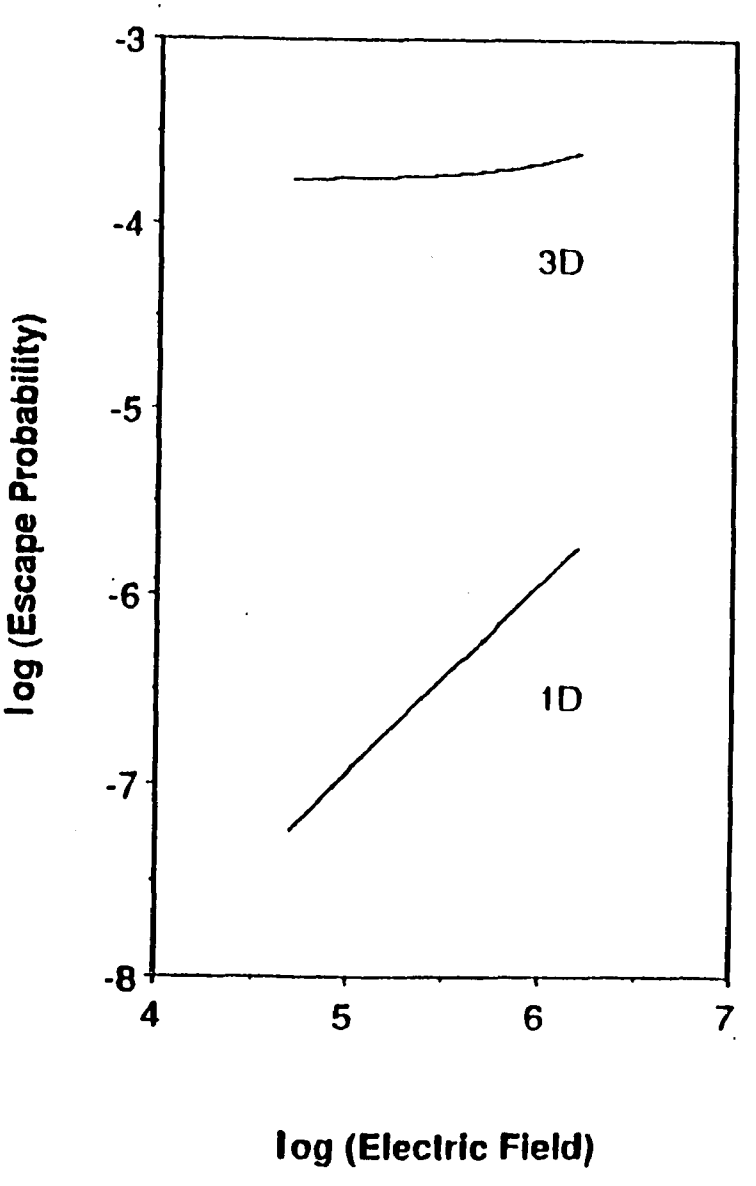

Fig. 4.4-2: Log-Log plot of the calculated escape probability vs electric field for the 1D and 3D case.

This is illustrated in Fig. 4.4-3. Experimentally, these two cases correspond to an Ohmic behavior of the photocurrent when the electric field is perpendicular to the stretching direction (3D) and a superlinear dependence when the electric field is parallel to the stretching direction (1D) as observed in the experimental results displayed in Figs. 4.3-3 and 4.3-4.

An obvious limitation of this interpretation is that the 1D and 3D cases are never perfectly realized in trans- polyacetylene. Deviations from the pure 1D behavior arise from the presence of

defects and chain terminations and/or the presence of interchain interactions due to nonvanishing values of the overlap integrals. Wilson[166] has given the expression for the 1D escape probability in the presence of defects which can act as traps for the carriers:

$$\phi_{1D} = [\, r_0/w + eEr_0/kT + O(E^2) \,]\, r_0/r_c \exp(-r_c/r_0) ,$$

$$r_0 < r_c , \quad E < kT/er_c , \qquad (4.4\text{-}17)$$

where w is the distance between traps along the chain. This equation indicates that even at zero field 1D is finite and given by

$$\phi_{1D} = \phi_{3D}\, (r_0^2/wr_c) \ . \qquad (4,4\text{-}18)$$

The purely 3D case is also not realized even when the field is applied perpendicular to the chains. For these reasons, stretched trans-polyacetylene films which consist of an assembly of 1D chains

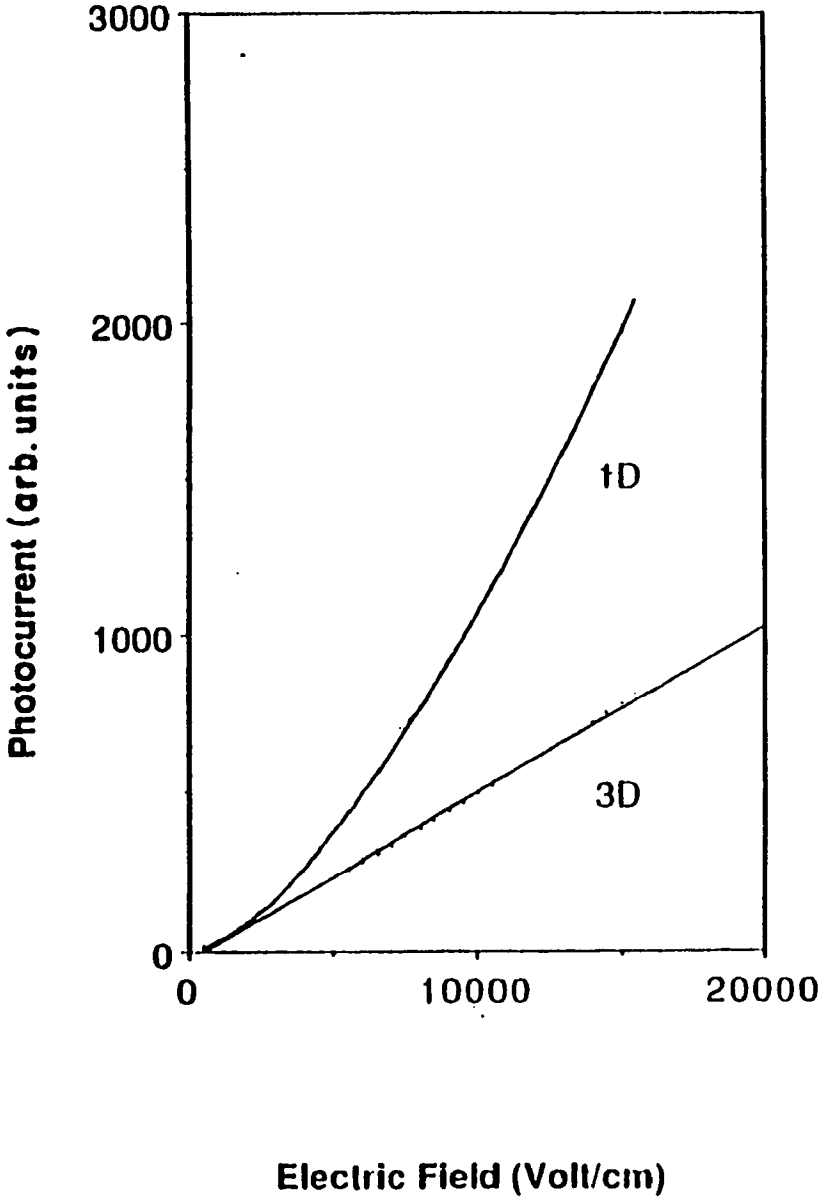

Fig. 4.4-3: Calculated photocurrent vs electric field for 1D and 3D case.

organized in a 3D network should exhibit a mixed type of dimensionality in which the parallel picosecond photocurrent should exhibit a quasi-1D behavior, while the perpendicular photocurrent should exhibit a quasi-isotropic behavior. The presence of defects, which disrupt the conjugation path thus reducing the 1D character of the charge transfer even for fields parallel to the chain, can be detected from the measured anisotropy of the dark current:

$$i_{\parallel} / i_{\perp} = \mu_{\parallel} / \mu_{\perp} = 25 \quad .$$

This value is considerably lower than the calculated anisotropy of the overlap integrals ($S_{parallel} = 0.23$, $S_{perpendicular} = 0.0027$ for the first intrachain and interchain neighbors respectively). This suggest that the chain terminations, cross links, and other chemical defects localize the carriers, reducing their mobility along the chain, while increasing the interchain transport as they act as hopping sites. It is interesting to note that the non-Ohmic behavior, characteristic of the quasi 1D photocurrent, is no longer observed in samples which were exposed to air for several hours. A reduction in the conductivity anisotropy is detected as well. The presence of defects in HOTPA seems to play a significant role in the temperature dependence of the picosecond photorespose. This point will be dealt with in the next section.

ii) Temperature dependence of the Picosecond Photocurrent

Figure 4.3-5 shows the temperature dependence of the cw and picosecond photoconductivity for the 1D and 3D configurations. The 1D fast photocurrent is practically independent of the temperature while the 3D fast photocurrent and the 1D and 3D cw photocurrent is temperature dependent .

The results can be qualitatively interpreted by considering the structure and morphology of polyacetylene films. These films are composed of fibrils of about 200 Å in diameter, which in the oriented sample, are aligned along a preferential (say Z) direction.[167] Within these fibrils the individual polyenic chains are arranged in a three dimensional lattice of high regularity. The conjugation length of the polyenic chains is limited by several chemical and structural defects such as cross links (carbon atoms with sp^3 hybridization) between neighboring chains, chain terminations, deviations from planarity and so on. The present of defects was considered above in the analysis of the I-V characteristics of HOTPA. From an electrical point of view a fibril can be considered as a bundle of segments of various length highly delocalized and weakly connected to each other. The physical structure plays a major role in the conductive properties of the polymer.

The peak picosecond photocurrent i_p is given by eq. (4.4-15) [165]. In the 1D configuration, most of the absorbed photons create pairs of oppositely charged carriers on the same chain. There is also a small but finite probability of direct interchain excitation. In any

case, the probability of escaping geminate recombination is higher, if the pair of carriers separate on different chains. After thermalization, the carriers which have escaped geminate recombination perform random walks along the chain. For a duration of time shorter than the time required for the carriers to hit the end of the segment in which they have been created, the carriers diffuses freely along the chain giving rise to band conduction along the Z direction.

For band conduction the Einstein relation for Brownian motion implies that μ should vary inversely with temperature ($\mu = \frac{eD}{kT}$) , D being the diffusion coefficient). Moreover, scattering processes of the diffusing carriers by optical and acoustical phonons should produce a temperature dependence of a variety of power laws[168] ($\mu \propto T^{-n}$).

Geminate (immediate) recombination is expected to be temperature dependent as shown in eqs. (4.4-12) and (4.4-13) Therefore, an exponential increase of the current with temperature is always expected. However, temperature independence of the picosecond 1D photoconductivity is somewhat puzzling as both the band conduction and the hopping conduction are expected to be strongly dependent upon temperature. It is therefore reasonable to assume that the initially photogenerated carriers have indeed unusual properties which are maintained only when they travel along the chain and prior to their capture at defect sites, supporting the widely accepted idea that the photogenerated charge carriers are solitons. [4] Indeed, a recent theoretical analysis has shown that the

mobility and lifetime of solitons do not depend much on temperature between 70 and 300 K.[169]

The situation for the picosecond photoconductivity perpendicular (3D) to the chain is somewhat different. For carriers on the chain, even the first step of their random walk motion will take place by phonon assisted tunneling, giving rise to perpendicular hopping conductivity. The carrier mobility will then have an Arrhenius form[170]:

$$\mu = \mu^{\circ} \exp(-E_A/kT) \qquad (4.4\text{-}4)$$

$$\mu^{\circ} = 1/6\, \nu_{ph} e R^2/kT \qquad (4.4\text{-}5)$$

where n_{ph} is the phonon frequency, R is the hopping distance and E_A is the activation energy for the hopping. In this case only polarons will be available to carry current because a single electron cannot jump from a chain to another and a simultaneous jump of a soliton/antisoliton pair is very unlikely indeed. According to Orenstein et al.[61] after hopping, the polaron is trapped by highly mobile neutral solitons, which are always present in undoped polyacetylene. Thus neglecting the temperature dependence of the carrier lifetime, one is led to conclude that the 0.048 eV activation energy observed for the fast, perpendicular photoconductive response (once the T independent background due possibly to chains misalignment has been subtracted) represents the activation energy for polaron hopping between neighboring chains.

The cw photoresponse is most likely controlled by the behavior of the charge carriers at long times. The measured T dependence which does not appear to be significantly affected upon changing the direction of the current flow, is more or less in agreement with the data obtained on isotropic samples by Etemad et al.[171] and by Sinclair et al. These authors quote an activation energy of 0.2 eV to be compared to 0.15 eV inferred from the present data. The activation energy controlling the slow response therefore appears to be substantially higher than the one needed for the hopping involved in the fast response.

A possible explanation for this behavior is based on the morphology of the polyacetylene films. At least three types of processes[172] contribute to the overall macroscopic cw conductivity, namely 1) band conduction associated with the carriers (possibly solitons) drifting along the chains before hitting defects of chain ends, 2) hopping of the carriers (polarons) between neighboring chains and 3) hopping of the carriers between fibrils. It can be reasonably assumed that this latter process is the one most severely limiting the macroscopic conductivity of the polymer as the interfibrillar distances are likely to be larger than the interchain separation. We can then conclude that the higher activation energy inferred from the T dependence of the cw response is related to the energy required for the interfibrillar hopping. These interparticle hops only control the long time photoconductivity since the early stages of the charge motion take place within the fibrill in which the carriers have been photogenerated.

Other explanations of the higher activation energy of the cw response are possible and involve the presence of defects and traps. Etemad et al. have suggested that at long times the remaining photogenerated solitons are trapped and the 0.15 eV - 0.20 eV is the activation energy required for electrons to hop from charged to neutral solitons. According to Kivelson[173] this mechanism predicts 3D conduction at low soliton concentrations, which is the case here. Therefore the present cw data, showing a negligible change of activation energy upon varying the direction of the dc field, supports both the interparticle hopping previously described, and the hopping of electrons from charged to neutral soliton suggested by Etemad.

We would like to give a possible reason for why the transient mobility we measured for highly oriented trans-(PA), is two orders of magnitude less than that measured for unoriented trans-(PA) by Sinclair et al.

The experimental set of Sinclair et al. was very similar to our. They used an Auston switch consisting of a 50 Ω microstrip transmission line (with a 0.2 mm gap in the upper conductor) fabricated by deposition of gold onto an alumina substrate. With a thin layer (approx. 0.1-0.2 μm thick) of trans-(PA) across the gap. On one side the switch was bias with 300 V, and the output signal was monitored with an PAR model 4400 boxcar system fitted with a Tektronix S-4 sampling head. A dye laser (PRA model LN105), pumped by a nitrogen laser operated at 8 Hz was used to produce 20 ps 1 μJ pulses at 2.1 eV. For an absorbed photon flux of 10^{15} cm^{-2} per pulse the photocurrent is 4 x 10^{-4} A with a 300 ps decay time. According to Sinclair this current corresponds to a conductivity of

about 0.3 S/cm. Using the following relationship for the photoinduced conductivity

$$\sigma_{ph} = (E/h\omega)e\eta\phi\mu \qquad (4.4\text{-}6)$$

where $(E/h\omega)$ is the number of absorbed photons per unit volume, $\eta = 1$ is the quantum efficiency, $\phi = 0.01$ is the probability to escape geminate (immediate) recombination, they calculated a mobility μ of approximately 1 $cm^2/V\text{-}s$ and a drift distance of about 400 angstroms in the measured decay time of 300 ps.

With picosecond time resolved photoconductivity it is possible to measure the mobility and relaxation time of the sample of interest. In those materials which have carrier relaxation times long enough to be resolved, the peak photocurrent is given by equation 4.4-1. The peak amplitude is proportional to the initial mobility and the slope of the initial relaxation of the displayed photocurrent yields an effective time constant for the relaxation of the carriers into localized states. For materials with carrier relaxation times faster than the time resolution of the oscilloscope, the photocurrent pulse is integrated to obtain the charge Q (the area under the photocurrent pulse displayed on the scope), in the pulse. The expression for the total charge Q is as follows [165]:

$$Q = \tau\eta\phi(1\text{-}R)(1\text{-}e^{-\alpha d})\frac{eV_b\mu P}{h\omega L^2} \qquad (4.4\text{-}7)$$

where η is the quantum efficiency for the conversion of each absorbed photon into a charge carrier. ϕ is the probability of escaping geminate recombination, R is the sample reflectivity, α is the absorption coefficient, d the film thickness (for our sample $\alpha d >> 1$), ω the photon frequency, V_b the bias voltage, L the distance between electrodes and P the pulse energy, μ is the transient mobility and τ is an effective time constant for the relaxation of the carriers. For this class of very fast materials the oscilloscope can at best measure the $\mu\tau$ product. To separate this product a high speed electronic correlation measurement [165] or some other method needs to be performed to determine the carrier relaxation time τ.

The short relaxation times observed in picosecond photoconductivity is due to the capture of photo-excited carriers by localized states (traps). These short relaxation times are not do to the transit time for carriers to drift from the point of generation to the electrodes. Carriers need not reach the electrodes in order to produce a current signal in the external circuit. Shockley used Green's reciprocation theorem of electrostatics to derive an expression for the induced currents which flow in the external circuit when a point charge is moving among the conductor. Equations 4.4-1 and 4.4-7 are the results of such an analysis. Hence, when a charge carrier is produced, there is induced an instantaneous current that is independent of the location of the charged carrier between the electrodes. The current remains constant until the carriers are immobilized or disappear by trapping or by discharge at the electrode.

It seems that Sinclair et al. calculated the photoinduced conductivity from the standard resistance R_s equation used in d.c. and steady state photoconductivity measurements:

$$R_s = L/A\sigma \qquad (4.4\text{-}8)$$

where R_s is the sample resistance, L is the length of the gap between the electrodes, A is the cross section of the sample, and σ is the photoconductivity. This equation assumes that the charge carriers drift from the generation point to the electrode. The net resistance R_t across the illuminated gap of a microstip transmission line is:

$$R_t = L^2/ N\eta\phi e\mu \qquad (4.4\text{-}9)$$

where L is the gap length, N is the number of absorbed photons, η is the quantum efficiency for the conversion of each absorbed photon into a charge carrier, ϕ is the probability of escaping geminate recombination, e is the electron charge, and μ is the transient mobility. Note the following: 1) $R_s \neq R_t$ and 2) R_t is proportional to L^2.

Our value of 0.04 $cm^2/V\text{-}s$ for the transient mobility of oriented trans-(PA) scales well with the mobility of amorphous silicon (RF Glow discharge Deposited) [165]. A picosecond 50 Ω optical switch with a 25 μm gap was used to measure the transient mobility of amorphous silicon(0.5 μm thick). The photocurrent decay time was 200 ps. For an incident pulse energy of 0.26 nJ (P_{avg} =21 mW, $1.4x10^{14}$ photons/cm^2, $7x10^{18}$ photons/cm^3, $1.2x10^{22}$ photons/cm^2s) and an electric field of $1.8x10^4$ V/cm (45 V), the peak value of the

photocurrent, i_p, is 0.4 ma. yielding $\eta\mu$ = 0.8 cm^2/V-s (η = 0.5). (Gap resistance: Dark, $R_d = 2x10^{11}\ \Omega$; Illuminated, $R_l = 2x10^5\ \Omega$). So with a voltage bias of 65 V, and an excitation energy of less than a 1 nJ the amorphous silicon switch was able to produce a photocurrent greater than that produced with the trans-(PA) switch (0.2 - 0.25 ma). Hence, it seems fitting that the charge carriers of amorphous silicon would have a higher mobility than that of oriented trans-(PA). In light of this, the value of 1 cm^2/V-s for the mobility of unoriented trans-(PA) calculated by Sinclair et al. is too large.

We can now calculate the mean drift distance (<x>=13 angstrom), the photoconductive gain ($G=2.6x10^{-6}$), and the photosensitivity (g=0.063 S/J), of our trans-polyacetylene optical switch with the following equations:

$$\langle x \rangle = \mu\tau E \qquad (4.4\text{-}10)$$

$$G = \mu\tau V_b/L^2 \qquad (4.4\text{-}11)$$

$$g = i_p/V_b P \qquad (4.4\text{-}12)$$

respectively.

4.5) Conclusion

The availability of oriented samples has enabled us to separate the contribution to the electrical transport properties coming from the motion of the charge carriers along (1D) and across (3D) the chains.

Our experimental findings on the photoconductive response of highly oriented trans-polyacetylene for above gap excitation can be summarized as follows:

i) The fast component of the photoconductivity parallel to the chains is temperature independent.

ii) The fast component of the photoconductivity perpendicular to the chains decreases exponentially with 1/T (E_A =0.048 eV).

iii) Both the parallel and the perpendicular cw photoconductivity decrease with 1/T exhibiting approximately the same activation energy (E_A =0.15 eV).

iv) The fast component of the photoresponse is roughly three orders of magnitude higher than the cw response. With a decay time of approximately 400 ps the mean drift distance of the charge carrier is about 13 angstroms.

v) The I-V characteristic curve of the 1D picosecond photoconductive response is superlinear for both above- and below gap excitation. The I-V characteristic curve for the 3D picosecond photoconductive response is linear. The dependence of the picosecond photocurrent on the direction of the carrier motion with respect to the polymer chain, was qualitatively accounted for by considering the dimensionality (1D and 3D) of of the escape probability $\phi(E)$, which stems from Onsagers model for electrolytic solutions..

The T independence of the fast component has been already reported by other groups. The present data on the oriented samples add the novel feature that only the parallel picosecond photoconductivity is T independent. This latter feature appears to indeed substantiate the claim that the initially photogenerated

carriers are quickly converted into soliton/antisoliton pairs [10]. However cw photoconductivity does not appear to be significantly affected by the T insensitivity of solitons.

In their recent study Roth and Bleier[69] have concluded that the distance traveled by the carriers before hitting an impurity is 35-50 Å. These authors conclude that the initial transport makes a negligible contribution to the overall conductivity, because charged solitons are a fast transient in the decay of the photoexcitation. Our cw data fully agrees with this conclusion as well as recent photoinduced absorption measurements[174], since they show that the soliton properties are exhibited only when the carriers drift along the chain and even then, only for the relatively short time (possibly a few picoseconds) needed to reach the end of the segment.

The short lifetime of the primarily photogenerated carriers (solitons), can also in our opinion be inferred from a recent study on the picosecond relaxation of the photoexcited states in polyacetylene carried out by Weidman and Fitchen[175]. By examining the relaxation of the photoexcitation in an isotropic sample in the time interval 1-100 ps, these authors were able to detect a transition time (t =25 ps) at which the exponent n of the power law decay, t^n, undergoes an abrupt change over from 0.5 to 0.3. The authors have interpreted the slower decay rate, as being associated with, the behavior of the carriers which perform thermally activated hopping from one segment to the next.

V Picosecond Photoconductivity Below Gap Excitation

5.1) Introduction

According to the Su, Schrieffer and Heeger (SSH) model, solitons can be photogenerated in trans-polyacetylene when an incident photon excites an e-h pair, and the lattice then distorts around the photogenerated charged carriers leading to a soliton-antisoliton (S^+S^-) pair. This model stimulated a host of experiments to challenge or prove the existence of solitons. The results of photoinduced experiments and simultaneous electrical conductivity and ESR measurements confirmed the predictions of Su and Schrieffer and also established the reversed spin-charge relationship of the soliton model [93] [176]. Theoretical calculations using the SSH or Takayama et al.[177] (TLM) models have shown that the energy to create a soliton at rest (E_S) was less than one-half the single particle gap (Δ). Therefore, direct photoproduction of soliton pairs at energies well below the principle interband absorption edge is possible as shown experimentally by Blanchet et al.[178].

The role played by nonlinear charge carriers such as solitons and polarons in the photoconductive response of trans-(PA) has been studied by several groups by comparing the excitation profile of the photoinduced absorption to that of the photoconductive response of the polymer [179, 147, 97, 145, 180]. The similarity between the two profiles is generally considered as evidence that charged solitons play a crucial role in the photocurrent of trans-(PA). However, most

of the past photoconductive experiments were performed with above gap ($h\omega > 2\Delta$) excitation where the charged soliton pairs are generated indirectly via electron-hole pairs. The photoconductive response of trans-(PA) with below gap excitation has received relatively little attention. In addition, there is strong evidence both from photoinduced absorption measurements and recent picosecond photoconductive measurements in trans-(PA) that the nature and characteristics of the charged carriers in trans-polyacetylene change rapidly with time. We have suggested, based on our temperature dependent picosecond photoconductive measurements in stretched samples, that the soliton like properties of photogenerated carriers in trans-(PA) are maintained only when they travel along the chains and for a duration of time shorter than the time required for the carriers to hit the end of the segment of the chain on which they have been created (for few picoseconds).

In this section, we have extended our temperature dependent picosecond photoconductive measurements in trans-(PA) with above gap excitation to include below gap excitation. Below gap ($hw < 2\Delta$) excitation has allowed us to reduce the generation of electron/hole pairs and isolate the possible contribution of charged solitons/polarons to the picosecond photocurrent.

5.2) Experimental Setup

The experimental setup for measuring the picosecond photocurrent for below gap excitation was similar to that shown schematically in Fig. 4.2-1, except that all the optics, such as the half-

wave plate, were suited for 1.06 μm (1.17 eV) optical pulses. To make sure that the HOPA sample was excited by only the fundamental (1.06 μm) output of the YAG laser, the KDP crystal was removed from the system. The excitation energy was approximately 36 μJ at a 10 Hz repetition rate and the applied bias was approximately 400 V.

5.3) Results

Figure 5.3-1 shows a semi-logarithmic plot of the fast photoconductive response as a function of temperature for the 1D (electric field parallel to the chain) and 3D (electric field perpendicular to the chain) case. The polarization of the excitation pulse (1.06 μm) was kept perpendicular to the stretching direction for both cases to keep the penetration depths identical and to obtain the strongest signal. In the 1D configuration the fast photocurrent is practically independent of the temperature between 300 and 160 K. In the 3D configuration the photocurrent decays with temperature between 300 and 200 K. The activation energy (E_a) in this region is approximately 0.063 eV. This response is very similar to that obtained for above gap excitation. Below 200 K there is a change of slope. This may be explained by assuming that the phonon activated hopping becomes relatively inefficient at low temperature and that tunneling through the barrier becomes the main mechanism for charge transfer between neighboring chains. Another possible explanation is that the change in slope is due to the contribution from misaligned chains. Shown in figure 5.3-2. is the linear

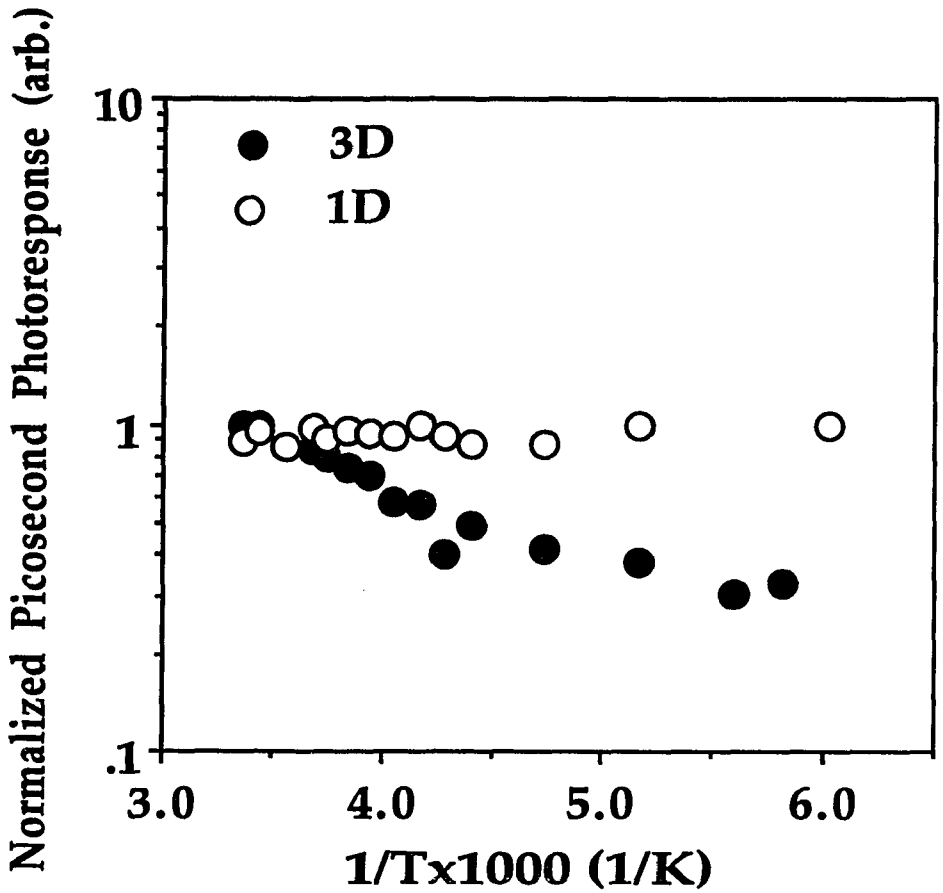

Fig 5.3-1: Semilogarithm plot of the temperature dependence of the 1D and 3D picosecond photoconductive response of trans-(PA) with below gap excitation.

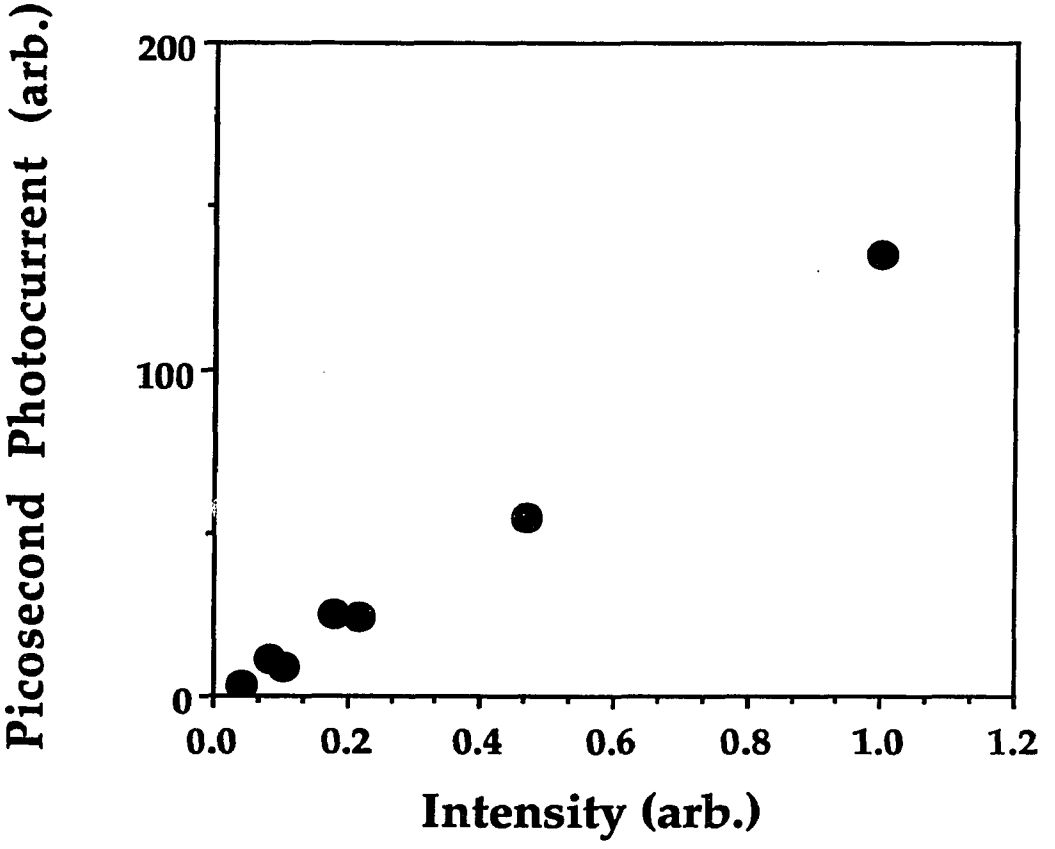

Fig 5.3-2: Intensity dependence of the Picosecond Photoconductivity of trans-(PA) with below gap excitation.

dependence of the picosecond photocurrent with respect to the intensity of the below gap (1.06 μm) excitation pulse at room temperature (300 K). This is characteristic of the photoresponse for both the 1D and 3D configurations.

5.4) Discussion

With oriented samples, it is possible to separate the contribution of charged carriers moving along from those moving across the polymer chains. The temperature dependence of the transient picosecond photoconductive response of stretched trans-(PA) in the 1D and 3D configurations for below gap excitation is very similar to our previous measurements with above gap excitation. The similarity of these two measurements imply that they arise from the same mechanism (solitons and polarons). For above gap excitation, the photogeneration of charged soliton pairs occur indirectly via an electron-hole pair. In the case of below gap excitation the photogeneration of the nonlinear charged carriers is direct. The energy gap (E_g) for trans-(PA) is approximately 1.8 eV. With an excitation energy of 1.17eV (1.06 μm) one would not expect the photoconductive response to occur except as a result of two photon absorption or through band-tailing. However, measurements of the photoconductivity under pressure have shown [86] that the absorption edge for trans-(PA) does not arise from static disorder or the associated band-tailing effect known in amorphous semiconductors. Two photon absorption cannot be totally ruled out, but earlier experimental results such as the observation of a threshold near the

soliton pair creation energy strongly suggest that the photocurrent at 1.17 eV is due to direct excitation of the charged carriers[181]. And the linear dependence of the photocurrent with respect to the laser intensity shown in figure 5.3-2 further substantiates the belief that direct excitation is the main photogenerating process occurring here [107].

Two other sources that may contribute to the fast photoconductive response of trans-(PA) with below gap excitation is the ionization of defect states (neutral solitons)[182] or impurity levels (charged states generated inadvertently during polymerization) located in the semiconductor gap. The contribution to the photocurrent by photoionization of the neutral soliton state is negligible as pointed out by Orenstein et al. [135] The impurities present in the film give rise to a dark conductivity found in the 10^{-6} - 10^{-7} $(\Omega cm)^{-1}$ range, which suggest that the sample was of good quality possessing a charge state density of less than 10^{18} cm^{-3} [183].

In the previous chapter, we reported that for above gap excitation ($h\omega > 2\Delta$) the picosecond photocurrent of stretched trans-(PA) was temperature independent in the 1D configuration (electric field parallel to stretching direction) and temperature dependent in the 3D configuration (electric field perpendicular to the stretching direction). The temperature independence of the transient photocurrent in the 1D configuration, violates both band conductionand hopping conduction since both are strongly dependent on temperature. It therefore seems reasonable to assume that the photogenerated carriers have unusual properties which are maintained only when traveling along the chain. It has been shown

through theoretical analysis that the mobility of solitons do not depend much on temperature between 70 and 300 K [169]. The explanation for the temperature dependence of the picosecond photocurrent in the 3D configuration is as follows. For carriers produced on the chain, the first step of their random walk motion would take place by phonon assisted hopping, giving rise to perpendicular hopping conductivity. In this case only polarons will be available to carry current because a single soliton can not jump from one chain to another and a simultaneous jump of a soliton/antisoliton pair is very unlikely. Thus one is led to conclude that the 63 meV activation energy (Ea) observed for the perpendicular picosecond photocurrent, represents the activation energy for a polaron to hop between neighboring chains.

The activation energy (E_a) in the 3D configuration for below gap (E_a= 63 meV) and above gap (E_a= 43 meV) excitations are of the same order of magnitude. The comparable values of the activation energy for both above and below gap excitation coupled with previous and present data strongly suggest that the charged carriers for both cases are the same. Also with below-gap excitation we have minimized the contribution of free electrons and holes to the transient photocurrent. The lower value of the activation energy for above gap excitation may be due to thermal heating by the incident optical pulse. For below gap excitation, heating effects should be much less important.

5.5 Conclusion

We have presented the first experimental study of the picosecond photoconductive response with below gap excitation of the highly oriented stretched trans-polyacetylene polymer. We have found that the transient 1D PC with below gap excitation is temperature independent as in our previous study with above gap excitation. And the transient 3D PC with below gap excitation is temperature dependent as in the case with above gap excitation. The activation energy of the 3D PC with below gap excitation is 63 meV. We have shown that the charged carriers that participate in the picosecond PC with above gap excitation are the very same carriers that are generated with below gap excitation. These results are further evidence that charged solitons and polarons probably play an important role in the transient photoconductive response of trans-(PA); and that these nonlinear carriers can be photogenerated by below gap excitation.

VI Picosecond Anisotropy Above and Below Gap

6.1) Introduction

Photoconductive and photoinduced absorption measurements in aligned trans-(PA) samples [184, 180, 185] using polarized excitation, helped to unravel the nature and characteristics of its mobile charge carriers. Bleier et. al.[186] studied the anisotropy of the picosecond photoconductive response of highly oriented Durham-Graz-type polyacetylene and found that the picosecond photocurrent with an excitation energy of 2.6 eV (above gap excitation) was about four times larger when the light is polarized perpendicular to the chains (after correcting for reflection losses the ratio reduced to 1.7). Bleir et al also claimed that the anisotropy ratio (1.7) is independent of both the excitation energy (from 1.7 to 3.2 eV.) and the intensity of the incident light.

In this section, we present evidence that under certain conditions the photoconductive anisotropy is strongly intensity dependent. Here, we show the results of a series of picosecond photoconductive measurements[187] which examines the anisotropy for both above and below gap excitation. We compare the above and below gap photoconductive responses of trans-(PA) in an effort to determine the nature and transport properties of the photoexcited charged carriers.

6.2) Experimental Set Up

The experimental setup for measuring the picosecond photocurrent was similar to that shown schematically in Fig. 4.2-1. The above gap photoexcitation was produced by 0.532 μm (2.4 eV), 25 ps pulses from a frequency doubled YAG laser. For below gap photoexcitation the fundamental frequency 1.06 μm (1.17eV) of the YAG was used. The maximum photon flux used in any experiment was approximately 6 x 10^{15} cm^{-2} (per pulse). A half-wave plate suited for each frequency was used to rotate the polarization of the optical pulses with respect to the stretching direction of the polymer. The optical switch was bias by a 400 V d.c. source, which is well within its ohmic range . The peak photocurrent was signal-averaged for approximately 100 shots using a boxcar integrator.

6.3) Results

Photoconductive measurements as a function of polarization (the angle between the optical electric field and the polymer chain) were carried out in the 1D configuration. The maximum signal is obtained in this configuration, for it has been shown by several groups that transport occurs primarily along the chain. The dependence of the photocurrent on polarization direction for the 1.06 μm and 0.53 μm excitation pulses are shown in Fig. 6.3-1. The incident photon flux density for the1.06 μm and 0.53 μm excitations are 0.036 GW/cm^2 and 0.043 GW/cm^2, respectively.

The anisotropy curve for above gap excitation (0.53 μm) has been normalized (to the number of absorbed photons) and corrected for any anisotropy that is due to reflectivity. Because of the sample thickness (approx. 20 μm), it is reasonable to assume that all incident photons that are not reflected are absorbed for above gap excitation. This was verified by measuring the transmission of the sample which proved to be opaque. However, for below gap excitation (1.06 μm) some of the incident photons are transmitted as well as reflected. Thus, the anisotropy curve was normalized and corrected for reflection, and transmission. θ is defined as the angle that the polarization of the optical field makes with the polymer chain (ie. the optical field is parallel to the polymer chain at θ=0 degrees and perpendicular at θ=90 degrees). The anisotropy ratio (defined as the ratio of the corrected photocurrent at θ=90 degrees to that at θ= 0 degree) for below gap excitation (1.06 μm) is approximately 2.4. The anisotropy ratio for above gap excitation (0.53 μm) is approximately 4.5. Any shifts of the minima or maxima from θ= 0 degrees or θ=90 degrees, respectively, in Fig. 6.3-1 is probably due to misalignment of the polymer chains with respect to the switch electrodes during the mounting of the sample. Note, the picosecond photoconductive response is maximum for perpendicular polarization for both the above and below gap excitations.

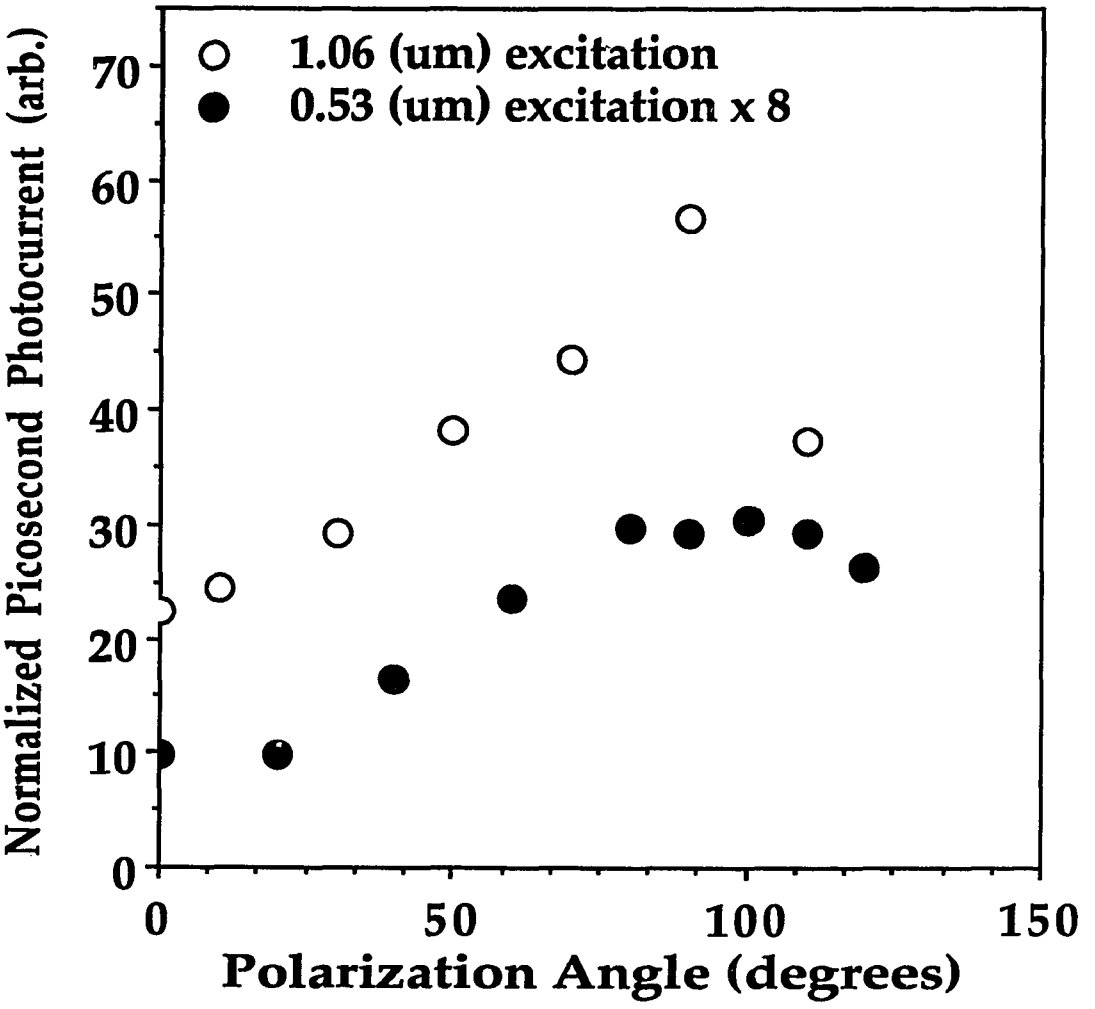

Fig. 6.3-1 Anisotropy of the corrected 1D picosecond photoconductive response with respect to the polarization of the incident above- (2.34 eV) and below- (1.17 eV) gap excitation . Notice, for proper scaling that 8x the above gap photoresponse is plotted.

In Fig. 6.3-2 the intensity dependence of the anisotropy ratio for above and below gap excitations is shown. Each curve has been corrected for the difference in absorbed photons, due to the polarization and frequency dependence of the reflectivity and transmission. There is a clear intensity dependence of the anisotropy ratio for above gap excitation, varying from 7.4 to 4.5. Note that the anisotropy ratio decreases as the intensity increases. The anisotropy ratio shown in Fig. 6.6-3 for below gap excitation is nearly independent of intensity at a value of approximately 2.4, in contrast to the above gap response. The intensity dependence of the picosecond photocurrent for below and above gap perpendicular excitation is shown in Fig. 6.3-3. Similarly shown in Fig. 6.3-4 is the intensity dependence of the picosecond photocurrent for below and above gap parallel excitation. In each figure the picosecond photocurrent is plotted with respect to the number of absorbed photons/cm^2. In Figures 6.3-3 and 6.3-4, the photocurrent is directly proportional to the laser intensity at each excitation wavelength and optical field polarization. In each case the photoconductive response is greater for below gap excitation. This point is dramatically illustrated in Fig. 6.3-4 where the actual photoconductive response for above gap parallel excitation has been multiplied by a factor of 5 and plotted.

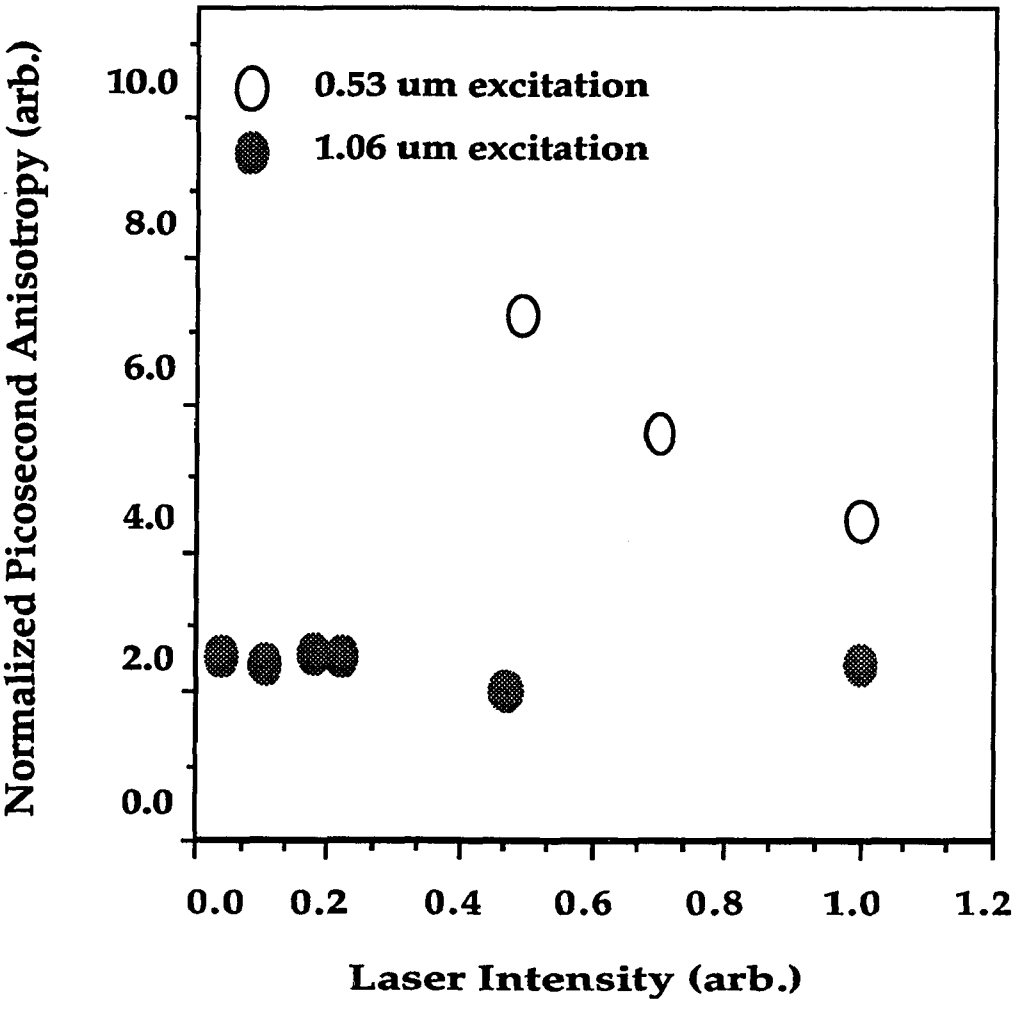

Fig. 6.3-2: Intensity dependence of the ratio of the transient photocurrent when the optical electric field is perpendicular to the chain, to that of the photocurrent when the electric field is parallel to the chain with a maximum laser intensity of 36.4 MW/cm2 and 43.3 Mw/cm2. respectively. Each curve has been corrected for reflection and transmission

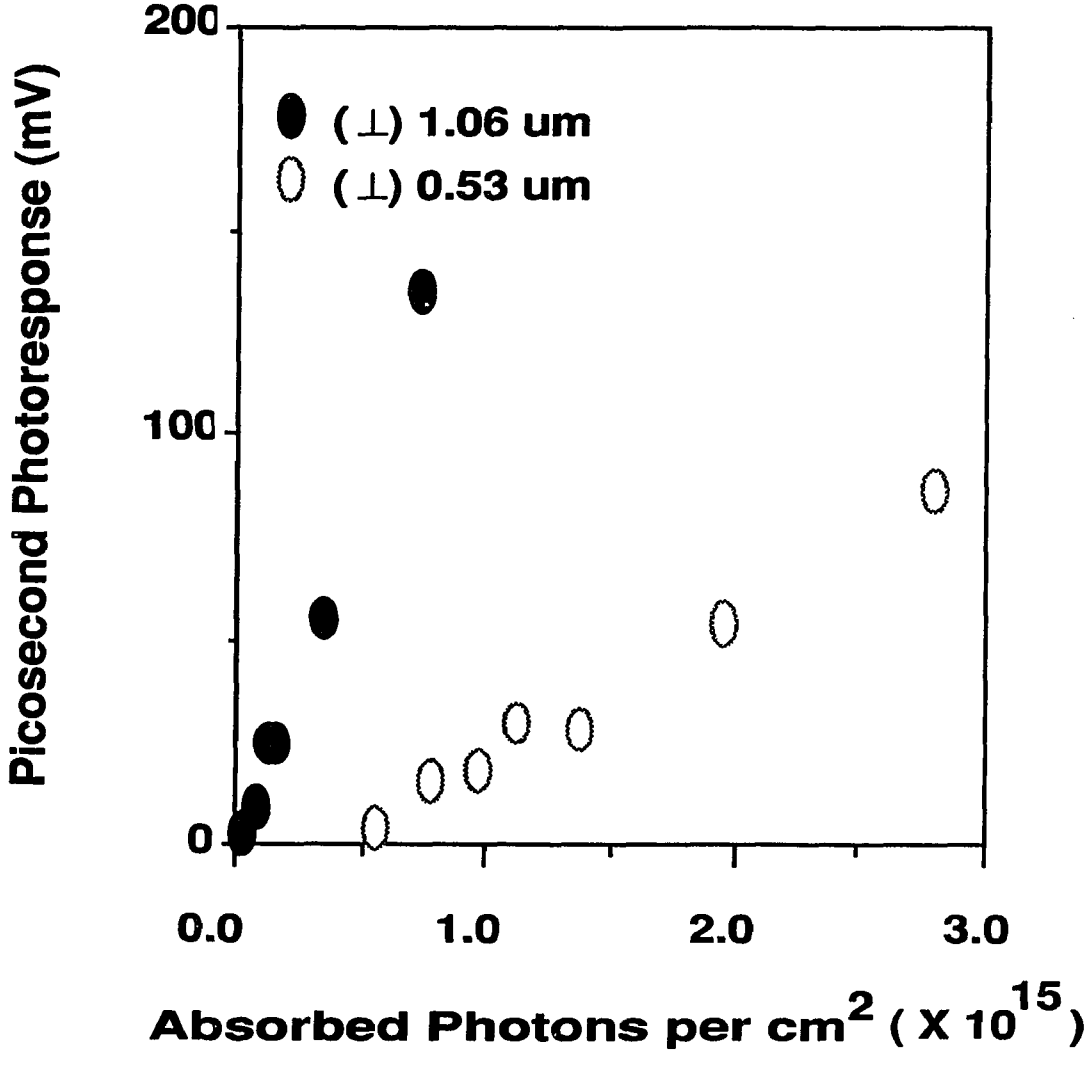

Fig. 6.3-3: 1D picosecond photocurrent with respect to the number of absorbed photons with perpendicular polarization of the above and below gap excitations.

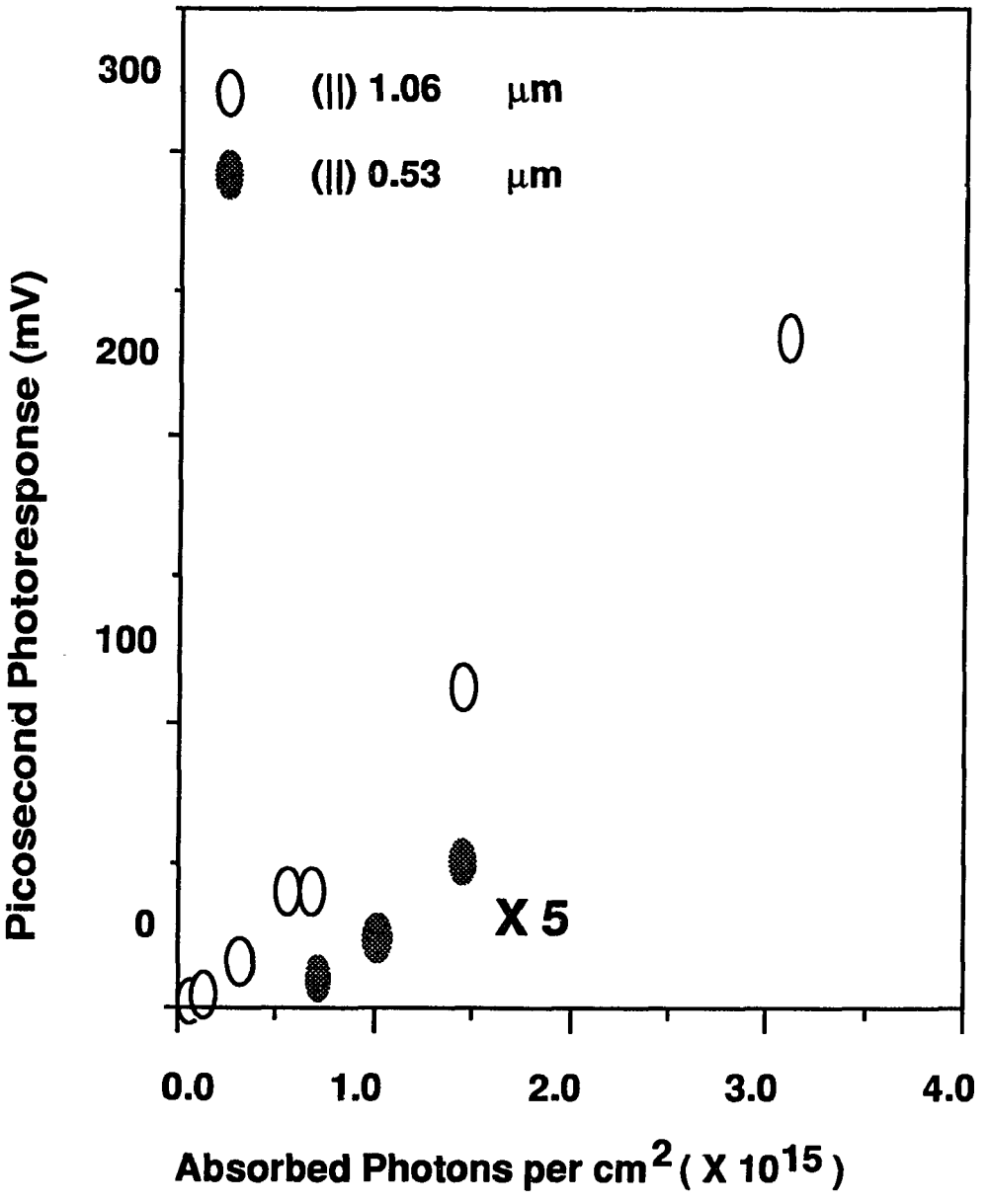

Fig. 6.3-4: 1D picosecond photocurrent with respect to the number of absorbed photons with parallel polarization of the above and below gap excitations. Notice, for proper scaling that 5 x the above gap photoresponse is plotted.

6.4) Discussion

The anisotropic character of charge transport in conjugated polymers arises from the large differences between intra and interchain overlap integrals. The large overlap between atomic wave functions along the chain gives rise to the formation of strong π covalent bonds, while small overlap between adjacent chains is responsible for the weak van der Waals bonding. This electronic structure is responsible for the electrical anisotropy (ie. ratio of the 1D photocurrent to the 3D photocurrent) of polyacetylene.

However, as previously discussed, trans-polyacetylene exhibits a so-called "pump anisotropy" for a given orientation of the applied dc electric field. The photoconductive response increases as the light polarization is changed from parallel to perpendicular with respect to the chain direction. This phenomenon which has been observed by various groups has received two different explanations. One school of thought is, the bimolecular recombination of the photocarriers, related to their topological nature (Dorsinville et al.; Blanchet et al.). In their model the polarization anisotropy is due to the difference in the nonlinear recombination for the two configurations (1D and 3D). The perpendicular and parallel absorption coefficients are 4×10^4 cm^{-1} and 6×10^5 cm^{-1}, respectively, at 2.4 eV, with the corresponding penetration depths of 25 μm and 1.7 μm [188]. Therefore, the penetration depth is much smaller and the charge density much greater for parallel excitation. Hence, nonlinear bimolecular recombination is more likely to occur for this polarization of the laser; reducing the number of charged carriers that participate in photoconduction. The opposite occurs with

perpendicular excitation where the charged carrier density is less, thus, allowing a greater number of the initially photogenerated charged carriers to contribute to the photocurrent.

The other model is related to the difference in geminate recombination rates between interchain and intrachain carriers in trans-(PA)[35]. Carriers created on different chains escape geminate recombination. With perpendicular polarization of the laser, more long lived interchain carriers can be directly photogenerated (Townsend and Friend; Bleir et al.)[189, 186]. The observation by Bleir et al., that the rate of decay of the slow photocurrent component is intensity independent seems to favour this interpretation. However, it is well known that only a small percentage of the initially photogenerated charged carriers contribute to the slow component. nonlinear bimolecular recombination may be affecting only the first stage of the dynamics of the charged carriers in trans-(PA) which occurs in the picosecond time regime. The slow component dynamics is mostly controlled by impurities and defects in the sample. Never the less, bimolecular recombination does not exclude direct photoexcitation of interchain carriers.

To explain the anisotropy of the photoconductive response of trans-(PA) with respect to pump polarization, a simple band structure model has been worked out with the help of Ricardo Tubino to compute the parallel and perpendicular absorption coefficients. A number of paper have appeared on this matter[190 191]. Ricardo and I present a relatively simplified model for interchain interactions which has the advantage of providing simple analytical expressions for the dipole moment components as function of only

one interchain parameter, therefore providing a simple semi-quantitative picture of the basic physics of the interchain coupling.

We assumed that self trapping of the photogenerated e-h pair into a soliton/antisoliton pair ($\tau_r=1/\Omega_{ph}$, Ω_{ph} is a typical phonon frequency) is much smaller than the interchain charge separation time ($\tau_h=h/\beta_x$, β_x is the interchain hopping integral), then the fraction $\varepsilon=(\tau_r/\tau_h)^2$ of the intrachain carriers will manage to transfer to different chains[192]. The basic assumption is then that only carriers that have separated on different chains or were created directly by interchain absorption can contribute to the overall photoconductive response' while carriers on the same chain or segment under go a quick (geminate) one-dimensional recombination. If this is the case, then the number of long lived carriers $N_{||}$ and $N_{\perp}$ created with parallel and perpendicular polarization of the beam to the chain respectively is described as follows:

$$N_{||}= (N\varepsilon)(1-R_{||}) \qquad (6.4\text{-}1)$$

$$N_{\perp}= N(\varepsilon +1-e^{-\alpha_{\perp}(10/\alpha_{||})})(1-R_{\perp}) \qquad (6.4\text{-}2)$$

where N is the number of impinging photons, ε is the quantum efficiency for interchain charge transfer (ε equal aprox. 0.01 according to Orenstein et al [135]) and $10/\alpha_{||}$ is the penetration depth of the radiation when it is polarized perpendicularly to the chains. This value for the penetration depth is estimated from the measured apparent perpendicular absorption which originates essentially from the chain misalignment.

According to Eq. 6.4-2 the number of long lived carriers created with perpendicular polarization depends on the perpendicular intrinsic absorption coefficient. To over come the difficulty connected with its direct measurement, we will outline a scheme used to evaluate the components of the transition moments by working out a simple extension of the tight binding model to include interchain interactions (Appendix II presents more details).

This model assumes linear chains organized in a three-dimensional crystal structure shown in Fig. (6.4-1) [193]. β_1 and β_2 indicate intrachain transfer integrals along the single and double bond respectively; β' the interchain transfer integral between chains within the unit cell and β_x, and β_y the transfer interchain integrals between translationally equivalent chains. It is apparent from the figure that $\beta_y << \beta_x$ and can be neglected. Moreover if one assumes that the transfer integral is proportional to the overlap integral[194] we get $\beta' << \beta_x$ because the overlap between p_z orbitals of the linear chain is very small (a p_z orbital points towards the nodal plane of the pz orbital of the neighboring chain of the same unit cell).

With these simplifications the matrix elements of the tight binding Hamiltonian becomes relatively simple and a basis of only two p_z orbitals needs to be considered:

$$\begin{vmatrix} \alpha - E & \beta_1 + \beta_2 \exp(-ik_z c) + \beta_x \exp(-ik_x a) \\ \beta_1 + \beta_2 \exp(-ik_z c) + \beta_x \exp(-ak_x a) & \alpha - E \end{vmatrix} \qquad (6.4\text{-}3)$$

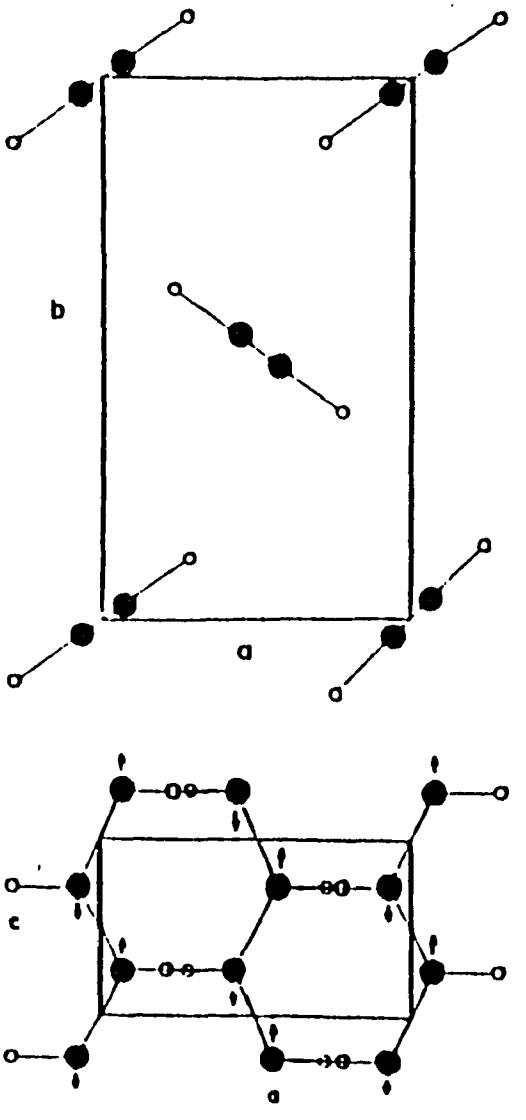

Fig. 6.4-1: Two schematic projections of the structure of Trans-(PA). a = 4.24 angstroms, b = 7.32 angstrom, c = 2.46 angstrom, and β = 91.5. The arrows are a schematic representation of the bond-alternation atomic displacements (from Fincher et al., 1982)

Diagonalization of this Hamiltonian yields both the band energies E and the wavefunctions which allow the calculation of the dipole transition moment using the equation[195]:

$$M_{nn'} = 1/V\int u_{n'k}(r)\,\nabla_k\, u_{nk}(r)\, d^3r \qquad (6.4\text{-}4)$$

where k is the wavevector corresponding to the optical vertical transition, V is the volume of the unit cell, $u_{n'k}$ is the unit cell periodic part of the Bloch wavefunction. Using this equation the following expression for the components of the transition moment are obtained:

$$M^x_{cv}(k)=(ia/4E^2)(E^2-E_0^2+\beta_x) \qquad (6.4\text{-}5)$$

$$M^z_{cv}(k)=(ic/4E^2)(E_0^2-E^2+\beta_2^2-\beta_1^2+\beta_2\beta_x\cos(\theta_c-\theta_a) \qquad (6.4\text{-}6)$$

where:

$$E_0^2=\beta_1^2+\beta_2^2+2\beta_2\beta_1\cos(\theta_c) \qquad (6.4\text{-}7)$$

$$E^2=E_0^2+\beta_x^2+2\beta_1\beta_x\cos(\theta_a)+2\beta_2\beta_x\cos(\theta_c-\theta_a) \qquad (6.4\text{-}8)$$

$\theta_a = k_x a$ and $\theta_c = k_c c$

Note that E_0 is the one dimensional energy band and $\pm E$ is the conduction/valence energy. Once the components of the transition moments are known the contribution to the optical susceptibility coming from the π electrons can be evaluated using the relation[196]:

$$\chi_\pi = \frac{2e^2\sigma}{\pi h}\int dk_z \int dk_x \frac{\Omega_{cv}(k)\left|M_{cv}(k)\right|^2}{\Omega_{cv}^2(k) - \left(\Omega - 1/\tau\right)^2} \qquad (6.4\text{–}9)$$

where e is the electronic charge and σ is the density of chains per unit cross area, $\Omega_{cv}(k)$ is the transition frequency and τ the lifetime of the optical excitation. The contribution coming from σ electrons is evaluated within the framework of the bond polarizability theory [192]. The value of the absorption coefficient can now be evaluated using standard relations which take into account local field corrections (Appendix II) [196].

We have computed the pump anisotropy at various energies (Table 1):

Table 1

Calculated "pump" anisotropies at various excitations

energy (eV)	$\alpha_{\|\|}$ (10^5 cm^{-1})	$\alpha_{\perp}$ (10^5 cm^{-1})	$\alpha_{\perp}/\alpha_{\|\|}$	$N_{\|\|}/N_{\perp}$
1.15	1.05	0.0018	0.0017	2.69
1.20	1.25	0.0024	0.0019	2.88
1.60	4.37	0.0424	0.0097	10.26
2.30	7.53	0.0260	0.0035	4.47
2.35	7.55	0.0256	0.0034	4.32

β_1=2.5 eV, β_2=3.3 eV, β_x=0.06 eV, $1/\Omega_{\|\|}$ =0.002 ps, $1/\Omega_{\perp}$=0.01 ps

This model predicts a pump anisotropy which is greater in the above gap region than in the below gap region in agreement with experimental findings. The model also predicts a substantial increase of the anisotropy in the gap region which has yet to be tested experimentally. The value β_x = 0.06 eV appears reasonable since the ratio β_x/β_2 compares favorably with the ratio between inter and intrachain overlap integrals[197].

The present data add the novel information that: 1) for above gap excitation the pump anisotropy depends on the intensity, 2) the below gap anisotropy is significantly smaller than the above gap anisotropy and is independent of the intensity and 3) the

photocurrent is greatest for below gap excitation. These results can be accounted for by using the bimolecular recombination model as follows: As the above gap excitation intensity increases, the charge density increases more rapidly for the perpendicular polarization of the laser than for the parallel polarization, reducing the above gap anisotropy ratio. The probability of generating free electron-hole pairs is greatly reduced with below gap excitation. Since, fewer photons are absorbed as well, this reduces the charged carrier density and the bimolecular recombination rate, for all polarizations. Hence, as the laser intensity increases, the relationship between the charge density for the perpendicular and parallel polarizations remain the same and in turn, the below gap anisotropy ratio is constant. This also explains why the below gap anisotropy is smaller than the above gap anisotropy. The role bimolecular recombination plays in reducing the number of charged carriers that participate in the picosecond photocurrent is made clear in Fig. 4 and Fig. 5. Here one can see that regardless of the polarization of the optical field (perpendicular or parallel) the photocurrent is always greatest for the case of below gap excitation where the bimolecular recombination rate is lowest.

The intensity dependence of the above gap anisotropy, is possibly influenced by heating effects following the laser pulse. A temperature increase is expected following illumination with above gap photons polarized along the polymer chains. Under these conditions the penetration depth is minimum ($d = 1/\alpha = (6x10^5)^{-1}$). Moreover, as we are considering short (25 picosecond) laser pulses, heat diffusion beyond the illumination volume can be neglected to a

first order approximation. The temperature increase following a pulse is given by

$$\Delta T = N\varepsilon/lc\rho$$

where N is the number of absorbed photons per cm^2 per pulse, l is the penetration depth, c is the specific heat, ρ is the density and ε is the photon energy. Assuming $N=10^{15}$ photons/cm^2 , $\rho=1.1$ g/cm^3, c=1 J/K° and $\varepsilon=2.34$ eV we get $\Delta T=263$ K° for parallel polarization. This heating following the pulse is large enough to increase the hopping conduction which has an activation energy of 0.05 eV. This could effectively reduce the above gap anisotropy as the laser intensity increases.

6.5 Conclusion

We have shown that the anisotropy ratio for above gap excitation decreases with laser intensity from a value of 7.4 to a value of 4.5 and that the anisotropy ratio for below gap excitation is independent of intensity at a value of 2.4. In addition, we find that the picosecond photocurrent is greatest for below gap excitation independent of the optical field polarization. An extended tight binding model that include the effects of coupling between the chains has been used to predict the anisotropy of the absorption coefficients of oriented trans-(PA). The pump anisotropy has been computed for various energies and is found to be greater in the above gap region than in the below gap region. The model predicts substantial increase of the anisotropy in the gap region as well. Both direct interchain photogeneration combined with laser heating effects and bimolecular recombination appears to account for the various features of the pump anisotropy experimentally observed.

VII Overall Conclusion

Polyacetylene a quasi one-dimensional organic semiconductor has received considerable attention from scientist and engineers because of the its relatively simple physical structure and seemingly endless technological applications. However, unlocking the treasures that lie within understanding the structure and properties (optical, electrical, etc.) of this materials is not a simple or easy task. This difficulty rest on several points: 1) The polyacetylene samples varies from research group to research group in quality and structure (fibrous, nonfibrous) depending on the technique (Shirakawa, Durham, Naarman-Theophilou, etc.) used to fabricate the polymer. This makes it a bit difficult to compare results between groups. Even samples produced with the same technique can vary considerably from one group to another. Thus the experimental results can vary as well. 2) Polyacetylene is not easy to handle because it reacts readily with air (surface oxidizes) and therefore must be stored in a vacuum or an inert gas atmosphere (ei. Argon, Nitrogen) away from intense heat and light. Care most be taken when transferring the polyacetylene sample from storage to the experimental site. The time the sample is exposed to air must be kept at a minimum. 3) The ideal structure of polyacetylene may be simple but the actual material has numerous defects and imperfections that effect and skew experimental results away from theoretical predictions. In

spite of these difficulties, a great deal of progress has been made in understanding this material.

We have studied the temperature, anisotropy, electric field, sample configuration (1D and 3D) and excitation energy dependence of the picosecond photoconductive response for above- and below-gap excitation of highly oriented stretched trans-(PA). Our experimental results can be summarized as follows:

i) The fast component of the photoconductivity parallel to the polymer chains (1D configuration) is temperature independent for both above- and below-gap excitation, respectively, 2.34 eV and 1.17 eV .

ii) The fast component of the photoconductivity perpendicular to the chains (3D configuration) decreases exponentially with 1/T for both above- and below- gap excitation each with an activation energy E_A of 48 meV and 63 meV respectively. Results i) and ii) leads us to believe two things: (1) Solitons and polarons are the main charge carriers in HOTPA. (2) These charge carriers can be directly photogenerated with below-gap excitation.

iii) Both the parallel and the perpendicular cw photoconductivity decrease with 1/T exhibiting approximately the same activation energy (E_A =0.15 eV).

iv) The fast component of the photoresponse is roughly three orders of magnitude higher than the cw response, with a decay time of approximately 400 ps. The transient mobility μ, is approximately 0.04 $cm^2/V\text{-}s$ along the chain. The mean drift distance of the photogenerated charge carriers $\langle x \rangle$, along the chain is about 13 angstroms, which is considerably smaller than previously estimated.

v) The I-V characteristic curve of the 1D picosecond photoconductive response is superlinear for both above- and below gap excitation. The I-V characteristic curve for the 3D picosecond photoconductive response is linear. The dependence of the picosecond photocurrent on the direction of the carrier motion with respect to the polymer chain, was qualitatively accounted for by considering the dimensionality (1D and 3D) of the escape probability $\phi(E)$.

vi) The intensity dependence of the picosecond 1D and 3D photocurrent varied linearly with the laser intensity, independent of the polarization and wavelength (0.53 μm or 1.06 μm) of the incident beam. These results implies that two photon-absorption does not produce the below-gap photoconductive response.

vii) The anisotropy with below gap excitation is constant at 2.4, while with above gap excitation it decreases from 7.4 to 4.5 as the laser intensity increases. We have also found that the photoconductive response is greatest for below gap excitation independent of the optical field polarization. The fact that the below-gap photoconductive response is greater than the above-gap response, further proves that two photon-absorption is probably not the source of the below-gap photocurrent. These results were accounted for by a combination of direct interchain generation, laser heating and bimolecular recombination.

VIII Future Research Directions

Rothberg et al.[198 199] measured the photoinduced 0.45 eV midgap absorption associated with photogeneration of charged solitons in trans-(PA). They found that the charged soliton absorption increases linearly with pump energy and then begins to saturate as higher pump fluences ($(1\text{-}2)\times10^{15}$ photons/cm^2) and were able to estimate the soliton lifetime at about 0.25 - 0.6 ps. The saturation was attributed to volume filling of the lattice by the photogenerated charged soliton pairs and is similar to bimolecular recombination. The similarity between the two model is that there is a limited amount of space available to the photogenerated charge carriers. Photoconductivity is proportional to the mobility μ and the number of photoexcitations, while photoinduced absorption is dependent on the number of photoexcitations alone. The best way to discern the difference in a change of mobility effect and a change in number of photocarrier effect, is to perform the picosecond photoconductivity and the femtosecond photoinduced absorption measurement simultaneously. As we can see from the soliton life time estimates of Rothberg et al (0.25 - 0.6 ps) our photoconductivity decay time (400 ps) is actually a convolution of numerous relaxations. One would like to look at the transient photoconductivity with the same time resolution (0.5 ps) of photoinduced absorption measurements in the 1D and 3D configuration at and below room temperature. It may be possible to determine directly the mobility of the charged solitons and polarons. One could determine the time dependence of the

charge carrier mobility and effectively identify the type of carrier by the magnitude of its mobility.

It is believed that optical phonons do not affect the drift rates of thermal soliton and polarons at room temperature and below because of their high energy. This idea is contested by others. Trans-(PA) possesses two strong Raman lines a 1121 cm-1 and 1521 cm-1. These lines are simultaneously induced with the midgap energybands and believed to be coupled to the soliton. Coherent excitation of either line while performing photoconductive measurements may allow direct observation of the interaction of solitons and polarons with optical phonons.

In chapter VI, our model predicts that the pump anisotropy is greater in the above-gap region than in the below-gap region and increases substantially in the gap region. With the appropriate tunable lasers (with sufficient power) it is possible to test these predictions. One might even repeat each of the experiments performed in this thesis, with photoexcitations throughout the visible spectrum into the far infrared region.

Appendix I - Theory of Picosecond Photoconductivity

A synopsis of the derivation [165] of the transient peak photocurrent will be given.

The transient photocurrent is not due to photogenerated carriers transversing from the point of generation to the electrode. The short relaxation times of the carriers are due to their capture by localized states (defects in the polymer). Electrons need not reach the electrodes to produce a current in the external circuit. Using Green's reciprocation theorem of electrostatics, Shockley[200] derived an expression for the induced current that flows in an external circuit connecting a system of conductors when a point charge is moving among the conductors. Assuming a space charge free conduction, the potential between the electrodes can be obtained from Laplace's equation.

$$d^2/dx^2\ V = 0$$

$$V = C_1 x + C_2$$

For a geometry as illustrated in Fig. (3.3-2-1) the boundary conditions are

(1) $V = V_b$; $x = -L/2$

(2) $V = 0 \quad ; \quad x = L/2$

The potential function is therefore

$$V = -V_b\, x/L + V_b/2 \qquad (1)$$

Green's reciprocation theorem states that if charges Q_1, Q_2, ...,Q_n on the conductor of a system give rise to potentials V_1, V_2, ..., V_n and if charges Q'_1, Q'_2, ..., Q'_n give rise to potentials V'_1, V'_2, ..., V'_n, then

$$\Sigma\, Qi\, V'i = \Sigma\, Qi'\, Vi$$

Green's reciprocation theorem was used to determine the charge induced on the electrodes by an electron-hole pair generated between the electrodes. Under the influence of the applied electric field, each carrier travels respectively towards the electrode of opposite polarity. The variables x_n and x_p are defined as the distance between the generated carrier and the electrode it is drifting towards for the electron and hole respectively. The bias electrode is referred to conductor 1 and the ground electrode conductor 4. Imagine two vanishingly small conductors placed at distance x_n from conductor 1 and x_p from conductor 4 and numbered 2 and 3 respectively.

Two problems are defined:

Problem (1). Let conductor 1 be at potential V_b, and conductors 2 and 3 be uncharged, and conductor 4 be at zero potential. The potentials and charges will satisfy the equations:

$V_1 = V_b$; Q_1

$V_2 = -V_b/L(x_n - L/2) + V_b/2$; $Q_2 = 0$

$V_3 = -V_b/L(L/2- x_p) + V_b/2$; $Q_3 = 0$

$V_4 = 0$; Q_4

Problem (2). Let conductors 1 and 4 be grounded and conductor 2 possess charge -e and conductor 3 possess charge e. The potentials and charges will satisfy the equations:

$V'_1 = 0$; Q'_1

V'_2 ; $Q'_2 = 0$

V'_3 ; $Q'_3 = 0$

$V'_4 = 0$; Q'_4

Green's reciprocations theorem yields

$$0 = Q'_1V_b + eV_b/L (x_n - L/2) - eV_b/2 - eV_b/L (L/2 - x_p) + eV_b/2$$

The induced charge is therefore given by

$$Q'_1 = Q(\text{induced}) = e - e/L(x_n + x_p) \qquad (2)$$

Note, that the induced charge increases as the distance between the charge carrier and the electrode decreases. As the charge carrier in the gap moves under the influence of the applied electric field, the magnitude of the induced charge in the electrodes change and it is

the rate of change of this induced charge that produces the current signal.

$$i(t) = d/dt\ [\ Q(\text{induced})\ ]$$

$$= d/dx\ [\ e - e/L(x_n + x_p)\ ]\ dx/dt$$

$$= -e/L(v_n + v_p)\ , \qquad (3)$$

where $v_n = \mu_n E$ and $v_p = \mu_p E$ represent the electron and hole drift velocities, respectively. Where μ_n and μ_p are the electron and hole mobilities respectively and E is the applied electric field. The moving charges induced a current i(t) in the external circuit which is proportional to their velocity. Thus, after a separated electron-hole pair is produced, there is induced an instantaneous current that is independent of the location of the electron or hole between the electrodes. The current remains constant until the carriers are immobilized by trapping (defects, impurities), geminate recombination or by discharge at the electrodes. The sign of the current is such that it reduces the stored charge of the electrode capacitance. For N electron-hole pairs,

$$i(t) = -Ne(\mu_n + \mu_p)E/L \qquad (4)$$

hence

$$i(t) = -Ne\mu V_b/L^2 \qquad (5)$$

where μ is defined as the average mobility of both the electrons and holes and V_b is the bias voltage.

The number of photogenerated carriers most be determine. From the continuity of light (Bouguer's Law), we find the decrease in its intensity when passing through a medium of thickness z

$$d/dz\ [I] = -\alpha(1-R)I\ , \qquad (6)$$

where α is the absorption constant and R is the reflectivity. Hence the fraction of the incident light intensity, I_0, transmitted through the medium as a function of z is

$$I(z) = (1-R)I_0\, e^{-\alpha z} \qquad (7)$$

The change in the generated carrier density per unit time may be described phenomenologically as

$$d/dt[n] + n/\tau = \eta\phi\alpha I/h\nu \qquad (8)$$

The right side of the equation represents the source of freed carriers by photoexcitation with η representing the quantum efficiency for generation and ϕ represents the probability of the photoexcited charge escaping geminate recombination. The second term on the left side of the equation n/τ is a damping term where τ is the relaxation time constant of the freed carriers into localized states. For picosecond excitation the initial laser intensity incident upon the

active region of the photodetector is approximated by a delta function,

$$I_0 = [\ P/(\pi L^2/4)\ ]\ \delta(t) \qquad (9)$$

where P is the optical pulse energy absorbed in the active region. Therefore we have,

$$d/dt[n] + n/\tau = \eta\phi\ (\alpha/h\nu)\ (1\text{-}R)\ [\ P/(\pi L^2/4)\ ]\ e^{-\alpha z}\ \delta(t) \qquad (10)$$

Integrating yields,

$$n(t) = \eta\phi\ (\alpha/h\nu)\ (1\text{-}R)\ [\ P/(\pi L^2/4)\ ]\ e^{-\alpha z}\ e^{-t/\tau} \qquad (11)$$

To obtain the number of optically excited carriers we must integrate the carrier density over the illuminated volume,

$$N(t) = \int_0^{L/2} 2\pi r\,dr \int_0^d n(t)\,dz \qquad (12)$$

where d is the film thickness

$$N(t) = \eta \frac{\alpha}{h\nu}(1\text{-}R) \frac{P}{\pi L^2/4} \int_0^{L/2} 2\pi r\,dr \int_0^d e^{-\alpha z}\,dz$$

subsequently

$$N(t) = \eta\phi\ [P/h\nu](1 - R)(1 - e^{-\alpha d})e^{-t/\tau} \qquad (13)$$

Substitution into eq. (5) yields

$$i(t) = e\eta\phi\ [P/h\nu](1 - R)(1 - e^{-\alpha d})\ \mu\ (V_b/L^2)\ e^{-t/\tau} \qquad (14)$$

Eq. (14) is used in a material with a relatively long carrier relaxation time. In such a material the time resolved peak amplitude of the photocurrent, i_p is used to determine the initial mobility. For example

$$i_p = i(t = t_{peak})$$

where t >> tpeak and $e^{-t/\tau}$ is approximately 1 and the expression for the transient photocurrent is as follow

$$i(t) = e\eta\phi\ [P/h\nu](1 - R)(1 - e^{-\alpha d})\ \mu\ (V_b/L^2) \qquad (15)$$

For those materials in which the carrier relaxation time is so fast that the peak amplitude of the photocurrent cannot be time resolved, the photocurrent is integrated to obtain the charge in the photocurrent pulse,

$$Q = e\eta\phi\ [P/h\nu](1 - R)(1 - e^{-\alpha d})\ \mu\tau\ (V_b/L^2) \qquad (16)$$

Equations 15 and 16 are the idealized photoresponse of the photodetector to a rectangular beam of circular cross-section focused to a radius L/2.

The illuminated gap resistance is

$$R_t = V_b/i_p$$

$$R_t = (h\nu/e) (L^2/\eta\phi\mu P) [1/(1 - R)] [1/(1 - e^{-\alpha d})] \quad (17)$$

Note, that R_t is proportional to L^2.

Appendix II - Electronic Absorption Spectrum Scheme

A scheme for evaluating the electronic absorption spectrum of a conjugated carbon chain, such as trans-(PA), will be presented here[201 202]. Flytzanis et al[203] addressed such a problem by using the one-electron tight-binding method to describe the π electronic states. They consider the case of a one dimensional crystal consisting of a single or two coupled infinite polyenic chains made of collinear carbon atoms. This assumption allowed only the evaluation of the components of the electronic transitions parallel to the chain. Here the formalism developed by Flytzanis et al. will be extended to include the effects of interchain coupling. The reduction of the band-gap energy and the appearance of a transition moment perpendicular to the chain should result do to interchain interactions. This has been shown experimentally by [86] Moses et al. with measurements of the photoconductivity under pressure. The electronic transition moment is given by

$$M_{nn'} = 1/V \int u_{n'k}(r)\, \nabla_k\, u_{nk}(r)\, d^3r \qquad (1)$$

where k is the wavevector corresponding to the vertical optical transition, V is the volume of the unit cell, $u_{n'k}$ is the unit cell periodic part of the Bloch wavefunction Φ:

$$\Phi_{nk}(r) = e^{ik\cdot r} u_{nk}(r) \qquad (2)$$

The crystal structure of trans-(PA) is shown in Fig. (6.4-1) . The unit cell contains two inequivalent matching [193] chains. The wave function Φ is constructed as a linear combination of the atomic orbitals belonging to the chains (tight binding approach):

$$\Phi_{nk}(r) = \left(N_1 N_2 N_3\right)^{-1/2} \sum_{l=1}^{N_1} \sum_{m=1}^{N_2} \sum_{n=1}^{N_3} e^{A(l,\,m,\,n)} B(l,m,n) \quad ,$$

$$A = k\bullet[\,(l-1)ai + (m-1)bj + (n-1)ck] \quad , \qquad (3)$$

$$B = c_1^{sk}\,\phi_{4l-3,\ 4m-3,\ 4n-3} + c_2^{sk}\,\phi_{4l-2,\ 4m-2,\ 4n-2} + c_3^{sk}\,\phi_{4l-1,\ 4m-1,\ 4n-1} + c_4^{sk}\,\phi_{4l\ 4m,\ 4n} \quad ,$$

where the ϕ's are the atomic wave functions for the p_z electrons, and c^{sk} are the expansion coefficients which can be determine by minimizing the total π electronic energy of the crystal. Inserting Eq. (3) into Eq.(1) and using the relation

$$\int \phi_i^{*} \times \phi_j \, d\tau = \delta_{ij} \qquad (4)$$

results in

being the x component of the electronic transition moment, with similar expressions representing the y and z components. Evaluation of Eq. (5) requires analytical expressions for the expansion

coefficients. With reference to Fig. (6.4-1) three interchain transfer parameters are seen to be present in polyacetylene, namely β_x, β_y (the transfer integral between translationally equivalent chains in the x and y directions), and β' (the transfer integral between chains in the unit cell). Neglecting β_y because b >> a, and using the Bloch theorem, we obtain the following set of equations for the c's:

$$(\alpha_1\text{-}E)\, c_1 + \beta c_2 + \gamma\, c_3 + (\gamma + \beta' e^{-i\theta c}) c_4 = 0, \qquad (6a)$$

$$\beta' c_1 + (\alpha_1 - E) c_2 + (\gamma + \beta' e^{-i\theta c}) c_3 + \gamma c_4 = 0 \qquad (6b)$$

$$\gamma^* c_1 + (\gamma^* + \beta' e^{-i\theta c}) c_2 + (\alpha_1\text{-}E)\, c_3 + \beta c_4 = 0 \qquad (6c)$$

$$(\gamma^* + \beta' e^{-i\theta c}) c_1 + \gamma^* c_3 + \beta' c_3 + (\alpha_1\text{-}E) c_4 = 0 \qquad (6d)$$

where

$$\alpha_1 = \alpha + 2\beta_x \cos\theta_a \ , \qquad (7a)$$

$$\beta = \beta_1 + \beta_2 e^{-i\theta c} + 2\beta_x \cos qa \ , \qquad (7b)$$

$$g = \beta'(1 + e\text{-}e^{-i\theta a})(1 + e^{-i\theta b}) \ , \qquad (7c)$$

$$\theta_a = k_x a; \quad \theta_b = k_y b; \quad \theta_c = k_z c \ . \qquad (7d)$$

Only if the terms $\beta' e^{-i\theta c}$ are neglected can a four-band analytical solution of Eqs. (7) be found. We shall concern ourselves with the two-band solution, which is obtained by putting $\beta' = 0$ (no interactions within the unit cell). Hence, the problem becomes a two dimensional one, with $M_{cv}(k)$ having only x and z components. The

following expression for the components of the transition moment are:

$$M^{x}_{cv}(k)=(ia/4E^2)(E^2-E_0^2+\beta_x) \quad (8)$$

$$M^{z}_{cv}(k)=(ic/4E^2)(E_0^2-E^2+\beta_2^2-\beta_1^2+\beta_2\beta_x\cos(\theta_c-\theta_a) \quad (9)$$

where:

$$E_0^2=\beta_1^2+\beta_2^2+2\beta_2\beta_1\cos(\theta_c) \quad (9a)$$

$$E^2=E_0^2+\beta_x^2+2\beta_1\beta_x\cos(\theta_a)+2\beta_2\beta_x\cos(\theta_c-\theta_a) \quad (9b)$$

$\theta_a= k_x a$ and $\theta_c= k_c c$

Note that E_0 is the one dimensional energy band and $\pm E$ is the conduction/valence energy. Once the components of the transition moments are known the contribution to the optical susceptibility coming from the π electrons can be evaluated using the relation [203]:

$$\chi_\pi=\frac{2e^2\sigma}{\pi h}\int_{-\pi/c}^{\pi/c} dk_z \int_{-\pi/a}^{\pi/a} dk_x \frac{\Omega_{cv}(k)\left|M_{cv}(k)\right|^2}{\Omega_{cv}^2(k)-\left(\Omega-1/\tau\right)^2} \quad (10)$$

where e is the electronic charge and σ is the density of chains per unit cross area, $\Omega_{cv}(k)$ is the transition frequency and τ the lifetime of the optical excitation. The value of the absorption coefficient can now be evaluated using standard relations, which take into account local field corrections to the perpendicular component of the dielectric constant:

$$\varepsilon_{\|} = 1 + 4\pi\chi_{\|}, \tag{11a}$$

$$\varepsilon_{\perp} = [1 + 2\pi\chi_{\perp}] / [1-2\pi\chi_{\perp}] \tag{11b}$$

$$\chi_{\|} = \chi_{\pi}^{\|} + \chi_{\sigma}^{\|} \tag{11c}$$

$$\chi_{\perp} = \chi_{\pi}^{\perp} + \chi_{\sigma}^{\perp} \tag{11d}$$

$$n = \{(1/2)\ [\varepsilon_1^2 + \varepsilon_2^2]^{1/2} + \varepsilon_1\}^{1/2} \tag{11e}$$

$$\kappa = \{(1/2)\ [(\varepsilon_1^2 + \varepsilon_2^2)^{1/2} - \varepsilon_1]\}^{1/2} \tag{11f}$$

$$\alpha = 2\omega\kappa/\chi \tag{11g}$$

$$R = [(n-1)^2 + \kappa^2] / [(n+1)^2 + \kappa^2 \tag{11h}$$

The contribution coming from σ electrons is evaluated within the framework of the bond polarizability theory [192]. The following values have been obtained elsewhere[204] χ = 1.87, and χ =1.98 .

Publications

1) Ultrafast Optoelectronic Ferromagnetic Semiconductor $CdCr_2Se_4$ Switch, Ardie D. Walser and R. R. Alfano. Applied Physics Letters 52 (7), 15 February 1988

2) Transient Photoconductivity in the Ferromagnetic Semiconductor $CdCr_2Se_4$. Ardie D. Walser and R. R. Alfano Applied Physics B, 47, 273 (1988) Springer-Verlag

3) Temperature Dependence of the Transient Photoconductivity in Stretched Trans-Polyacetylene Films. A. Walser, A. Seas. Communications, 67, 33 (1988)

4) Temperature Dependence of the Picosecond Photocurrent in Stretched Trans-Polyacetylene Films with Below Gap Excitation, A. D. Walser, R. Dorsinville, R. Tubino and R. R. Alfano. Mat. Res. Soc. Symp Proc. Vol. 173, pg. 437 (1990)

5) "Steady State & fast photoconductive response of highly oriented ^{205}polyacetylene", R. Tubino, R. Dorsinville, A. Walser, A. Seas and R. R. Alfano. Synth. Metals, 28, D175 (1989)

6) Temperature Dependence of the Transient Photoconductive Response in Stretched Trans-Polyacetylene Films with Below Gap Excitation, A. D. Walser, R. Dorsinville, R Tubino and R. R. Alfano. Journal of Applied Physics (to be published, Dec. 15, 1990)

7) Anisotropy of the Picosecond Photocurrent in Stretched Trans-Polyacetylene for Above and Below Gap Excitation, A. D. Walser, R. Dorsinville, R. Tubino, and R. R. Alfano Phys. Rev. B (accepted for publication 1991)

8) Pump Polarization Anisotropy with Above and Below Gap Excitation In Oriented $(CH)_x$, D. Comoretto, G. Musso, R. Tubino, A. Walser, R. Dorsinville, and R. R. Alfano, Synth. Metals (accepted for publication 1991)

Patents

1) Ultrahigh Speed Optical and Electrical Pulse Analysis using a Transmission Strip Line Photocathode in a Photomultiplier or Microchannel Plate Structure, R. R. Alfano and A. D. Walser, United States Patent # 4,853,595 August 1, 1989

2) Femtosecond Sampling Oscilloscope for Voltage Waveforms, R. R. Alfano and A. D. Walser, United States Patent # 4,931,704 June 5, 1990

Conferences

1) APS March Meeting (New Orleans) 3/21-25/1988 Temperature Dependence of the Picosecond Photoconductive Response in Highly Oriented Trans-polyacetylene Films, A. D. Walser, A. Seas, R. Dorsinville, R. R. Alfano, R. Tubino,Bulletin of the American Physical Society. Vol. 33, No. 3, 181-866, Talk No. 122 7 pg. 492

2) APS March Meeting (New Orleans) 3/23/1988 Ultrafast Optoelectronic Ferromagnetic Semiconductor $CdCr_2Se_4$ Switch. A. D. Walser and R. R. Alfano Poster Session 20C

3) First Edward Bouchet International Conference on Physics and Technology. June 9-11 1988 (Trieste Italy) Speaker

4) Annual Meeting of the Optical Society of America October 31-November 4, 1988 Santa Clara Convention Center, Santa Clara, California. Temperature Dependence of the Picosecond Photoconductive Response of Conducting Polymer Films Re: 0178

5) 12th Annual Meeting of The National Society of Black Physicists and 16th Annual Day Of Scientific Lectures April 5-7, 1989, AT&T Bell Laboratories Holmdel NJ Speaker

6) Temperature Dependence of the Picosecond Photocurrent in Stretched Trans-Polyacetylene Films with Below Gap Excitation. Materials Research Society Symposium, Nov. 27-Dec. 2, 1989. Boston MA

References

1 Chiang, C. K., Y. W. Park, A. J. Heeger, H. Shirakawa, E. J. Louis, and A. G. MacDiarmid, J. Chem. Phys. 69, 5098 (1978).

2 Chiang, C. K., M. A. Druy, S. C. Gau, A. J. Heeger, E. J. Louis, A. G. MacDiarmid, Y. W. Park, and H. Shirakawa, J. Am. Chem. Soc.100 1013 (1978).

3 Chiang, C. K., C. R. Fincher, Jr., Y. W. Parker, A. J. Heeger, H. Shirakawa, E. J. Louis, S. C. Gau, and A. G. MacDiarmid, Phys. Rev. Let. 39, 1098 (1977)

4 Etemad, S., A. J. Heeger and A. G. MacDiarmid, Annu. Rev. Phys. Chem. 33, 443 (1982)

5 Su, W. P., J. R. Schrieffer, and A. J. Heeger, Phys. Rev. Letters 42, 1698 (1979)

6 Peierls, R., Quantum Theory of Solids. Oxford University Press, London (p 108) (1955)

7 Pople, J. A., and S. H. Walmsley Mol. Phys. 5, 15 (1962)

8 Longuet-Higgens, H. C., and L. Salem, Proc. R. Soc. London Ser. A 251, 172 (1959)

9 Salem, L., The Molecular Orbital Theory of Conjugated Systems (Benjamin, New York). (1966)

10 Su, W. P., and J. R. Schrieffer, Pro. Nat. Acad. Sci. U.S.A., 77, 5626 (1980)

11 Su, W. P., J. R. Schrieffer, and A. J. Heeger, Phys. Rev. B22, 2099 1980

12 Su, W. P., J. R. Schrieffer, and A. J. Heeger, Phys. Rev. B28, 28,1138 (E) (1983)

13 Ball, R., W. P. Su and J. R. Scrieffer, J. Phys. Paris Colloq., 44, C3-429 1983)

14 Brazovskii, S. A., and N. N. Kirova, Pis, ma Zh. Eksp. Teor. Fiz., 33, 6 (1981) JETP Lett., 36, 4 (1981)

15 Kertesz, M., Adv. Quantum Chem., 15, 161 (1982)

16 Campbell, D. K. and A. R. Bishop, Phys. Rev. B 24, 4859 (1981)

17 Campbell, D. K. and A. R. Bishop, Nucl. Phys. B 200, 297 (1982)

18 Gross, D. J., and A. Neveu, Phys. Rev. D 10, 3235 (1974)

19 Natta, G., G. Mazzanti, and P. Corradini, Atti Accad. Naz. Lincei Rend. Cl. Sci. Fis. Mat. Nat., 25, 3 (1958)

20 Ito, T., H. Shirakawa, and S. Ikeda, J. Polym. Sci. Polym. Chem. Ed., 12, 11 (1974).

21 Shirakawa, H., and S. Ikeda, Synth. Met. 1, 175, (1979/1980)

22 Druy, M. A., C. H. Tsang, N. Brown, A. J. Heeger, and A. G. MacDiarmid, J. Polym. Sci. Polym. Phys. Ed., 18, 429 (1980)

23 Park, Y. W., M. A. Druy, C. K. Chiang, A. G. MacDiarmid, A. J. Heeger, H. Shirakawa, and S. Ikeda, J. Polym. Sci. Polym. Lett. Ed., 17, 195 (1979)

24 Fincher Jr., C. R., Jr., C. E. Chen, A. J. Heeger, and A. G. MacDiarmid, Phys. Rev. Lett., 48 100 (1982).

25 Lugli, G., U. Pedretti, and G. Perego, Journal of Polymer Science, Polymer Letters. Ed. 23, 129 (1985)

26 Piaggio, P., G. Dellepiane, R. Tubino, L. Piseri and G. Lugli, Solid State Commun. 49, 895 (1984)

27 Bleir, H., S. Roth, H. Lobentanzer and G. Leising, Europhysics Lett., 4 (12) 1397 (1987)

28 Edward, J. H., and W. J. Feast, Polymer 21, 595 (1980)

29 Edward, J. H., and W. J. Feast, and D. C. Bott, Polymer 25, 395 (1984)

30 Bradely, D. D. C., H. Friend, T. Hartman, E. A. Moseglia, M. M. Sckolowski, and P. D. Townsend, Synth. Met. 17 (1987)

31 Kahlert, H., A. Leitner and G. Leising, Synth. Met. 17, 467 (1987)

32 Goldberg, I. B., H. R. Crowe, P. R. Newman, A. J. Heeger, and A. G. MacDiarmid, J. Chem. Phys. 70, 1132 (1979)

33 Weinberger, B. R., E. Ehrenfreund, A. J. Heeger, and A. G. MacDiarmid J. Chem. Phys. 72, 4749 (1980)

34 Fincher, C. R., M. Ozaki, A. J. Heeger, and A. G. MacDiarmid Phys. Rev. B 19, 4140 (1979)

35 Rabolt, J. F., T. C. Clarke, and G. B. Street, J. Chem. Phys. 71, 4614 (1979)

36 Etemad, S., A. Pron, A. J. Heeger, A. G. MacDiarmid, E. J. Mele, and M. J. Rice Phys. Rev. B 23, 5137 (1981)

37 Thomann, H., L. R. Dalton, M. Grabowski, Y. Tomkiewicz, N. S. Shiren, and T. C. Clarke, Phys. Rev. Lett. 50, 533 (1983)

38 Kuroda, S., H. Bando, and H. Shirakawa, Solid State Commun. 52, 893 (1984) (1985)

39 Kuroda, S., H. Bando, and H. Shirakawa, j. Phys. Soc. Jpn. 54, 3956 (1985)

40 Grupp, A., P. Hofer, H. Kass, M. Mehring, R. Weizenhofer, and G. Wegner, 1987, in Electronic Properties of Conjugated Polymers, edited by H. Kuzmany, M. Mehring, and S. Roth, Springer Series in Solid State Sciences No. 76 (Springer, Berlin), p. 156 (1987)

41 Kass, H., P. Hofer, A. Grupp, P. K. Kahol, R. Weizenhofer, G. Wegner, and M. Mehring, Europhys. Lett. 4, 947 (1987)

42 Kuroda, S., and H. Shirakawa, Synth. Met. 17, 423 (1987)

43 Subbaswany, K. R., and M. Grabowski, Phys. Rev. B 24, 2168 (1981)

44 Heeger, A. J. , and J. R. Schrieffer, Solid State Commun. 48, 207 (1983)

45 Nechtschein, M., F. Devreux, F. Genoud, M. Guglielmi, and K. Holczer, J. Phys. (Paris) Collog. 44, C3-209 (1983a)

46 Nechtschein, M., F. Devreux, F. Genoud, M. Guglielmi, and K. Holczer, Phys. Rev. B 27, 61 (1983b)

47 Jeffries, C. D., Dynamic Nuclear Polarization (Interscience, New York) (1963)

48 Nechtschein, M., F. Devreux, R. L. Greene, T. C. Clark and G. B. Street, Phys. Rev. Lett. 44, 356 (1980)

49 Clark, W. G., K. Glover, G. Mozurkewich, S. Etemad, and M. Marfield, Mol. Cryst. Liq. Cryst. 117 (part A), 447 (1985)

50 Holczer, K., F. Devreux, M. Nechtschein, and J. P. Travers Solid State Commun. 39, 881 (1981)

51 Rabolt, J. F., T. C. Clarke, and G. B. Street, J. Chem. Phys. 71, 4614 (1979)

52 Rabolt, J. F., T. C. Clarke, and G. B. Street, J. Chem. Phys. 71, 4614 (1979)

53 Fincher, C. R., M. Ozaki, A. J. Heeger, and A. G. MacDiarmid,

Phys. Rev. B 19, 4140 (1979)

54 Paggio, D., G. Dellepiane, L. Pisari, R. Tubino, and C. Taliana, Solid State Commun. 50, 947 (1984)

55 Leising, G., R. Vitz, B. Angele, W. Ottinger, and F. Stelzer, Mol. Cryst. Liq. Crst. 117 (Part A), 327 (1985)

56 Tanaka, M., A. Watanabe, and J. Tanaka, Bull. Chem. Soc. Jpn. 53, 645, 3430 (1980)

57 Feldblum, A., J. H. Kaufman, S. Etemad, A. J. Heeger, T. -C. Chung and A. G. Macdiarmid, Phys. Rev. B 26, 815 (1982)

58 Chung, T. -C., F. Moraes, J. D. Flood, and A. J. Heeger Phys. Rev. B 29, 2341 (1984)

59 Tomkiewicz, Y., A. R. Taranko, and T. D. Schultz, Phys. Rev. Lett. 42, 1532 (1979)

60 Tomkiewicz, Y., N. S. Shiren, T. D. Schultz, H. Thomann, L. R. Dalton, A. Zettl, G. Gruner and T. C. Clarke, Mol. Crst. Liq. Cryst. 83 (part D), 1049 (1981)

61 Chen, J. T. -C. Chung, F. Moraes, and A. J. Heeger, Solid State Commun. 53, 757 (1985)

62 Moraes, F. J. Chen, T. -C. Chung, and A. J. Heeger Synth. Met. 11, 271 (1985)

63 Chen, J., A. J. Heeger, Phys. Rev. B 33, 1990 (1986a)

64 Fincher, C. R., Jr., M. Ozaki, M. Tanaka, D. Peebles, L. Lauchlan, and A. J. Heeger Phys. Rev. B 20, 1589 (1979)

65 Meyer, W. H., Mol. Cryst. Liq. Cryst., 77 (1981)

66 Meyer, W. H., Synth. Met. 4, 81 (1981)

67 Kiess, H., D. Baeriswyl, and G. Harbeke Mol. Cryst. Liq. Cryst., 77, 147 (1981)

68 Harada, I., Y. Furukawa, M. Tasumi, H. Shirakawa, and S. Ikeda, J. Chem. Phys. 73, 4746 (1980)

69 Kuzmany, H., Phys. Status Solidi B 97, 521, (1980)

70 Lichtman, L. S., A. Sarhangi, and D. B. Fitchen, Solid State Commun. 36, 869, (1980)

71 Fitchen, D. B., Mol. Cryst. Liq. Cryst. 83, 1127 (1982)

72 Kuzmany, H., E. A. Imhoff, D. B. Fitchen, and A. Surhangi, Phys. Rev. B 26, 7109 (1982)

73 Lefrant, S. J. Phys. (Paris) 44, C3-247 (1983)

74 Mulazzi, E., G. P. Brivio, E. Faulques, and S. Lefrant, Solid State Commun. 53, 583 (1985)

75 Harada, Issei, Mitsuo Tasumi, Hideki Shirakawa, and Sakuji Ikeda Chem. Lett. (Japan) 1411 (1978)

76 Rimai, L., M. E. Heyde, and D. Gill, J. Am. Chem. Soc., 95, 4493 (1973)

77 Gill, D., R. G. Kilponen, and L. Rimai, Chem. Phys. Lett., 8, 634 (1971)

78 Teitelbaum, R. C. , S. L. Ruby, and T. J. Marks, J. Am. Chem. Soc., 100 3215 (1978)

79 Harada, I., Y. Furukawa, M. Tasumi, H. Shirakawa, and S. Ikeda, J. Chem. Phys. 73, 4746 (1980)

80 Vardeny, Z., E. Ehrenfreund, O. Brafman, and B. Horovitz, Phys. Rev. Lett. 51, 2326 (1983)

81 Vardeny, Z., E. Ehrenfreund, O. Brafman, and B. Horovitz, Phys. Rev. Lett. 54, 75 (1985)

82 Horovitz, B., Z. Vardeny, E. Ehrenfreund, and O. Brafman, Synth. Met. 11, 139 (1984)

83 Lauchlan, L., S. P. Chen, S. Etemad, M. Kletter, A. J. Heeger and A. G. MacDiarmid Phys. Rev. B 27, 2301 (1983)

84 Tubino, R. Dorsinville, W. Lam, R. R. Alfano, and Joseph L. Birman, Phys. Rev. B 30, 6601 (1984)

85 Destri, S., A. Bolognesi, and M. Cattelani, Die Makromol, Chem. Rapid Commun. Germany 5, 353 (1984)

86 Moses, D., A. Feldblum, E. Ehrenfreund, A. J. Heeger, T. C. Chung, and A. G. MacDiarmid, Phys. Rev. B 26, 3361 (1982)

87 Hausser, K. W., R. Kuhn, A. Smakula, and K. H. Kreuchen Phys. Chem. Abt. B 29, 363 (1935)

88 Piseri, L., R. Tubino, E. Mulazzi and G. Dellepiane, in Raman Spectroscopy: Linear and Nonlinear, edited by J. Lascombe and P,v. Huong (wiley, New York, 1982), p. 583

89 Lauchlan, L., S. Etemad, T. C. Chung, A. J. Heeger, and A. G. MacDiarmid Phys. Rev. B 24, 3701 (1981)

90 Blanchet, G. B., C. R. Fincher, T.-C. Chung, and A. J. Heeger Phys. Rev. Lett. 50, 1938 (1983)

91 Vardeny, Z., J. Orenstein, and G. L. Baker, Phys. Rev. Latt. 50, 2032 (1983a)

92 Vardeny, Z., J. Orenstein, and G. L. Baker, J. Phys. (Paris) 44, C3-325 (1983b)

93 Orenstein, J., and G. L. Baker, Phys. Rev. Lett. 49, 1043 (1982)

94 Blanchet G. B., C. R. Fincher and A. J. Heeger, Phys. Rev. Lett. 51, 2132 (1983)

95 Rice, M. J., Phys. Rev. Lett. 51, 142 (1983)

96 Sun, X. L. Chen and E. X. Yu, Solid state Commun 53, 973 (1980)

97 R. Dorsinville, S. Krimchansky, R. R. Alfano, J. L. Birman, R. Tubino, and G. Dellepiane, Solid State Commun. 56, 857 (1985).

98 Vardeny, Z., J. Strait, D. Moses, T. -C Chung,a dn A. J. Heeger Phys. Rev. Lett. 49, 1657 (1982)

99 Shank, C. V., R. Yen, R. L. Fork, J. Orenstein, and G. L. Baker Phys. Rev. Lett. 49, 1660 (1982)

100 Rothberg, L., T. M. Jedju, S. Etemad, and G. L. Baker Phys. Rev. Lett. 57, 3229 (1986)

101 Sinclair, M., D. Moses, and A. J. Heeger, Solid State Commun. 57, 343 (1986)

102 Bleir, H., S. Roth, and G. Leising, Synth. Met. 17, 521 (1987)

103 Kivelson, S., and W. -K. Wu, Phys. Rev. B 34, 5423 (1986b)

104 Flood, J. D., and A. J. Heeger Phys. Rev. B 28, 2556 (1983)

105 Moraes, F., Y. W. Park and A. J. Heeger Synth. Met. 13, 113 (1986)

106 Hoffman, D., 1984, Ph.D. Thesis (Ohio State University) (1984)

107 Jayaraman, S., and Lee, C. H. Appl. Phys. Lett. 20, 392-395 (1972)

108 Auston, D. H. Appl. Phys. Lett. 26, 101-103 (1975)

109 Lawton, R. A. and Scavannec, A. Electron. Lett. 11, 74-75 (1975)

110 Mathur, V. K., Chang, C. S., Cao, W. L., Rhee, M. J., and Lee, C. H. IEEE J. Quantum Electron. QE-18, 205-209. (1982)

111 Leonberger, F. J., and Moulton, P. R. Appl. Phys. Lett. 35, 712-714 (1979).

112 Auston, D. H., Lavallard, P., Sol, N., and Kaplan, D. Appl. Phys. Lett. 36, 66-68 (1980a)

113 DeFonzo, A. P. Appl. Phys. Lett. 39, 480-482 (1981)

114 Margulis, W., and Sibbett, W. Opt. Commun. 31, 224 (1981)

115 Walser, A. D., and Alfano, R. R. Appl. Phys. Lett. 52, 592 -594 (1988)

116 Ho, P. T., Lee, C. H., Stephenson, T. C. and Cavanagh, R. B. Opt. Commun 46, 202-204 (1983)

117 Johnson, A. M., Lum, R. M., Simpson, W. M., and Klingert, J. To be published in IEEE J. Quanyum Electronics July 1987

118 Lawton, R. A., and Andrews, J. R. IEEE J. Trans. Instrum. Meas. IM-25, 56 (1976a)

119 Auston, D. H., Johnson, A. M., Smith, P. R., and Bean, J. C. Appl. Phys. Lett. 37, 371-373 (1980b)

120 Valdmanis, J. A., Mourou, G. A., and Gabel, C. W. IEEE J. Quantum Electron. QE-19, 664-667 (1983)

121 Mourou, G. A., and Knox, W. Appl. Phys. Lett. 36, 624 (1980)

122 LeFur, P., and Auston, D. H. Appl. Phys. Lett. 28, 21-23 (1976)

123 Agostinelli, J., Mourou, G. A., and Gabel, C. W. Appl. Phys. Lett. 35, 731 (1979)

124 Proud, J. M., and Norman, S. L., IEEE Trans. Microwave Theory Tech. MTT-26, 137-140 (1978)

125 Johnson, A. M. , Auston, D. H., IEEE J. Quantum Electron. QE.11, 283-287 (1975)

126 Platte, W., and Appelhans, G. Electron. Lett. 12, 270-271 (1976)

127 Mourou, G. A., Stancampiano, C. V., and Blumenthal, D. Appl. Phys. Lett. 38, 470-472. (1976)

128 Lawton, R. A., and Scavannec, A. Electron Lett. 11, 74-75 (1975)

129 Hammond, R. B., Paulter, N. G., Iverson, A. E., and Smith R. C. Tech. Dig.- Int. Electron. Devices Meet. pp. 157-159 (1981)

130 Gurston, M. A. R., Microwave Transmission-Line Impedance Data London: Van Nostrand Reinhold, pp. 38-39 (1972)

131 Schneider, M. V., "Microstrip Lines for Microwave Integrated Circuits", Bell System Tech J., Vol. 48, pp. 1421-1444 (1969)

132 Wheeler, H. A., "Transmission Line Properties of Parallel Strips Seperated by a Dielectric Sheet, " IEEE Trans. Microwave Theory Tech. Vol. MTT-13, pp 172-185 (1965)

133 Wheeler, H. A., "Transmission Line Properties of a Strip on a Dielectric Sheet on a Plane, " IEEE Trans. Microwave Theory Tech. Vol. MTT-25, pp 631-647 (Aug. 1977)

134 Hammerstad, E. O., "Equations for Microstrip Circuit Design," in Proc. European Microwave Conf., pp. 268-272 (1975)

135 Orenstein, J., Z. Vardeny, G. L. Baker, G. Eagle and S. Etemad, Phys. Rev., B30, 786 (1984)

136 Townsend, P. D. Tonsend and R. H. Friend, Synthetic Metals, 17, 361 (1987)

137 Danielsen, P. L., Synthetic Metals, 20, 125 (1987)

138 Gartstein, Y., N., and A. A. Zakhidov, to be published

139 Jeyadev, S., and E. M. Conwell, Phys. Rev. B, 35, 5917 (1987)

140 Tani, T., P. H. Grant, W. D. Gill, G. B. Street, and T. C. Clark Solid State Commun. 33, 499 (1980)

141 Etemad, S., T. Mitani, M. Ozaki, T. C. Chung, A. J. Heeger and A. G. MacDiarmid Solid State Commun. 40, 741 (1981)

142 Weinberger, B. R., Phys. Rev. Lett. 50, 1693 (1983)

143 Weinberger, B. R., Phys. Rev. Lett. 33, 86 (1984)

144 Kiess, H., R. Keller, D. Baeriswyl, and G. Harbeke, Solid State Commun. 44, 1443 (1982)

145 Tubino, R., R. Dorsinville, A. Seas, J. Birman, and R. R. Alfano Phys. Rev. B 38, 8318 (1988)

146 Siddiqui, A. S., J. Phys. C 17, 683 (1984)

147 Dorsinville, R., R. Tubino, J. L. Birman, and R. R. Alfano, Synth. Met. 17, 509 (1987)

148 Roth, S., and H. Bleir, Synthetic Metals, 17, 503 (1987)

149 Townsend, P. D., and R. H. Friend Synthetic Metals. 17, 361 (1987)

150 Onsager, L. J., Chem. Phys. 2, 599 (1934)

151 Onsager, L. J., Phys. Rev. 54, 554 (1938)

152 Kao, K. C., W. Hwang, Electrical Transport in Solids Pergamon Press (1981)

153 Pai, D. M., J. Appl. Phys. 46, 5122 (1975)

154 Pai, D. M., and Enck, R. C., Phys. Rev. B 11, 5163 (1975)

155 Batt, R. H., C. L. Braun, and J. F. Horing, J. Chem. Phys. 49, 1967 (1968)

156 Geacintov, N. E., M. Pope, Proceeding of the 3rd International Conference on Photoconductivity in Organic Crystals (ed. E. M. Pell) Pergamon Press (Oxford) 289 (1971)

157 Melz, P. J., J. Chem. Phys. 57, 1964 (1972)

158 Batt, R. H., C. L. Braun, and J. F. Horing, J. Chem. Phys. 49, 1967 (1968)

159 Chance, R. R., and C. L. Braun, J. Chem. Phys. 64, 3573 (1976)

160 Pfister, G., and D. J. Williams, J. Chem. Phys. 61, 2516 (1974)

161 Haberkorn, R., M. E. Michel-Beeyerle, Chem. Phys. Lett. 23, 128 (1973)

162 Frakevich, E. L., A. A. Lymarev and I. A. Sokolik, Chem Phys. Lett. 159, 113 (1989)

163 Knight, J. C., E. A. Davies, J. Phys. Chem. Solids 35, 543 (1974)

164 Haberkorn, R., M. E. Michel-Beeyerle, Chem. Phys. Lett. 23, 128 (1973)

165 Johnson, Anthony Micheal, Carrier Transport in Amorphous Silicon Utilizing Picosecond Photoconductivity, dissertation, The City University of New York (1981)

166 Wilson, E. G., J. Phys. C 13, 2885 (1980)

167 T. Ito, H. Shirakawa, S. Ikeda, Journal of Polymer Science, Polymer Letters, Ed. 12, 11 (1974)

168 M. Pope and C. E. Swendberg, "Electronic Processes in Organic Crystals," Clarendon Press, Oxford, 1982

169 E. M. Conwell, S. Jeyadev, (to be published)

170 J. C. W. Chien, "Polyacetylene," Academic Press, New York, 1984, p. 483

171 S. Etemad, T. Mitani, M. Ozaki, T. C. Chung, A. J. Heeger. A. G. MacDiarmid, Solid State Communications, 40, 75 (1981)

172 S. Roth, K. Ehinger, K. Menke, M. Peo, R. J. Schweizer, Journal de Physique, C3, 69 (1983)

173 S. Kivelson, Physical Review Letters, 46, 1344 (1981)

174 L. Rothberg, T. M. Jedju, S. Etemad, G.L. Baker, IEEE Journal of Quantum Electronics, 24, 311 (1988)

175 D. L. Weidman, D. B. Fitchen, Synthetic Metals, 17, 355 (1987)

176 Vardeny, Z., J. Strait, D. Moses, T. T. Chung and A. J. Heeger Phys. Rev. Lett. 49, 1657 (1982)

177 Takayama, H., Y. R. Lin-Lin, and K. Maki, Phys. Rev. B, 21, 2388 (1980)

178 Blanchet, Graciela B, C. R. Fincher, T. C. Chung, and A. J. Heeger, Phys. Rev. Lett. 50, 1938 (1983)

179 Walser, A., A. Seas, R. Dorsinville, R. R. Alfano, and R. Tubino Solid State Communications, 67, 333 (1988)

180 Sinclair, M., D. Moses, R. H. Friend and A. J. Heeger Phys. Rev. B, 36, 4296 (1987)

181 Lauchlan, L., S. Etemad, T. C. Chung, A. J. Heeger, and A. G. MacDiarmad Phys. Rev. B. 24, 3701 (1981)

182 Goldberg, J. H., H. R. Crow, P. R. Newman, A. J. Heeger, and A. G. MacDiarmid J. Chem. Phys. 70, 1132 (1979)

183 Chiang, C. K., C. R. Fincher, Y. W. Park, A. J. Heeger, H. Shirakawa, E. J. Loius, S. C. Gau, and A. D. MacDiarmid Phys. Rev. Lett. 39, 1098 (1977)

184 R. Dorsinville, S. Krimchansky, R. R. Alfano, J. L. Birman, R. Tubino & G. Dellepiane Solid State Comm. 56, 857 (1980)

185 H. Bleir, S. Roth, H. Lobentanzer and G. Leising Europhysics Lett., 4 (12) 1397 (1987)

186 Bleier, H., S. Roth, Y. Q. Shen, and D. Scafer-Siebert Phys Rev. B 38, 6031 (1988)

187 A. D. Walser, R. Dorsinville, R. Tubino and R. R. Alfano (To be Published 1991)

188 G. Leising, Synth Metals 28, D215 (1989)

189 P. D. Townsend and R. H. Friend Phys. Rev. B 40, 3112 (1989)

190 Danielsen, P. L., J. Phys. C19, L741 (1986)

191 Phillpot, S. R., D. Baeriswyl, A. R. Bishop and P. S. Lomdahl Phys. Rev. B35, 7533 (1987)

192 Piseri, L., and R. Tubino. Phys. Rev. B11, 5145 (1975)

193 Fincher Jr., C. R., C. E. Chen, A. J. Heeger, A. G. MacDiarmid and J. B. Hastings, Phys. Rev. Lett. 48, 100 (1982)

194 Mulliken, R. S., J. Chem. Phys. 46, 497, 675 (1949)

195 Genkin, V. N., and P. M. Mednis, Zh. Exp. Teor. Fiz. 54, 1137 (1968) (Soviet, Phys. JETP 27, 609 (1968))

196 Cojan, C. G. P. Agrawal and C. Flytzanis, Phys. Rev. B15, 909 (1977)

197 Dove. R., Private Communication

198 Rothberg, L., T. Jedju, S. Etemad and G. L. Baker, Phys. Rev. B 36, 7529 (1987)

199 Rothberg, L., T. M. Jedju, P. D. Townsend, S. Etemad, and G. L. Baker Phys. Rev. Lett. 65, 100 (1990)

200 Shockley, W., J. Appl. Phys. 9, 635 (1938)

201 Comoretto, D., R. Tubino, G. Dellepiane, G. F. Musso, A. Borghesi, A. Piaggi, and G. Lanzani, Phys. Rev. B 41, 3534 (1990)

202 Comoretto, D., G. Dellepiane, G. F. Musso, R. Tubino, A. Walser, R. Dorsinville and R. R. Alfano (To be published Synthetic Metals (1991)

203 Cojan, C. G. P. Agrawal and C. Flytzanis, Phys. Rev. B15, 909 (1977)

204 Lanzani, G., S. Luzzati, R. Tubino, and G. Dellepiane, J. Chem. Phys. 91 (2), 732 (1989)